Electrical Conduction in Fluorite-Structure Related Oxides

March, 1987

Doctor Thesis

University of Tokyo

Masaru MIYAYAMA

Preface

The fluorite-structured oxides are one of the most important materials in both scientific and industrial fields. Their most significant property is the oxygen-ion conduction. From the report by C. Wagner in 1943 on conduction mechanism of stabilized fluorite ZrO_2, many investigations have been conducted on defect chemistry, ionic conduction mechanism and applications for fluorite-type oxides. Nowadays, oxygen sensors and oxygen pumps using ZrO_2-based materials are already used in a variety of industrial areas, and fuel cells are going to be realized.

Some oxides with fluorite-related structures show polymorphic transformations accompanied by volume changes at low temperatures. The transformation between tetragonal and monoclinic forms, induced by applied stress, absorbs the fracture energy and hence enhances the mechanical properties (strength and toughness) in partially-stabilized or tetragonal ZrO_2 ceramics. These materials are being watched with keenest interest as a promising toughened ceramics.

The oxygen-ion conduction in the fluorite-type oxides essentially derive from their open and symmetrical crystal structure. Accordingly, a slight change in the crystal structure greatly affects the oxygen-ion conduction. Although there has been many investigations on the conduction mechanism for the

fluorite-type oxides, investigations including influences of structural changes are very few.

Grain boundary, present in polycrystals, is known to inhibit the oxygen-ion conduction in most of fluorite-type oxides. However, since the effect depends on microstructure of polycrystals and impurity concentration, grain-boundary resistivity has not yet been interpreted inclusively.

In the present study, Bi_2O_3- and ZrO_2-based compounds were selected as the fluorite-structure related oxides, and the correlation of the oxygen-ion conduction with crystal structure, defect structure and polycrystalline structure was investigated.

The constitution of the present thesis is briefly described in the following ;

In Chapter **I**, the crystal structures in Bi_2O_3 polymorphis, fundamental theories for oxygen-ion and ion-electron mixed conduction and some experimental techniques for electrical measurements are reviewed.

In Chapter **II**, the polymorphic transformations in pure- and doped Bi_2O_3 and the electrical conduction behavior in each form (monoclinic α, tetragonal β, bcc γ and fcc δ forms) are revealed. On the bases of the obtained results, the correlation between crystal structure and oxygen-ion conduction is discussed.

In Chapter **III**, the oxygen-ion conductivities in solid solutions and two-phase mixed composites in Bi_2O_3-ZrO_2-Y_2O_3 system are shown, and the conduction mechanism in the composites is discussed.

In Chapter **IV**, the effects of microstructure (grain size) and impurity(Al_2O_3) concentration on grain-boundary resistivity in stabilized ZrO_2 are revealed. The origin of grain-boundary resistivity is also discussed.

In Chapter **V**, electrical conduction behavior in Sb_2O_4 and Y_2O_3, which are used as dopants for Bi_2O_3 or ZrO_2, is revealed.

CONTENTS

Chapter I

Introduction

I - 1. Crystal structures of polymorphic forms in Bi_2O_3

Bismuth sesquioxide has four polymorphic forms : monoclinic α stable at room-temperature, cubic δ at high temperatures, and metastable tetragonal β and bcc γ forms. The crystal structures of α, β and γ forms can be related to that of the δ form. Structural informations are given in Table 1.

1-1. δ -Bi_2O_3

The cubic δ form has an oxygen-deficient structure of the fluorite-type, in which the bismuth atoms are located on fcc sites and one-forth of oxygen atoms are missing.

There is some contraversy concerning the structure and space group on this form. Sillen proposed a simple cubic structure (Pn3m) in which oxygen atoms are ordered along <111>[1,2]. Gattow and Schroder proposed the average distribution of 6 O atoms in 8 tetrahedral(8c) sites (Fm3m)[3]. The high ionic conductivity and the high disorder(a large enthalpy change and a large entropy gain for $\alpha \rightarrow \delta$ transition[4]) in the δ form does not support the Sillen's model, at least, at high temperatures. In contrast, the displacement of O atoms from the normal tetrahedral sites was observed by neutron diffraction at high temperatures.[5,6] The O

Table 1-1. Structural Information for Bismuth Oxide Polymorphs

	Space Group / Lattice Constant(A)	Atom	x	y	z	ref
α-Bi_2O_3	$P2_1/c$	4 Bi^{+3}	0.524	0.183	0.361	
	a = 5.848	4 Bi^{+3}	0.041	0.043	0.776	
	b = 8.166	4 O^{-2}	0.780	0.300	0.710	13
	c = 7.510	4 O^{-2}	0.242	0.044	0.134	
	= 113	4 O^{-2}	0.271	0.024	0.513	
β-Bi_2O_3	$P42_1c$	8 Bi^{+3}	0.021	0.256	0.236	
	a = 7.742	8 O^{-2}	0.290	0.320	0.027	11
	c = 5.631	4 O^{-2}	0.0	0.50	0.146	
δ-Bi_2O_3	Pn3m(Sillen)	4 Bi^{+3}	0.75	0.75	0.75	1
	a = 5.525	6 O^{-2}	0.0	0.50	0.50	
	Fm3m(Gattow)	4 Bi^{+3}	0.0	0.0	0.0	3
	a = 5.66(750°C)	6 O^{-2}	0.25	0.25	0.25 #1	
	Fm3m(Harwig)	4 Bi^{+3}	0.0	0.0	0.0	
	a = 5.6595(774°C)	6 O^{-2}	x	x	x #2	5
				(x = 0.25 + d)		
γ-Bi_2O_3	I23	24 Bi^{+3}	0.176	0.318	0.014	
($Bi_{26}O_{40}$)		1 Bi^{+3}	0.0	0.0	0.0	
	a = 10.268	1 Bi^{+5}	0.0	0.0	0.0	19
		8 O^{-2}	0.689	0.689	0.689	
		24 O^{-2}	0.635	0.752	0.989	
		8 O^{-2}	0.893	0.893	0.893	

Site Occupancy ; #1 : 3/4, #2 : 3/16

atoms are distributed at the 32f positions, xxx ; x = 0.25 +d , with occupation probability 3/16. The structures are shown in Fig.1. For pure δ form, the displacement parameter d is 0.066, but it decreases with increasing dopant-concentration and then finally diminishes (at 32.5 mol% in case of Gd_2O_3).[7]

In the solid solutions of δ-Bi_2O_3 with M_2O_3 or M_2O_5, a trivalent or a pentavalent cation is substituted for Bi^{3+}.[8,9] Hence, in case of M_2O_5, the oxygen vacancy concentration decreases with increasing M_2O_5 content according the expression,

$$Bi_{2(1-x)}M_{2x}O_{3+2x}V_{1-2x} \qquad (1)$$

where V is the oxygen vacancy.

1-2. β-Bi_2O_3

The tetragonal β form has a distorted deficient fluorite structure with ordered vacant sites in the oxygen sublattice. Early workers suggested that the β form was a simple two-dimensional superstructure of δ-Bi_2O_3 with ordered vacancies in the <111> direction.[10] Aurivillius and Malmros redetermined the β structure and concluded that β-Bi_2O_3 crystallizes in the $P42_1c$ space group and the structure is penetrated by tunnels in the <001> direction formed by oxygen vacancies.[11] Projection of the β- Bi_2O_3 structure on the (001) plane is shown in Fig.2. The O atoms are divided in two types, O(1) and O(2), and positions of O(1) are shifted largely from those in the δ form. It is also suggested that the tunnels may accomodate extra oxygen atoms if Bi^{3+} is substituted by pentavalent cations.[11]

1-3. α-Bi_2O_3

The monoclinic α form is the low-temperature stable form which crystallizes in the $P2_1/c$ space group.[1,12,13] A projection of the structure on the (010) plane is given by Fig.3. The structure consists of layers of Bi atoms parallel to the (100)

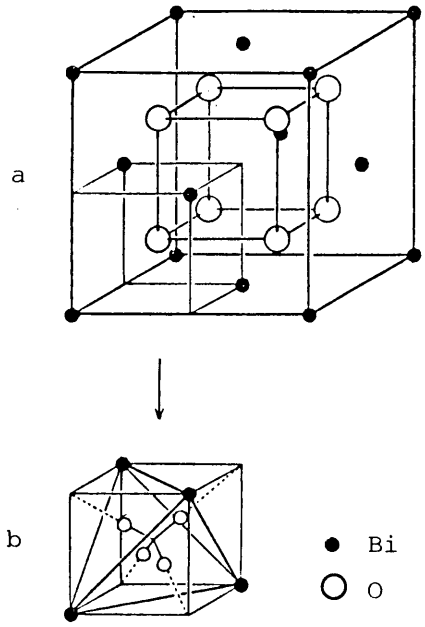

Fig.1-1.
Fluorite structure of δ-Bi_2O_3.
a) Gattow model:[3)]
average distribution of 6 O atoms at 8c sites of Fm3m.
b) Wills model:[5)]
average distribution of 6 O atoms at 32f sites of Fm3m.

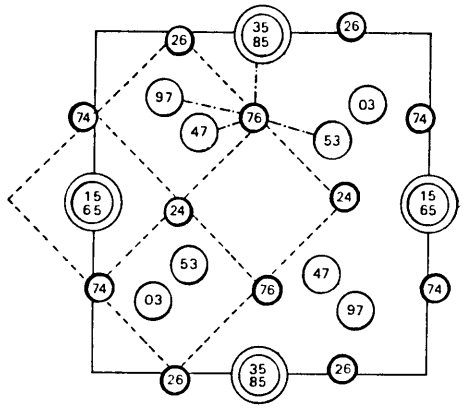

Fig. 1-2.
Projection of β-Bi_2O_3 structure on the (001) plane. 11)
The bismuth cube of the fluorite structure is indicated.

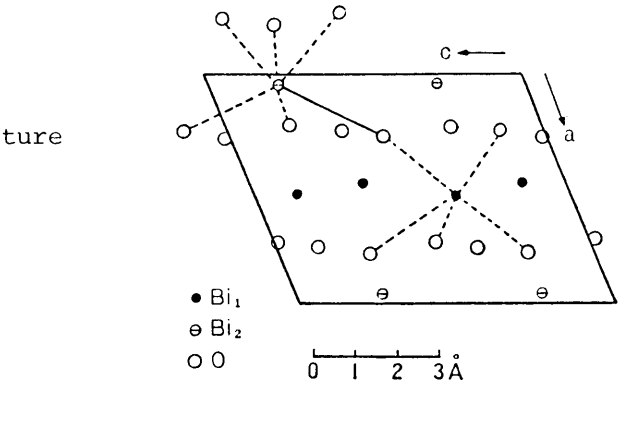

Fig. 1-3.
Projection of α-Bi_2O_3 structure on the (010) plane. 13)

plane at x = 0 and 0.5. These layers are separated by sheets of O atoms at x = 0.25 and 0.75. There are two types of oxygen coordination around Bi atoms, one 5-coordinated around Bi_1(x = 0.5) and one 6-coordinated around Bi_2(x = 0). The oxygen polyhedrons are described as distorted octahedrons, in which an oxygen is removed for 5-coordinated Bi_1.

The relations of Bi sublattice to the fcc cation sublattice of δ-Bi_2O_3 are shown in Fig.4.[14] For the sake of clarity, the positions of the Bi atoms are indicated by the two-fold screw axis and the structure of α form is described as pseudo-orthorhombic. It is found that Bi atoms in the orthorhombic lattice situate in the zigzag configuration in a axis direction and displacements of Bi atoms in c axis direction make a fcc cation sublattice. In the same manner, an introduction of oxygen vacancies and displacements of O atom positions give the oxygen sublattice of the δ form. Accordingly, the oxygen sublattice in α-Bi_2O_3 is related to that of a highly ordered deficient-fluorite structure.

1-4. γ-Bi_2O_3

The bcc γ form can be stabilized by the addition of small amounts of dopant oxides to form the sillenite group of compounds $6Bi_2O_3.MO_2$ ($Bi_{24}M_2O_{40}$) in the I23 space group. In the sillenite compounds, the M^{4+} ions are tetrahedrally coordinated and occupy the body centered sites and the cube corners, linked by hepta-coordinated Bi atoms.[15] The schematic figure of the structure and the projection of Bi sublattice on (001)plane are shown in Fig.5.

The pure γ-Bi_2O_3 was first proposed by Sillen[1] to be isomorphous with the bcc $Bi_{24}Si_2O_{40}$ where Bi atoms occupy the Si positions in the cell. Other studies suggested that γ-Bi_2O_3 contains $Bi_{26}O_{39}$ in the unit cell.[16,17] Levin and Roth indicated that the pure γ-Bi_2O_3 has the largest cell dimension of the serius of sillenite compounds reported.[18] Craig and Stephenson

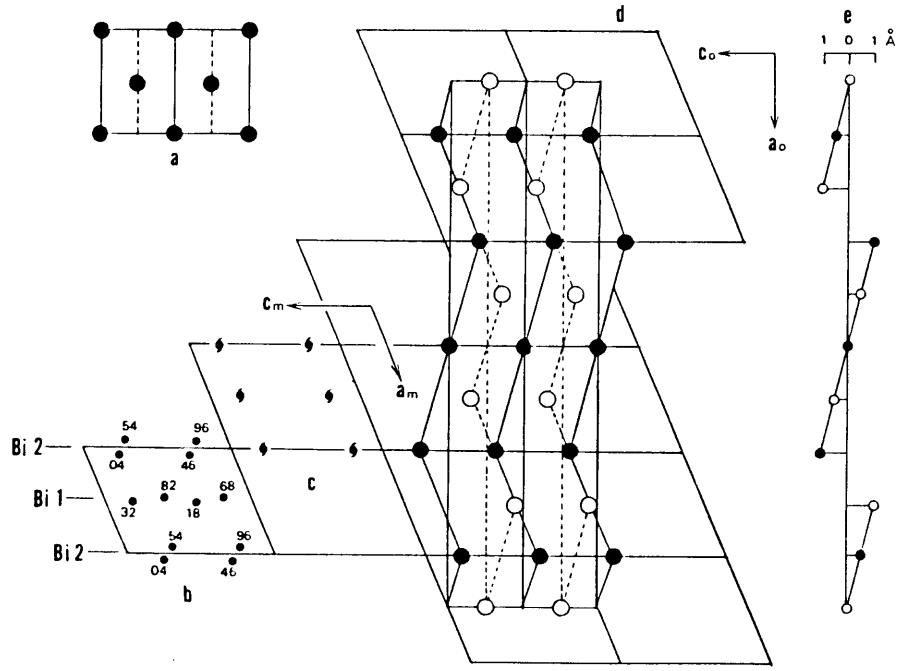

Fig. 1-4. Comparison of the Bi sublattice of α-Bi_2O_3 with the ideal fcc Bi sublattice of δ-Bi_2O_3.[5]

a) projection on the $(101)_f$ plane of the fcc Bi sublattice of δ-Bi_2O_3.
b) projection on the $(010)_m$ plane of the Bi sublattice of α-Bi_2O_3.
c) positions of the two-fold screw axes in $P2_1/c$.
d) projection on the $(010)_o$ plane of the orthorhombic ten-fold cell of α-Bi_2O_3.
e) average displacements on the $<001>_m$ direction of the Bi atoms in the layers at $x = \pm n$, $1/2 \pm n$ at the $\alpha \rightarrow \delta$ transition.

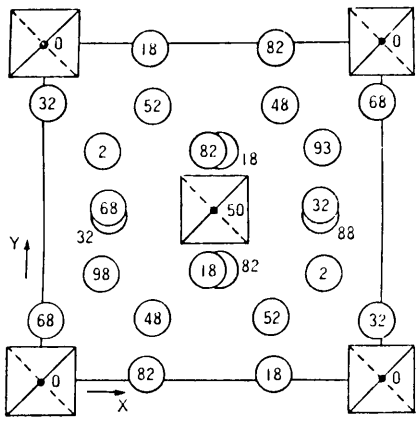

Fig. 1-5. Projection on the (001) plane of the Bi sublattice of bcc $Bi_{12}GeO_{20}$. 15)

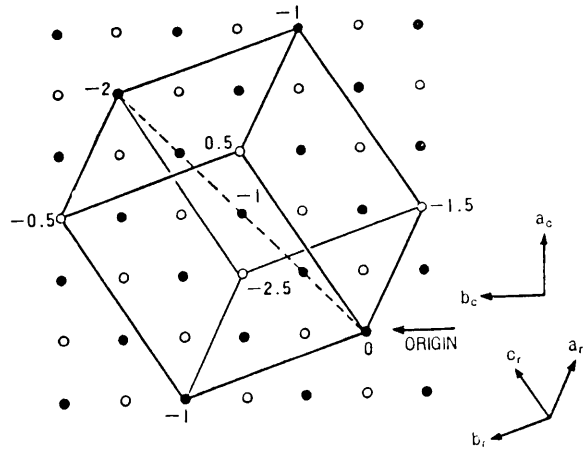

Fig. 1-6. Projection of the fcc Bi sublattice of δ-Bi_2O_3 on the (001) plane. A bcc super cell is outlined.[5]
: Bi at $z = \pm n$, : Bi at $z = 1/2 \pm n$.

suggested that the γ-Bi_2O_3 is isomorphous with $Bi_{24}^{3+}Bi^{5+}Fe\ O_{40}$ and has the composition $Bi_{25}^{3+}Bi^{5+}O_{40}$, where the two tetrahedral sites are occupied by one Bi^{3+} and one Bi^{5+} ion.[19] Devalette et al. reported that $Bi_{12}[A_{1/2}B_{1/2}]O_{20}$ and $Bi_{12}[Zn_{1/3}B_{2/3}]O_{20}$ (A = Fe, Ga and B = P, As, Bi) are derived from $Bi_{12}GeO_{20}$ by couple substitutions.[20] However, the existance of the Bi^{5+} ion has not yet been verified directly. Accordingly it is not clear at present whether the oxygen sublattice of pure γ-Bi_2O_3 is occupied completely or not.

The structural relation in γ- and δ-Bi_2O_3 is demonstrated by the introduction of a body-centered rhombohedral super cell in the fcc lattice of the γ form, as shown in Fig.6.[14] This super cell contains $13Bi_2O_3$ units as the γ form. Assuming the unit cell of 5.53 A for fcc lattice, the cell dimension is 10.34 A and $\alpha = 85.9°$ which approximately agree with 10.27 A in the γ form.

REFERENCES in I-1

1. L.G. Sillen, Ark. Kemi. Mineral. Geol., 12A, 1 (1937).
2. J.W. Medernach and R.L. Snyder, J. Am. Ceram. Soc., 61, 494 (1978).
3. G. Gattow and H. Schroeder, Z. Anorg. Allg. Chem., 318, 176 (1962).
4. H.A. Harwig and A.G.Gerards, Thermochim. Acta, 28, 121 (1979)
5. H.A. Harwig, Z. Anorg. Allg. Chem., 444, 151 (1978).
6. M.J. Verkerk, G.M.H. van de Velde, A.J. Burggraaf and R.B. Helmholdt, J. Phys. Chem. Solids, 43, 1129 (1982).
7. K. Koto, H. Mori and Y. Ito, Solid State Ionics, 18&19, 720 (1986).

8. T. Takahashi, H. Iwahara and T. Arao, J. Appl. Electrochem., 5, 187 (1975).
9. T. Takahashi, H. Iwahara and T. Esaka, J. Electrochem. Soc., 124, 1563 (1977).
10. G. Gattow and D. Schuetze, Z. Anorg. Allg. Chem., 328, 44 (1964).
11. B. Aurivillius and G. Malmros, Trans. R. Inst. Technol., Stockholm, 1972, 3.
12. L.G. Sillen, Z. Kristallogr., 103, 274 (1941).
13. G. Malmros, Acta Chem. Scand., 24, 384 (1970).
14. H.A. Harwig and J.W. Weenk, Z. Anorg. Allg. Chem., 444, 167 (1978).
15. S. C. Abrahams, P. B. Jamieson and J.L. Bernstein, J. Chem. Phys., 47, 4034 (1967).
16. W. C. Schumb and E. S. Rittner, J. Am. Chem. Soc., 65, 1055 (1943).
17. B. Aurivillius and L. G. Sillen, Nature (London), 155, 305 (1945).
18. E.M. Levin and R.S. Roth, J. Res. Natl. Bur. Stand. Sect A, 68, 197 (1964).
19. D.C. Craig and N.C. Stephenson, J. Solid State Chem., 15, 1 (1975).
20. M. Devalette, G. Meunier, C. Mazeau, A. Morell and P. Hagenmuller, C. R. Acad. Sc. Paris, 291, 251 (1980).

I - 2. Basic theories for ionic and mixed conduction

In this section, effects of temperature, dopant concentration and oxygen partial pressure on the conductivity are described for oxygen-deficient oxides. Discussion will be restricted to the oxides where oxygen vacancies, present in quantity by nature (Bi_2O_3) or generated by the introduction of lower-valent cations (ZrO_2), are the majority charge carriers.[1-3] The notation used in the following equations is due to Kroger and Vink[1].

The electrical conductivity of one charge carrier i can be expressed as

$$\sigma_i = c_i Z_i e \mu_i \qquad (1)$$

where c_i is the number of carriers per unit volume, Z_i the number of electron charge e of the carrier, and μ_i the mobility. The total conductivity σ_t is then represented as the sum of the conductivities of each of the charge carriers.

2-1. The effect of temperature

Empirically it has been found that the temperature dependence of the ionic conductivity can be expressed by the next form;

$$\sigma T = A \exp(-E_a/kT) \qquad (2)$$

where A is a constant (preexponential term), E_a the apparent activation energy and k is the Boltzmann constant.

For the migration of oxygen vacancies, we can expand the mobility

$$\mu = r(Ze/kT)a^2\gamma \exp(-\Delta G_m/kT) \quad (3)$$

where r is a geometric factor, γ the junp attempt frequency, ΔG_m the Gibbs free energy for the jump, a the jump distance, e, k and T have their usual meanings, and Z = 2. Now, $\Delta G_m = \Delta H_m - T\Delta S_m$ where ΔH_m and ΔS_m are the enthalpy and entropy for migration, thus Eq.3 becomes

$$\mu = (B/T) \exp(-\Delta H_m/kT) \quad (4)$$

where constant B contains the temperature-independent terms, assuming ΔS_m to be temperature-independent. The number of charge carrier is simply given by,

$$c = [V_O^{\cdot\cdot}](1-[V_O^{\cdot\cdot}])N \quad (5)$$

which for small values of $[V_O^{\cdot\cdot}]$ approximates $[V_O^{\cdot\cdot}]N$, where N is the number of anion sites per unit volume. Substituting Eqs.4 and 5 into Eq.1, we obtain

$$\sigma = (B'/T)[V_O^{\cdot\cdot}]\exp(-\Delta H_m/kT) \quad (6)$$

where $B' = NeZB \quad (7)$

2-2. The effects of dopant concentration and association[2,3]

When the lower-valent cation $Mf^{(4-n)+}$ substitute for the cation in M_2O_4, oxygen vacancies are generated as charge compensating defects;

$$Y_2O_3 \xrightarrow{2ZrO_2} 2Y_{Zr}' + 3O_O^{*} + V_O^{\cdot\cdot} \quad (n=1) \quad (8)$$

Case 1 : Free vacancies

In the case where all the oxygen vacancies are free, the condition of electro-neutrality determines that

$$[V_O^{\cdot\cdot}] = n[Mf_M](1/2) \quad (9)$$

where term (1/2) is due to anion/cation ratio. Substituting Eq.9 into Eq.6 gives

$$\sigma T = B'(n/4)C\exp(-\Delta H_m/kT) \quad (10)$$

where C is the total dopant concentration.

Case 2 : n = 2 e.g. Ca^{2+} in ZrO_2

The vacacies are not free but bound to dopant cations to form defect associates. This binding energy is mainly due to the Coulombic attraction energy of the defects by their effective charges. For the case n = 2, only one simple defect associate is possible, the neutral associate $(Mf_M V_O)$. For the dissociation of the associate, applying the law of mass action gives,

$$[Mf_M''][V_O^{\cdot\cdot}]/[(Mf_M V_O)] = K_{A2}(T) \quad (11)$$

Electroneutrality is $2[V_O^{\cdot\cdot}] = 2[Mf_M''](1/2)$ (12)

For full association of defects, $[(Mf_M V_O)] = C$ (13)

The equilibrium constant $K_{A2}(T)$ can be expressed as

$$K_{A2}(T) = (1/W)\exp(-\Delta H_{A2}/kT) \quad (14)$$

where W is the number of orientations of associate and ΔH_{A2} the enthalpy of association. By combining Eqs.11-14, we obtain

$$[V_O^{\cdot\cdot}] = (C/2W)^{1/2}\exp(-\Delta H_{A2}/2kT) \quad (15)$$

Substitution of Eq.15 into Eq.6 gives

$$\sigma T = B'(C/2W)^{1/2}\exp[-(\Delta H_m + \Delta H_{A2}/2)] \quad (16)$$

Case 3 : n = 1 e.g. Y^{3+} in ZrO_2

Two defect associates are possible, a charged associate $(Mf_M V_O)^{\cdot}$ or a neutral associate $(2Mf_M V_O)$. Assuming the dissociation of the charged associate, we can obtain the next equation in the same manner described above,

$$\sigma T = (B'/W)\exp[-(\Delta H_m + \Delta H_{A1})/kT] \quad (17)$$

Case 4 : n = 0 e.g. Y^{3+} in Bi_2O_3

In this case total concentration of oxygen vacancy is fixed to be 0.25. Assuming the dissociation of the charged associate $(Mf_M V_O)^{\cdot\cdot}$, we can obtain the next equations

$$[V_O^{\cdot\cdot}] + (1/2)[(Mf_M V_O)^{\cdot\cdot}] = 0.25 \quad (18)$$

$$C = [Mf_M^{*}] + [(Mf_M V_O)^{\cdot\cdot}] \quad (19)$$

and $$[Mf_M^{*}][V_O^{\cdot\cdot}]/[(Mf_M V_O)^{\cdot\cdot}] = K_{AO}(T) \quad (20)$$

where $$K_{AO}(T) = (1/W)\exp(-\Delta H_{AO}/kT) \quad (21)$$

In case of full association for small C, $[(Mf_M V_O)^{\cdot\cdot}] = C$, which leads to $[V_O^{\cdot\cdot}] = 0.25 - C/2$ and hence,

$$\sigma T = B'(0.25-C/2)\exp(-\Delta H_m/kT) \quad (22)$$

When C is larger than 0.5, $[(Mf_M V_O)^{\cdot\cdot}] = 0.5$. Eqs.19 and 20 gives $[V_O^{\cdot\cdot}] = K_{AO}(T)/(2C-1)$ and then,

$$\sigma T = [B'/W(2C-1)]\exp[-(\Delta H_m + \Delta H_{AO})/kT] \quad (23)$$

Comparing with the empirical relation Eq.2, A and E_a in cases 1-4 are listed in Table 1.

An agreement of estimated and observed composition-dependences of A and E_a is achieved only in the dilute solution range ($[V_O^{\cdot\cdot}] < 0.04$) of case 2, and qualitatively in case 4.[3] In the concentrated range, observed A and E_a in cases 2 and 3 increase with increasing dopant concentration resulting in a decrease in conductivity.[3] this phenomena have not been fully accounted for in a quantitative way, though defect ordering, clustering, electrostatic interactions, precipitation of a second phase etc. have been invoked.[4,5] As for the case 4, discussion will be conducted in Chap.II-5.

Table I-2-1. The form of the preexponential factor A and activation energy E_a

Case	n	A	E_a
1	-	$B'(n/4)C$	ΔH_m
2	2	$B'(C/2W)^{1/2}$	$\Delta H_m + \Delta H_{A2}/2$
3	1	$B'(1/W)$	$\Delta H_m + \Delta H_{A1}$
4	$0 (C \ll 0.5)$	$B'(0.25-C/2)$	ΔH_m
	$0 (C > 0.5)$	$B'[1/(2C-1)W]$	$\Delta H_m + \Delta H_{AO}$

2-3. The effect of the ambient atmosphere

In oxides containing a large amount of oxygen vacancy, the oxygen-ion conductivity is independent on oxygen partial pressure (PO_2) due to almost unchanged concentration of the vacancy. However, concentrations of electronic defects change markedly with PO_2 and those conductivities become comparable at very high or low PO_2.

At high PO_2 where oxygen is being incorporated into the lattice, defect equilibrium can be expressed as,

$$1/2\ O_2(g) + V_O^{\cdot\cdot} \longrightarrow O_O^{*} + 2h^{\cdot} \qquad (24)$$

where $h^{\cdot}$ represents an electron hole. By applying the law of mass action to Eq.24, we obtain

$$[O_O^{*}][h^{\cdot}]^2/[V_O^{\cdot\cdot}]PO_2^{1/2} = K_1 \qquad (25)$$

when $[V_O^{\cdot\cdot}]$ is large and fixed, Eq.25 can be rewritten using $[h^{\cdot}]=p$ and approximately $[O_O^{*}]=1$ as,

$$p = ([V_O^{\cdot\cdot}]K_1)^{1/2}PO_2^{1/4} \qquad (26)$$

Assuming the constant hole-mobility, the conductivity due to electron holes varies with $PO_2^{1/4}$.

At low PO_2, we can write a similar equation describing the loss of oxygen from the lattice,

$$O_O^{*} \longrightarrow V_O^{\cdot\cdot} + 1/2\ O_2(g) + 2e' \qquad (27)$$

where e' represents an electron. the law of mass action gives next equation assuming the equilibrium constant K_2 and constant $[V_O^{\cdot\cdot}]$,

$$n = (K_2/[V_O^{\cdot\cdot}])^{1/2}PO_2^{-1/4} \qquad (28)$$

Thus, the electron conductivity is expressed as

$$\sigma_e = (e\mu_e)(K_2/[V_O^{\cdot\cdot}])^{1/2}PO_2^{-1/4} \qquad (29)$$

Experimental set-up for the PO_2 dependence of conductivity used in the present study is shown in Fig.1.

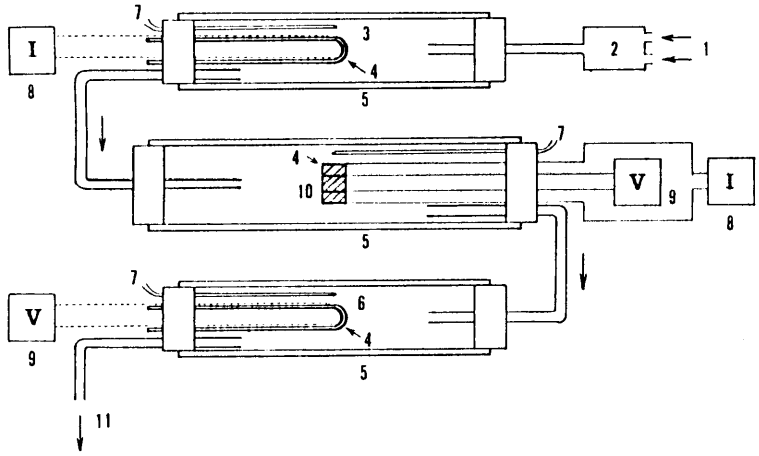

Fig. 2-1. Experimental set-up for PO_2 dependence of conductivity.

1:Gas inlet, 2:Gas mixer, 3:Zirconia cell for oxygen pump, 4: Pt paste electrode, 5:Alumina tube, 6: Zirconia cell for PO_2 monitoring, 7: Thermocouple, 8: DC current supply, 9:Voltmeter, 10:Specimen, 11:Gas outlet.

REFERENCES in I-2

1. F. A. Kroeger and H. J. Vink, "Solid State Physics" Vol.3 (F. Seitz and D. Turnbull, eds.), Academic Press, New York, 1956, p.307.
2. R.J. Brook, "Electrical Conductivity in Ceramics and Glass, Part A" (N.M.Tallan ed.) Marcel Dekker, New York, 1974,p.179.
3. J.A. Kilner and B.C.H. Steel, "Nonstoichiometric Oxides" (O. T. Sorenson ed.) Academic Press, New York, 1981, p.233.
4. E.C. Subbarao, "Advances in Ceramics" Vol.3 (A.H. Heuer and L.W. Hobbs eds.) The Am. Ceram. Soc., Ohio, 1981, p.1.
5 J.F. Baumard and P. Abelard, ibid, Vol.12 (A.H. Heuer, N. Claussen, M. Ruhle eds.) 1983, p.555.

I - 3. Some experimental method

3-1. Complex impedance method

The ionic conductivity in polycrystalline specimens contains contributions of grain, grain boundaries and electrodes. The dc methods cannot eliminate the contribution of grain boundaries (and electrodes), and hence this often leads to errors for the analysis of true electrical behavior of the bulk. The spliting can be achieved by use of the complex impedance method.

When resistance R and capacitance C are connected in parallel, total impedance of the circuit is expressed as

$$Z = (1/R + jwC)^{-1} \quad \text{or} \quad Z = R(1 + jw\tau)^{-1} \qquad (1)$$

where w is the circular frequency(= $2\pi f$), τ the relaxation time(or time constant, $\tau = RC$). This impedance can be represented as a semicircle in the complex impedance plane($Z = Z' - jZ''$). An idealized plot for a polycrystalline specimen with partially blocking electrodes is shown in Fig.1a and an equivalent circuit corresponding to the impedance plot is shown in Fig.1b.[1,2] Three semicircles in Fig.1a represent grain resistance/cell capacitance, grain-boundary dispersion and electrode dispersion from high frequencies. They have been identified by a comparison with single crystals and by variations of the length/area ratio and

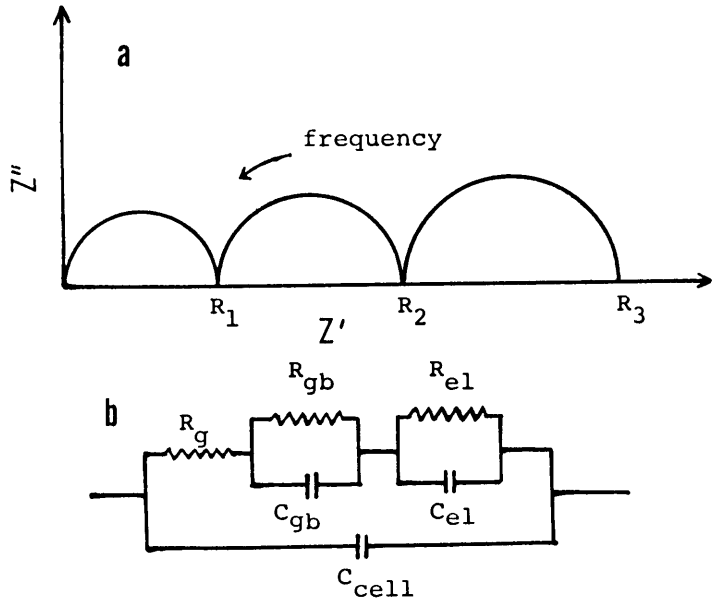

Fig. 3-1. (a) An idealized complex impedance plot for a sintered oxide. (b) An equivalent circuit representing the specimen corresponding to (a).
g : grain(bulk), gb : grain boundary, el : electrode.

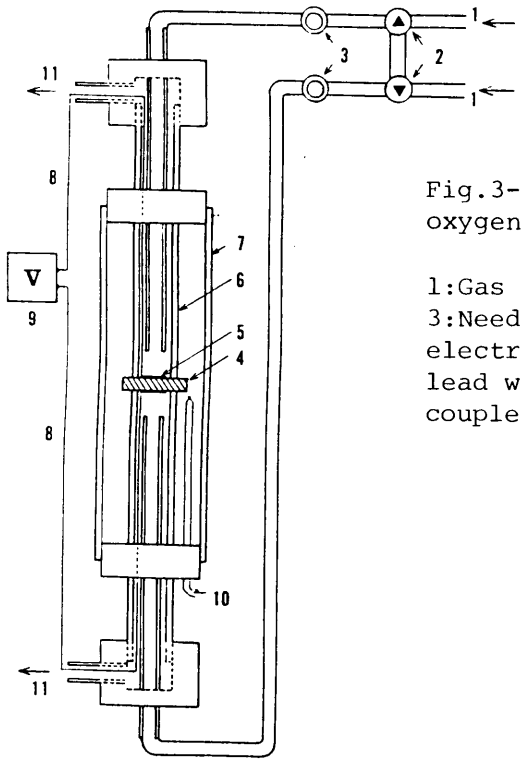

Fig.3-2. Construction of the oxygen concentration cell.

1:Gas inlet, 2:Three-way stop cock, 3:Needle valve, 4:Specimen, 5:Pt electrode, 6,7:Alumina tube, 8: Pt lead wire, 9:Voltmeter, 10,Thermo-couple, 11:Gas outlet.

oxygen partial pressure.[1] Accordingly, the intercepts on the real axis of Fig.1a, R_1, R_2, R_3, are related to the equivalent circuit as $R_1 = R_g$, $R_2 = R_g + R_{gb}$, $R_3 = R_2 + R_e$ (2)
For the dc methods, the measured resistance corresponds to R_2 for 4-probe and R_3 for 2-probe dc method.

These semicircles will be well-defined provided that their relaxation times are well separated. The relaxation times in an equal level allow an extensive overlap of semicircles. In addition, when the relaxation time is not definitive in each dispersion, depression of semicircle can be observed.

3-2. Ionic transference number

When describing a solid in which there are more than one cherge carrier, a useful concept is the transference number for each carrier. The ionic transference number is defined as

$$t_{ion} = \sigma_{ion}/\sigma_{total} \qquad (3)$$

(1) Concentration cell method

The electromotive force E of the next concentration cell

$O_2(PO_2')$,Pt | solid electrolyte | Pt, $O_2(PO_2")$ $(PO_2'>PO_2")$

is given by

$$E = \frac{RT}{4F}\int_{PO_2"}^{PO_2'} t_i \, d \ln PO_2 \qquad (4)$$

Assuming a constant t_i (t_i : average ionic transference number) through the electrolyte, Eq.4 can be rewritten as,

$$E = t_i \frac{RT}{4F} \ln \frac{PO_2'}{PO_2"} \qquad (5)$$

When the idealized emf for pure ionic conductors is defined as E_{th} ($t_i = 1$ in Eq.5, apparent (average) transference number is given by $t_i = E / E_{th}$ (6)
Since the electron conductivity is determined by Eq.29 in I-2-3, we obtain the next equation for ion-electron mixed conductors,

$$t_i = \frac{1}{1 + (PO_2/P\ominus)^{-1/4}} \tag{7}$$

where $P\ominus = (\mu e/\sigma_i)^4 (K/[V_O^{\cdot\cdot}])^2$ (8)

The $P\ominus$ corresponds to an PO_2 at which t_i becomes 0.5 ($\sigma_i = \sigma_e$).[3]
By substituting Eq.7 in Eq.4 and integrating, we obtain

$$E = \frac{RT}{F} \ln \left\{ \frac{PO_2'^{1/4} + P\ominus^{1/4}}{PO_2''^{1/4} + P\ominus^{1/4}} \right\} \tag{9}$$

When the hole conduction is added, emf is given by the next equation assuming PO_2 where $\sigma_i = \sigma_p$ to $P\oplus$,

$$E = \frac{RT}{F} \left[\ln \left\{ \frac{PO_2'^{1/4} + P\ominus^{1/4}}{PO_2''^{1/4} + P\ominus^{1/4}} \right\} + \ln \left\{ \frac{PO_2''^{1/4} + P\oplus^{1/4}}{PO_2'^{1/4} + P\oplus^{1/4}} \right\} \right] \tag{10}$$

Construction of the oxygen concentration cell used in the present study is shown in Fig.2.

(2) Polarization method

When an ion-blocking electrode and a reversible electrode are applied at both sides of a mixed conductor, the ionic current I_i can flow only just after applying voltage and is blocked after reaching an steady-state. In the steady-state, electronic current per unit area can be expressed by the following equation,[4,5]

$$I_e = \frac{RT}{LF} \left[\sigma_n \left\{ \exp\left(\frac{EF}{RT}\right) - 1 \right\} + \sigma_p \left\{ 1 - \exp\left(-\frac{EF}{RT}\right) \right\} \right] \tag{11}$$

where L is the thickness of the sample, q the charge on an electron, E applied voltage and σ_e and σ_p are the electron and hole conductivities at the reversible-electrode side. Accordingly by measuring I_e as a function of E, we can obtain the both electron and hole conductivities in a mixed conductor.[5]

As a simplified method, we can obtain t_i by comparing currents at zero and infinite time after biassing under a fixed voltage as,[6] $t_i = 1 - I(\infty)/I(0)$ (12)
where $I(0)$ and $I(\infty)$ are the currents at zero and infinite time(in a steady state), respectively. Construction of the polarization cell used in the present study is shown in Fig.3.

REFERENCES in I-3

1. J.E. Bauerle, J. Phys. Chem. Solids, 30, 2657 (1969).
2. M.J. Verkerk, B.J. Middelhuis and A.J. Burggraaf, Solid State Ionics, 6, 159 (1982).
3. H. Schmalzried, Z. Elektrochem., 66, 572 (1962).
4. C. Wagner, Z. Elektrochem., 60, 4 (1956), 63, 1027 (1959).
5. J.W. Patterson, E.C. Bogren and R.A. Rapp, J. Electrochem. Soc., 114, 752 (1967).
6. R.W. Vest and N.M. Tallan, J. Appl. Phys., 36, 543 (1965).

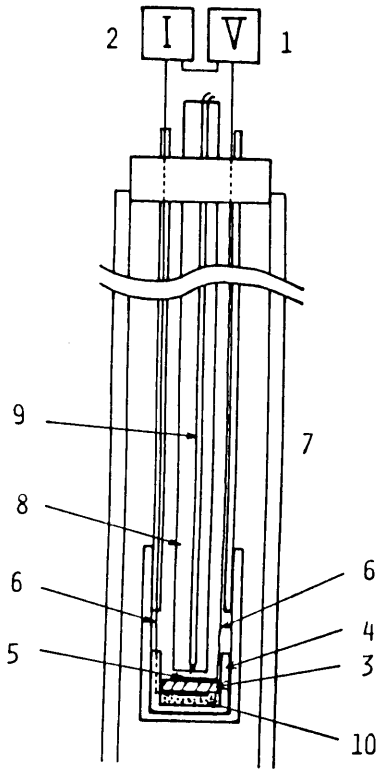

Fig. 3-3. Construction of polarization cell.

1:DC constant power supply,
2:Ammeter, 3:Electrolyte,
4:Quartz glass holder,
5:Gold sputtered electrode,
6:Pt wire, 7:Alumina tube,
8:Alumina rod,
9:Thermocouple,
10:Blocking electrode(In metal).

Chapter II

Electrical Conduction in Bi_2O_3 Polymorphs

II - 1. Polymorphic transformation in pure and Sb_2O_3-doped Bi_2O_3

INTRODUCTION

Bismuth sesquioxide (Bi_2O_3) has four polymorphic forms ; a monoclinic α form stable at low temperatures below 730°C, a cubic δ form stable at high temperatures up to the melting point (825°C), and a metastable tetragonal β form and bcc γ form which appear during cooling of the δ form[1-8]. The appearance of the metastable forms is reported to depend on the highest temperature passed through and the cooling rate[5-8].

Although there are many works on the polymorphic transformation of Bi_2O_3, electrical property of each polymorph has not been investigated in detail, especially for the two metastable forms. In ZnO varistors to which Bi_2O_3 is used as an additive, it is reported that there is a relationship between Bi_2O_3 polymorphs at grain boundaries and the non-linear characteristics[9,10]. Antimony sesquioxide (Sb_2O_3) is known as an additive for ZnO varistors, as well as Bi_2O_3, to improve the non-linear characteristics. However, polymorphs and their transformations in the system Bi_2O_3-Sb_2O_3 is not clear.

Accordingly, for the first step to investigate the electrical properties, changes in resistivity accompanied by the polymorphic transformations were measured for pure and Sb_2O_3-doped Bi_2O_3.

EXPERIMENTAL

Bismuth sesquioxide (99.99 % pure) was mixed with 1 mol% Sb_2O_3, calcined at 700°C for 3 h, and ground. Polymorphic transformation was examined for pure and doped Bi_2O_3 by differential thermal analysis (DTA) using Pt pans and α-Al_2O_3 as a standard. Phase identification was performed with X-ray diffraction on specimens, which were pressed into pellets (10 mm × 2 mm thick) and quenched into water from various temperatures. Specimens for resistivity measurements were prepared by pressing powders at 50 MPa into rectangular bars (10×3×20 mm), sintered at 700°C for 5 h and furnace-cooled. The X-ray diffraction analysis showed that the sintered specimens were all in the α form.

Electrical resistivity was measured by a four-probe dc method at 200° to 800°C in air. Heating and cooling rate during the measurements was 4°C/min.

RESULTS AND DISCUSSION

(1) pure Bi_2O_3

Peaks of DTA are shown in Fig.1. The results are almost same to that reported by Matsuzaki et al.[5,6], i.e. transformations were $\alpha \rightarrow \delta$ form $\rightarrow$ melt and the temperature of $\alpha \rightarrow \delta$ transformation was 730°C. When the δ form was cooled from 750°C, it transformed into the α form directly at 710°C. When cooled from 790°C, transformations were $\delta \rightarrow \beta \rightarrow \alpha$ form at a usual cooling rate (>1.25°C/min) as shown in Fig.1. In case of a slow cooling

rate (0.625°C/min), a gradual endothermic peak appeared at 600-400°C , and γ form was sometimes retained at room temperature. Matsuzaki et al.[5,6] reported the transformations of melt→δ→γ form at a cooling rate of 1°C/min. Accordingly, the gradual peak can be regarded to be of δ → γ transformation. The observed transformations in pure Bi_2O_3 are summarized in Fig.2. Specimens, quenched at any temperatures below the melting point, were all in α form.

Figure 3 shows the resistivity - temperature characteristics. Changes in resistivity were observed at the temperatures of transformations. Amongthem, the change accompanied by α → δ transformation was large, about three orders of magnitude.

(2) Sb_2O_3-doped Bi_2O_3

The DTA peaks are shown in Fig.4. The transformations on heating and on cooling from 750°C were same to those in pure Bi_2O_3. In the case of cooling from 790°C, the δ form transformed into γ form at 620 to 640°C and the γ form was kept down to room temperature. The β form was observed in specimens which were once heated at 790°C and quenched from 650-790°C . The γ and β forms obtained at room temperature transformed into α form and then δ form on heating as shown in Fig.5. Observed transformations are summarized in Fig.6.

The resistivity - temperature characteristics of doped Bi_2O_3 on cooling from 750 and 790°C are shown in Fig.7. A change in resistivity accompanied by δ→γ transformation was about two orders of magnitude and more gradual than that by δ→β transformation in pure Bi_2O_3. Figure 8 shows resistivities of the β and γ forms on heating. Although changes in resistivity with β→α and γ→α transformations were small, changes in activation energy were clearly observed. The activation energy was 1.20-1.31 eV for the β form, 0.81-0.94 eV for the γ form and about 0.5 eV at >350°C and 0.85 ev at <350°C for the α form.

Fig. 1-1.

DTA curves of pure Bi_2O_3 on heating and on cooling from 750°C and 790°C.

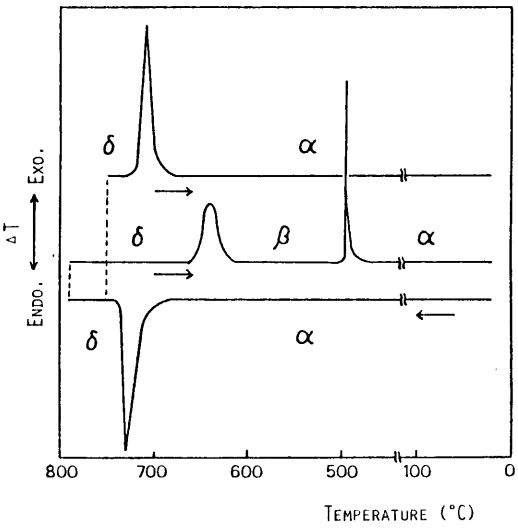

Fig. 1-2.

Polymorphic transformations of pure Bi_2O_3.

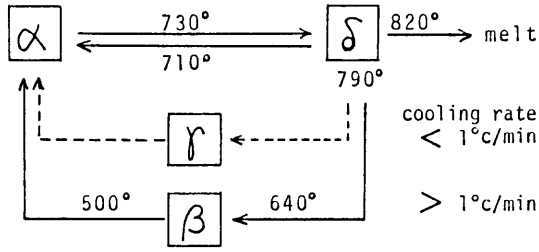

Fig. 1-3.

Resistivity-temperature characteristics of pure Bi_2O_3 on heating and on cooling from 750°C and 790°C.

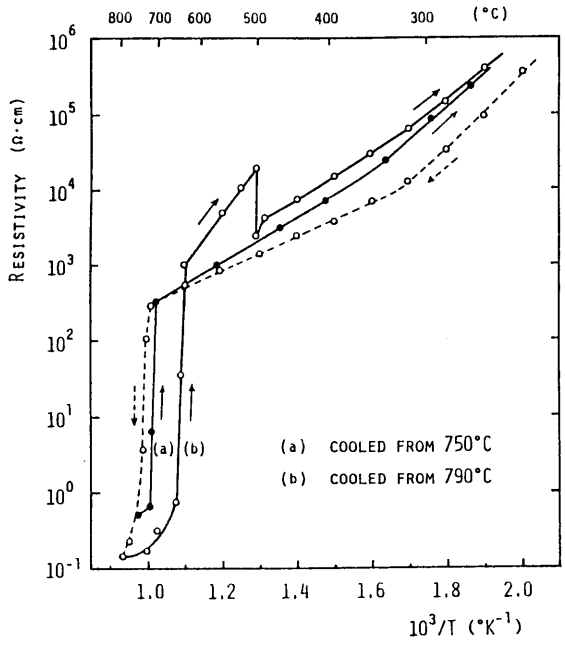

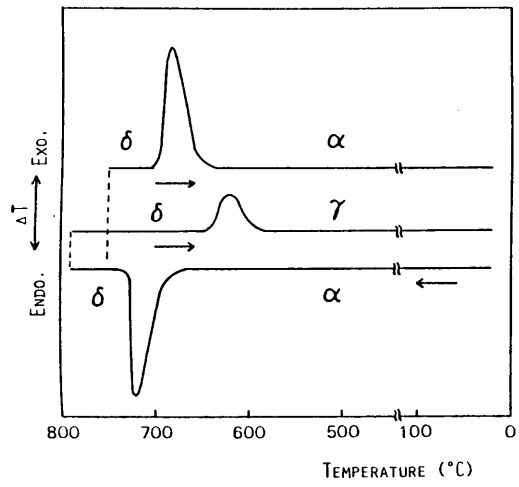

Fig. 1-4.

DTA curves of Sb_2O_3(1 mol%)-doped Bi_2O_3 on heating and on cooling from 750°C and 790°C.

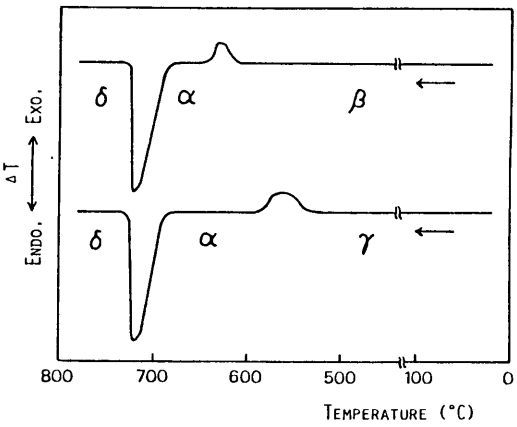

Fig. 1-5.

DTA curves of Sb_2O_3(1 mol%)-doped β- and γ-Bi_2O_3 on heating.

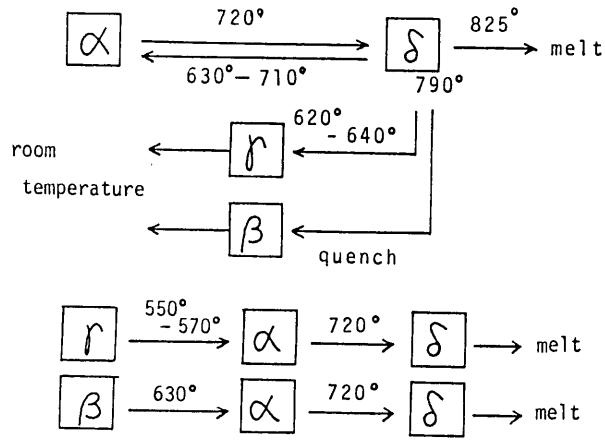

Fig. 1-6.

Polymorphic transformations of Sb_2O_3(1 mol%)-doped Bi_2O_3.

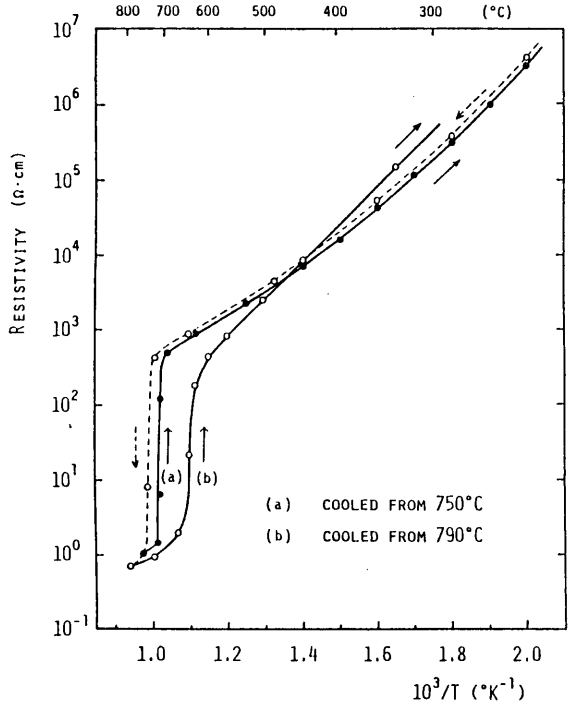

Fig. 1-7.
Resistivity-temperature characteristics of Sb_2O_3(1 mol%)-doped Bi_2O_3 on heating and on cooling from 750°C and 790°C.

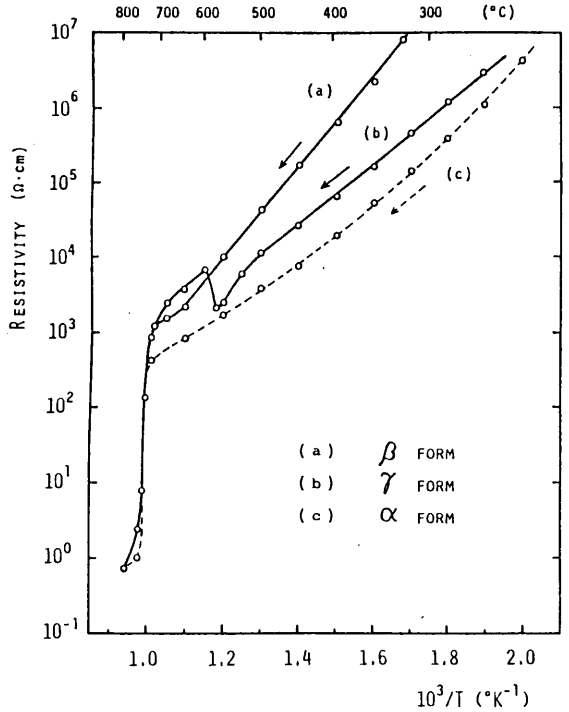

Fig. 1-8.
Resistivity-temperature characteristics of Sb_2O_3(1 mol%) doped β- and γ-Bi_2O_3 on heating.

CONCLUSION in II-1

(1) Metastable β and γ forms were obtained at room temperature with 1 mol% doping of Sb_2O_3, when the δ form was quenched and cooled slowly from temperatures above 790°C, respectively.

(2) The electrical resistivity of pure and doped Bi_2O_3 showed changes in resistivity or changes in activation energy accompanied by polymorphic transformations.

(3) The resistivity of β form was larger than that of γ and α forms at 200 to 500°C. the δ form was with very low resistivity. The activation energy E in the β, γ and α form was $E_\beta > E_\gamma > E_\alpha$.

REFERENCES in II-1

1 W.C. Schumb and E.S.Ritter,J.Am.Chem. Soc.,65, 1055 (1943).

2 E.M. Levin and R.S. Roth, J. Res. Natl. Bur. Standards, 68A, 189 (1964).

3 G. Gattow and H. Schroder, Z.Anorg.Allg.Chem., 318, 176 (1962)

4 G. Gattow and D. Schutze, ibid., 328, 44 (1964).

5 R. Matsuzaki, A. Sofue and Y. Saeki, Nippon-Kagakukai-Shi, 1973, 491.

6 R. Matsuzaki, H. Masumizu and Y. Saeki, DENKI KAGAKU, 42, 578 (1974).

7 J.W. Medernach and R.L. Snyder, J. Am. Ceram. Soc., 61, 494 (1978).

8 H.A.Harwig and A.G.Gerards,Thermochim.Acta,28,121 (1979).

9 A. Iga, M. Matsuoka and T. Masuyama, Jpn. J. Appl. Phys., 15, 1161 (1976).

II - 2. P-type electronic conduction in monoclinic α - Bi_2O_3

INTRODUCTION

Electrical conduction in monoclinic α-Bi_2O_3 has been investigated by only a few workers before 1960's[1-3]. The α-Bi_2O_3 behaves like a p-type semiconductor up to 650°C in air, but there are some indications that it changes over to n-type behavior below 600°C at oxygen partial pressure (PO_2) below 10^{-1} Pa[1-3]. In the p-type region, resistivity is reported to show $PO_2^{-1/4}$ dependence at PO_2 above 10^1Pa.

In the present section, PO_2 dependence of resistivity in pure and Sb_2O_3-doped α-Bi_2O_3 was measured in a wide range of PO_2, in order to compare an ionic conduction in α form to that in other polymorphs.

EXPERIMENTAL

Sintered specimens of pure and Sb_2O_3-doped α-Bi_2O_3 for resistivity measurements were prepared by the same method

described in II-1. The X-ray diffracion analysis showed that the specimens were in α form.

Electrical resistivity was measured at 500°C by a four probe dc method. Oxygen partial pressure (PO_2) was controled by passing Ar-O_2 mixed gas and using a stabilized zirconia cell as an oxygen pump. The PO_2 was monitored by emf of a stabilized zirconia cell.

RESULTS AND DISCUSSION

Figure 1 shows PO_2 dependence of resistivity for pure and doped α form at 500°C. the resistivity increased in proportion to $PO_2^{-1/4}$ down to about 10^{-4}Pa. Below 10^{-4}Pa, resistivity decreased with decreasing PO_2 for pure α form, but it remained almost constant for doped α form. These results suggest that the predominant conduction in α form changes from p-type electronic (hole) to n-type electronic (electron) or ionic conduction at PO_2 of 10^{-4}Pa at 500°C. It is not clear whether the constant resistivity of doped specimen below 10^{-4}Pa is due to ionic or to electron/hole conduction. However, even if the conduction is ionic, the ionic resistivity is two or three orders of magnitude higher than that in Sb_2O_3-doped β- and γ-Bi_2O_3 (see II-3 and 4). Measurement of ionic transference number also suggested the dominant conduction in α form to be electronic (see II-4).

The resistivity of Sb_2O_3-doped specimen was a little higher than that of pure specimen. Since doped Sb^{3+} ions are known to oxidize partly to Sb^{5+} in the host lattice (this oxidation was confirmed in doped β and γ form, see II-3,4), next equation can be assumed to occur;

$$Sb_2O_3 + 2h^{\cdot} \xrightarrow{Bi_2O_3} 2Sb_{Bi}^{\cdot\cdot} + 3O_O^{*} \qquad (1)$$

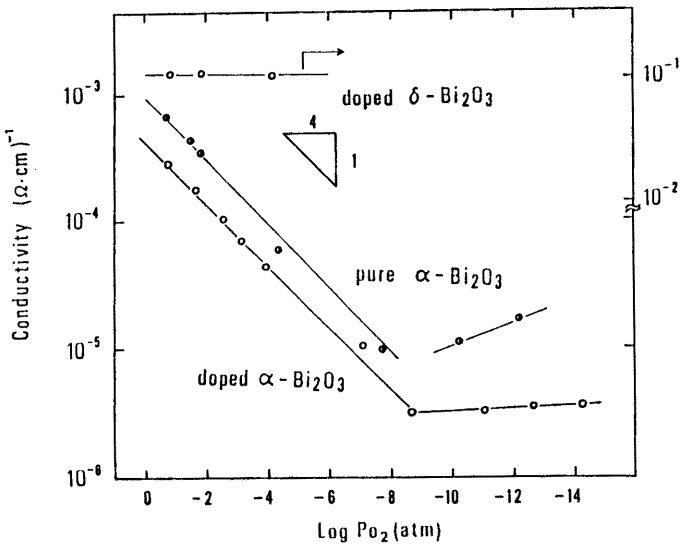

Fig. 2-1. PO_2 dependences of conductivity in pure and doped α-Bi_2O_3 at 500°C.

where $Sb_{Bi}^{\cdot\cdot}$ is a pentavalent antimony ion substituted for a trivalent bismuth ion, O_O^* is an oxygen at a normal site and h' is a hole. the equation brings about a decrease in hole concentration, resulting in an increase of resistivity.

Two defect equilibriums can be postulated to explain the $PO_2^{-1/4}$ dependence of resistivity ($PO_2^{1/4}$dependence of hole concentration) ;

1: cation vacancy model: if incorporated oxygens produce a bismuth vacancy and it release two holes, a defect equilibrium would be

$$3/4\ O_2 = 3/2\ O_O^* + V_{Bi}'' + 2h^{\cdot} \qquad (2)$$

where V_{Bi}'' is a doubly ionized bismuth vacancy. Since the neutral condition is $[V_{Bi}''] = 2[h^{\cdot}]$ where [ ] means concentration, the mass action law gives $PO_2^{1/4}$ dependence of the hole concentration.

2: consumed oxygen vacancy model: if the lattice of Bi_2O_3 has

a large amount of oxygen vacancy, an oxygen incorporated at the vacancy release two holes as,

$$1/2\ O_2 + V_O^{\cdot\cdot} = O_O^{*} + 2h^{\cdot} \qquad (3)$$

where $V_O^{\cdot\cdot}$ is a doubly ionized oxygen vacancy. In the condition of a constant concentration of oxygen vacancy, the mass action law gives $PO_2^{1/4}$ of the hole concentration.
However, it is difficult to determine the dominant reaction only from the present data.

CONCLUSION in II-2

(1) Pure and Sb_2O_3-doped α-Bi_2O_3 showed a p-type electronic (hole) conduction at PO_2 of 10^5 to 10^{-4}Pa at 500°C.

(2) The resistivity in α-Bi_2O_3 in the above PO_2 region showed $PO_2^{-1/4}$ dependence, suggesting presence of bismuth vacancies or excess oxygen vacancies.

REFERENCES in II-2

1. R. Mansfield, Proc. Phys. Soc. (London), B62, 476 (1949).
2. K. Hauffe and H. Peters, Z. Physik. Chem., 201, 121 (1952).
3. C.N.R. Rao, G.V. Subba Rao and S. Ramdas, J. Phys. Chem., 75, 672 (1969).

II - 3. Mixed conduction in tetragonal β- Bi_2O_3

3-1. Stabilization of β- Bi_2O_3 by Sb_2O_3 doping

INTRODUCTION

Of the four polymorphic forms of Bi_2O_3, the tetragonal β form is metastable and exists between 500° and 640°C on cooling δ from above 790°C[1-4]. After Gattow and Schroeder[5] investigated impurity-stabilized β-Bi_2O_3, many studies of impurity additions were undertaken[6-9]. Factors for stabilization of the β form have not yet been clarified whereas those of the metastable bcc γ form have. Aurivillius and Malmlos[10] proposed that the crystal structure of the β form was penetrated by tunnels and that excess oxygen atoms might be accommodated in these tunnels if pentavalent cations were substituted for Bi^{3+}. In the present section, stabilization of β-Bi_2O_3 by Sb_2O_3 doping and oxidation of Sb^{3+} in β-Bi_2O_3 were investigated.

EXPERIMENTAL

Monoclinic α-Bi_2O_3 powder (99.99%), with particles 4 - 10 μm was mixed with a desired amount of Sb_2O_3 (99.99%) calcined in air at 800°C for 2 h in a Pt crucible, and cooled in furnace or

quenched in water to room temperature. The polymorphic forms were examined by X-ray diffraction. The Sb^{3+} and Sb^{5+} concentrations were determined by wet chemical method[12] and TG-DTA.

RESULTS AND DISCUSSION

The polymorphic forms obtained at room temperature are shown in Table 1. Doping antimony > 10 at% gave rise to the cubic δ form with a small amount of unidentified phase, whereas the β form was obtained as a single phase with the doping antimony 4 to 10 at%. Another metastable γ form was obtained with 1 to 3 at% antimony. With the increase of antimony content, the a-axis increased and the c-axis decreased as shown in Fig.1.

Antimony sesquioxide heated in air at 500°C is oxidized to Sb_2O_4, which has a network structure containing equal amounts of Sb^{3+} and Sb^{5+}.[13] However, wet chemical analysis showed that more than 75% of antimony was valenced to Sb^{5+} in the β specimens as shown in Fig.2. Thermal gravimetry-DTA showed that the weight of Bi_2O_3 mixed with 10 mol% Sb_2O_3 increased through two stages, the first at 500°C, where Sb_2O_3 oxidized to Sb_2O_4; and the second at 700 - 750 °C, where the α form transformed to the δ form.

The second increase suggests that the oxidation of Sb^{3+} proceeds with its dissolution into the δ form. The δ form transformed to the β form during cooling without any appreciable weight change. The total increase was 0.4 to 0.5 wt%, which corresponds to the calculated weight increse when 57 to 71 % of Sb^{3+} was oxidized to Sb^{5+}. The atomic percent of Sb^{5+} is in good agreement with that determined by wet chemical analysis, though the value determined from TG was slightly smaller. These results indicate that the tetragonal β-Bi_2O_3 is obtained at room temperature with doping of Sb_2O_3, and that excess oxygen atoms generated by oxidation of Sb^{3+} to Sb^{5+} exist in β-Bi_2O_3. The presence of Sb^{5+} may be an important factor in the stabilization of β-Bi_2O_3, but further investigation is necessary to fully understand the details.

Table 3.1-1 **Polymorphs Observed at Room Temperature in Sintered β-Bi_2O_3 Doped with Sb_2O_3**

Sb_2O_3 (mol%)	Sintering temp. (°C)	Polymorph observed: Water-quenched specimens	Polymorph observed: Furnace-cooled specimens
1–3	800	β*	γ*
4	800	β	β
5–7	830	δ†	β
10	850	δ‡	β‡

*Minor α X-ray diffraction peaks detected in 1 mol% specimens. †Minor β peaks detected in 5 mol% specimens. ‡Unidentified minor X-ray diffraction peaks detected.

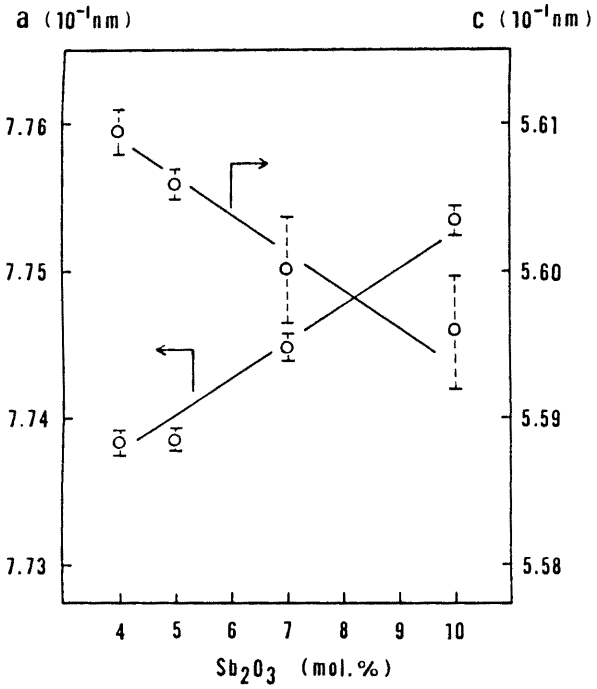

Fig. 3.1-1.

Lattice constants of β-Bi_2O_3 furnace-cooled from 800°C.

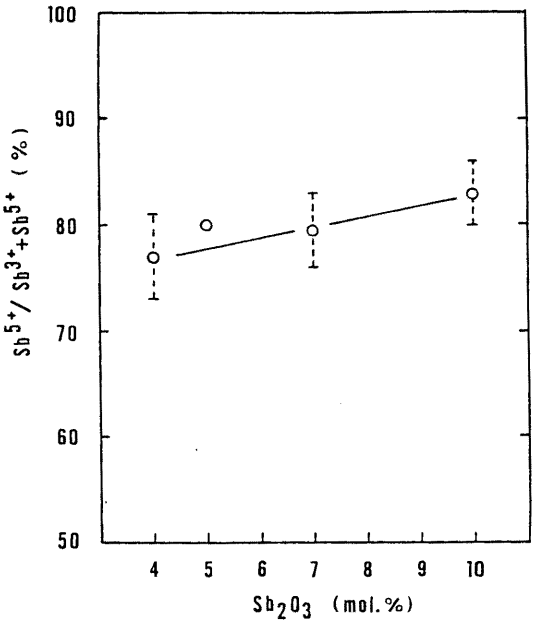

Fig. 3.1-2.

Concentration of Sb^{5+} in β-Bi_2O_3.

3 - 2. Pure β - Bi_2O_3

INTRODUCTION

It has been proposed that β-Bi_2O_3 has a distorted two-dimentional superstructure of the fcc δ-Bi_2O_3 with slight deviations in oxygen atom positions.[6,10,14-15] Since the δ-form is known to show high oxygen-ion conductivity[17-20], the electrical conduction in the β-form is of interest in view of the structural relation. However, few investigations have been reported on the conductivity behavior. The frequency dispersion of impedance reported by Harwig and Gerards[20] suggests an ionic conduction in the β form in air, although the conductivity is several orders of magnitude lower than that of the δ form. In this section, the electrical conduction in pure β-Bi_2O_3 was investigated by measuring conductivity, ionic transference number, and Seebeck coefficient.

EXPERIMENTAL

Powder of α-Bi_2O_3 (99.99 % pure) with particle size of 4-10 μm was pressed into pellets (10 mm in diam. by 3 mm) or rods (5 by 3 by 15 mm) under 54 MPa and sintered at 700°C for 5 h in air. The X-ray diffraction analysis showed that the specimens were in monoclinic α-form. Apparent density of the sintered specimens

was about 85 % of theoretical.

Electrical conductivity was measured by a four-probe dc method. Platinum powder paste was baked at 700°C onto specimens as electrodes. For Seebeck coefficient measurements, two Pt-Pt13Rh thermocouples were attached to two ends of the specimens, and the temperature difference (≃6K) was controled using the temperature gradient in the furnace. Oxygen partial pressure (PO_2) was controled by passing Ar-O_2 mixed gas and using a stabilized zirconia oxygen pump. The PO_2 was monitored by a zirconia cell. Ionic transference number was determined from the emf of an oxygen concentration cell. Platinum paste andPt powder (2000 mesh) was mixed and baked at 700°C in order to get porous electrodes. Air and oxygen gas at 10^5 Pa were used as anode and cathode gas, respectively.

RESULTS AND DISCUSSION

When the specimens (αform at room temperature) were heated up to 790 °C and then cooled, conductivity showed jumps accompanied by polymorphic transformations as shown in Fig.1-3 in sec Conductivity at 500° to 640°C on cooling is of the β form, as described in II-1.

Generally, holes and electrons in oxygen-ion conductors are generated by the following defect equilibriums;

$$1/2\ O_2 + V_O^{\cdot\cdot} = O_O^{*} + 2h^{\cdot} \qquad (1)$$

$$O_O^{*} = 1/2\ O_2 + V_O^{\cdot\cdot} + 2e' \qquad (2)$$

where Kroeger & Vink notation was used. When the concentration of $V_O^{\cdot\cdot}$ is fixed, the mass action law gives $PO_2^{1/4}$ and $PO_2^{-1/4}$ dependences for hole (σ_p) and electron (σ_n) conductivity, respectively, as described in Chap.I.

Figure 1 shows the PO_2 dependence of conductivity in the β form. The conductivity increased with decreasing PO_2, and it was proportional to $PO_2^{-1/4}$ below 10^{-5} atom. This suggests that n-

type electronic conduction is predominant in β-Bi_2O_3 under low PO_2 and oxygen vacancies with a high concentration are contained in the structure of β-Bi_2O_3. Accordingly, the total conductivity σ_t is expressed by the following equation;

$$\sigma_t = \sigma_i + \sigma_p^\circ (PO_2/10^5Pa)^{1/4} + \sigma_n^\circ (PO_2/10^5Pa)^{-1/4} \quad (3)$$

where σ_i is oxygen-ion conductivity, σ_n° and σ_p° are electron and hole conductivity at PO_2 of 10^5Pa, respectively. the measured total conductivity was separated to three conductivities and they are represented in Fig.2 as dotted lines. The full line in Fig.2 is the sum of those three conductivities.

Figure 2 shows temperature dependences of σ_i and σ_n°, calculated from σ_n at PO_2 of 10^5Pa in Fig.2. They are expressed as

$$\sigma_i\ (\Omega\cdot cm)^{-1} = 2.33\times10^7 \exp[-182(kJ/mol)/RT] \quad (4)$$

$$\sigma_n^\circ(\Omega\cdot cm)^{-1} = 4.77\times10^2 \exp[-111(kJ/mol)/RT] \quad (5)$$

where R and T have their usual meanings. It was difficult to obtain an accurate value of σ_p in the PO_2 range measured, but next equation was roughly estimated

$$\sigma_p^\circ(\Omega\cdot cm)^{-1} = 1.37\times10^9 \exp[-224(kJ/mol)/RT] \quad (6)$$

The oxygen partial pressure (Pθ), at which ion and electron conductivities become an equal value, was estimated from Fig.2[21,22]. The Pθ value (Pa) was expressed as

$$\log P\theta = 1.56\times10^4/T - 14.7 \quad (7)$$

The obtained activation energy (182 kJ/mol) for ionic conduction in β-Bi_2O_3 is much larger than that in δ-Bi_2O_3 stabilized by doping of various oxides (60-110 kJ/mol).[17] Table 1 shows structural data for β- and δ-Bi_2O_3. The tetragonal structure of the β form is shortened in a-axis direction and is extended in c-axis direction compared to the ideal structure. The ratio of lattice constant a/c should be $\sqrt{2}$ for the ideal tetragonal structure without a distortion. However, actual a/c is 1.375 ($0.97\sqrt{2}$). Mole volume of β form is also smaller than that of δ form, and it is reported that the volume decreased 2.1 %

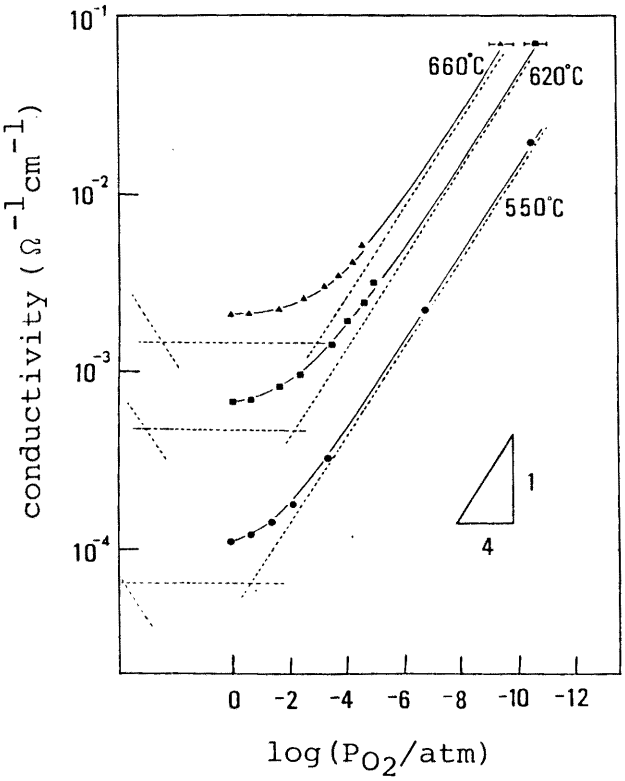

Fig. 3.2-1.
Oxygen partial pressure dependence of conductivity for pure β-Bi_2O_3.
▲, ■, ● : measured conductivity
——— : calculated total conductivity
- - - - : electron, hole or ion conductivity

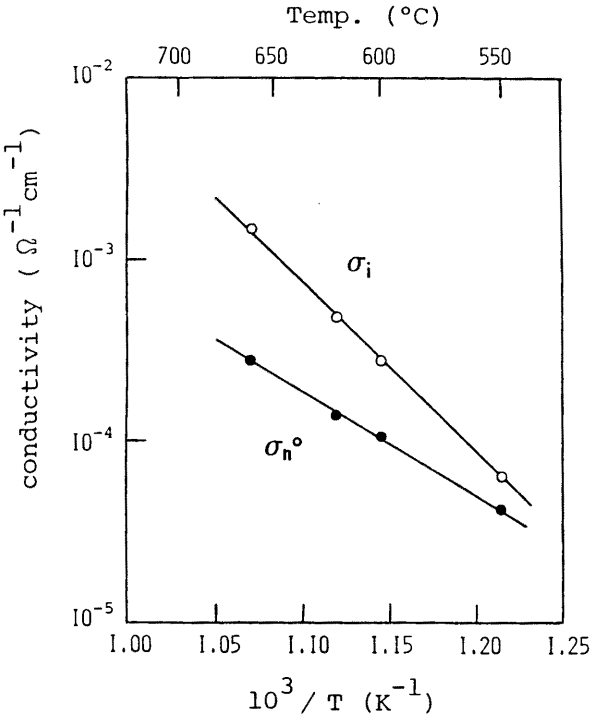

Fig. 3.2-2.
Temperature dependences of ionic conductivity and electron conductivity at 10^5 Pa. (1 atm).

Table 1. Structural data for δ- and β-Bi_2O_3

	δ form		β form
Space group	Pn3m	Fm3m	$P42_1c$
Lattice parameters(A)	a=5.525	a=5.66 (750°C)	a=7.742 c=5.631
Shortest interatomic distances(A)	Bi-O 2.40 O-O 2.76	Bi-O 2.45 O-O 2.83	Bi-O 1.96-3.04 O-O 2.73-3.04
Z(number of chemical formula)	2	2	4
ref.	16	5	10

accompanied by δ to β transformation.[1] The shortest interatomic distances are constant in δ form, but they are varying in a wide range in β form. From these structural data, it is assumed that the structure of the β form is dense (closer packing of atoms) and has unequivalent oxygen sites, in comparison with a open structure with equivalent oxygen sites of the β form. The high activation energy for oxygen-ion conduction in the β form would be due to the distorted tetragonal structure. In addition, Aurivillius pointed out that there exist tunnels in the structure of β form made by ordering of oxygen vacancies in the <001> direction.[10] Such a structure has a possibility for an anistropic conduction, resulting in an increase in activation energy and a decrease in conductivity for polycrystalline specimens. Electrical measurements for single crystals would be required to clarify the anistropic conduction behavior.

In the case for ion-electron mixed conduction, the emf E of oxygen concentration cell is expressed as the next equation,

$$E = \frac{RT}{F} \ln \left\{ \frac{P_{O_2}^{1/4} + P_{\ominus}^{1/4}}{P_{O_2}'^{1/4} + P_{\ominus}^{1/4}} \right\} \qquad (8)$$

In the case for mixed conduction of ion, electron and hole, the

emf is represented as the next equation ;

$$E = \frac{RT}{F}\left[\ln\left\{\frac{PO_2'^{1/4} + P\ominus^{1/4}}{PO_2''^{1/4} + P\ominus^{1/4}}\right\} + \ln\left\{\frac{PO_2''^{1/4} + P\oplus^{1/4}}{PO_2'^{1/4} + P\oplus^{1/4}}\right\}\right] \quad (9)$$

where $P\oplus$ is the PO_2 at which ion and hole conductivities are equal.

Figure 3 shows average transference numbers t_i in α, β and δ forms. Line (I) indicates t_i calculated with Eqs.7 and 8, and (II) calculated with Eqs.7, 9 and $P\oplus$ values estimated from Eqs.4 and 6. The measured t_i in the β form was in the range of 35 - 65 %, and found to be close to the values of line (II) calculated taking both electron and hole conductivities into account.

Figure 4 shows PO_2 dependences of Seebeck coefficient Q in the β form at 615°C. The sign of Q was positive at PO_2 of 10^5Pa, but it converted to be negative just below 10^5Pa. This implies a change of major charge carrier from positive species (oxygen vacancy or hole) to negative one (electron) with decreasing PO_2. When electron is only charge carrier, Q is expressed as the next equation[23];

$$Q = -\frac{k}{e}\left(\ln\frac{N_c}{n_e} + A\right) \quad (10)$$

where N_c is the number of state, n_e electron concentration and A constant associated with energy transport. Equation 10 can be rewritten as a function of n_e, as ;

$$eQ/2.303k = \log n_e + \text{const.} \quad (11)$$

At below 10^0 Pa, the left term of Eq.11 increased with decreasing log PO_2 with a slope of about -1/4, as shown in Fig.4. This suggests that the electron concentration increases in proportion to $PO_2^{-1/4}$. This result is in a good agreement with the PO_2 dependence of conductivity under low PO_2.

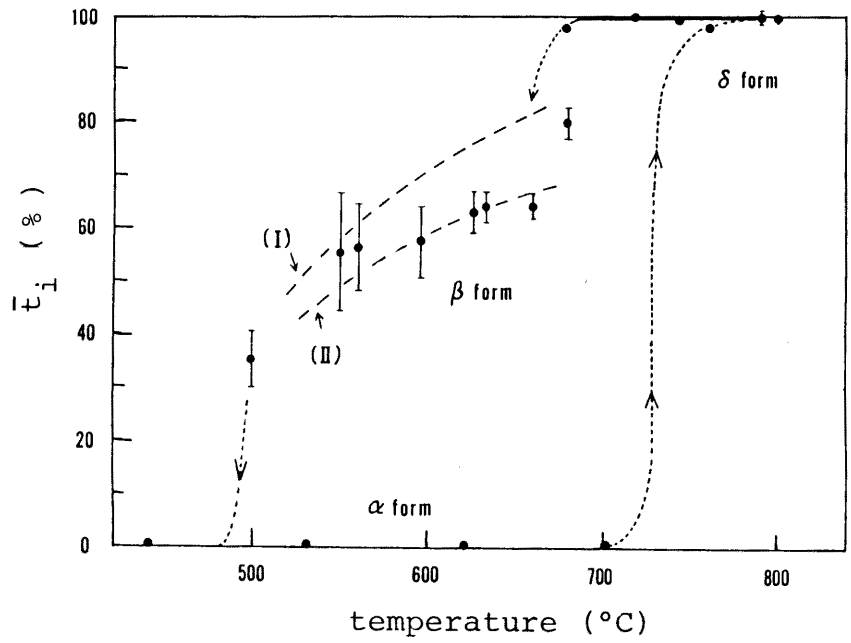

Fig. 3.2-3.

Temperature dependence of average ionic transference number $\bar{t}_i$.
(I),(II) : calculated with the equation (8),(9).

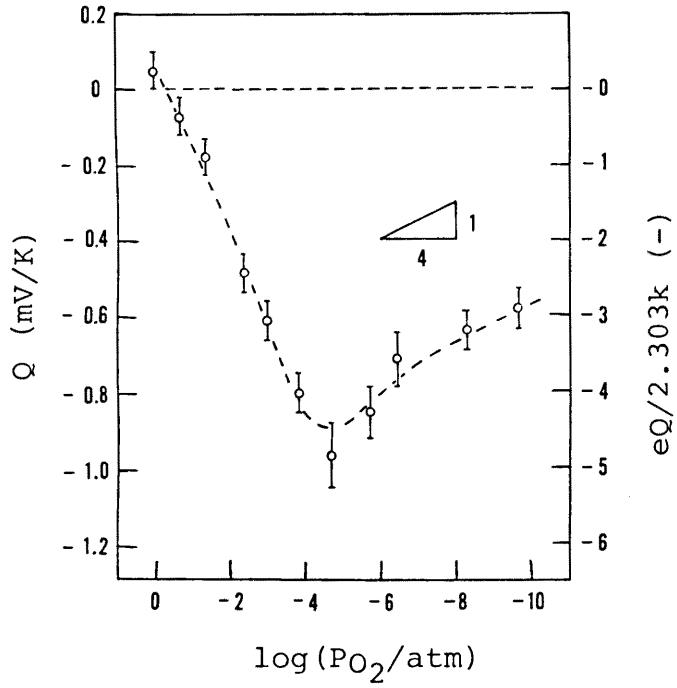

Fig. 3.2-4.
Oxygen pressure dependence of Seebeck coefficient Q of β-Bi_2O_3 at 615°C.

3 - 3. Sb_2O_3-doped β - Bi_2O_3

INTRODUCTION

In the last section, the pure β form was found to show an ionic and electronic mixed conduction where the electron conduction was predominant below the oxygen partial pressure (PO_2) of 10^0 Pa. As for the doped β form, high ionic transference numbers of more than 85% for the systems Bi_2O_3-Y_2O_3 and Bi_2O_3-MoO_3 at high PO_2 were reported.[24,25] However, the conduction mechanism in the doped β form still remains obscure. It was described in II-3-1 that the β form was stabilized by doping with Sb_2O_3 and more than 5% of the Sb atoms exhibited a valence of 5+ in the β specimens. In the present section, the electrical conduction in β-Bi_2O_3 doped with Sb_2O_3 was investigated.

EXPERIMENTAL

The powders of α-Bi_2O_3 and Sb_2O_3 (both 99.99%) were mixed, calcined in air at 730°C for 2 h in a Pt crucible, finely ground, and pressed into pellets (10 mm in diam. by 3 mm) or rods (5 by 3 by 10 mm) under 54 MPa. The pressed bodies were sintered for 5 h in air and then furnace-cooled or water-quenched. The sintering

temperature was 800°C for 1 - 4 mol% Sb_2O_3 and 830°C for 5 - 10 mol% Sb_2O_3. The polymorphic forms were identified by X-ray diffraction(XRD).Electrical conductivity was measured by two-probe ac method at a frequency of 10kHz and by a four-probe dc method. The conductivities by both methods agreed within experimental error. Baked platinum paste was used as electrodes.

The Seebeck coefficient and ionic transference number was determined by the methods described in II-3-2.

RESULTS AND DISCUSSION

Beta Bi_2O_3 was obtained in specimens with 1 - 4 mol% Sb_2O_3 by quenching and in specimens with 4 - 10 mol% Sb_2O_3 by furnace-cooling, as shown in Table 1 in II-3-1. The apparent densities were 81 to 84 % of theoretical for the water-quenched specimens and 88 to 92 % for the furnace-cooled specimens. The lattice parameters changed monotonically with the Bi_2O_3 content, as reported in II-3-1.

The temperature dependence of the electrical conductivity for β-Bi_2O_3 doped with 4 to 10 mol% Sb_2O_3 on heating in air is shown in Fig. 1. High-temperature XRD confirmed that abrupt changes of the conductivity at about 635 ° and 710°C resulted from polymorphic transformation into the α and δ forms, respectively. Apparent activation energies were about 95 - 105 and 80 kJ/mol above and below 350 °C, respectively. The composition dependence of conductivity will be discussed in detail later.

For the water-quenched β specimens, the conductivities were about one order of magnitude lower than those of the furnace-cooled specimens. The conductuvity shows a density dependence, so that the lower conductivities are assumed to be caused by lower densities in the quenched spacimens.

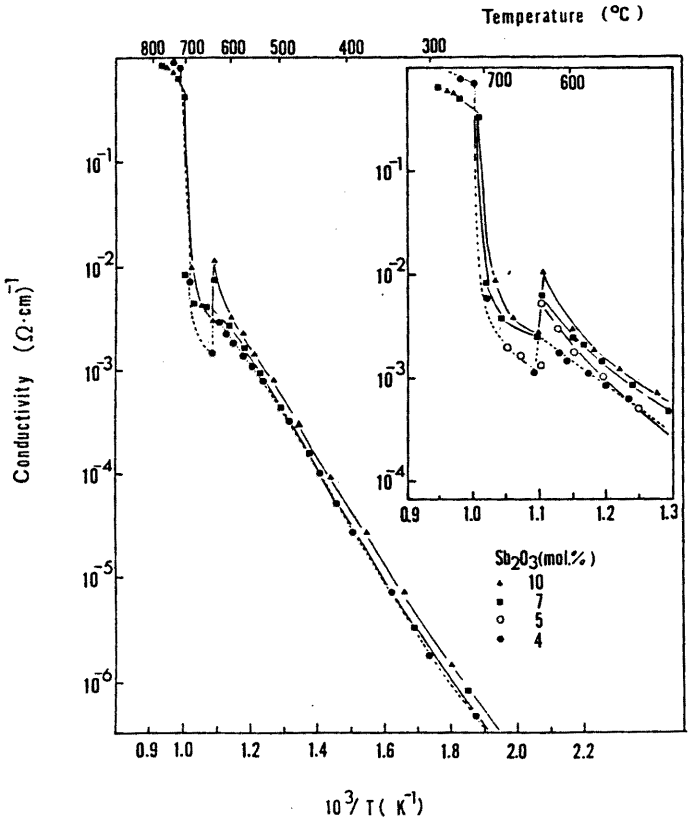

Fig. 3.3-1.

Temperature dependence of conductivity for Sb_2O_3-doped β-Bi_2O_3 heated in air. Insert shows details of high temperature data.

Figure 2 shows the dependence of the conductivity on PO_2 and Sb_2O_3 content at 500 °C. The conductivities showed a mixed conduction behavir, where they increased in proportion to $PO_2^{-1/n}$ (n=positive integer) in the low PO_2 region. The n-type PO_2 dependence (-1/n) decreased gradually from -1/4 to -1/16 with increasing Sb_2O_3 content and the p-type PO_2 dependence become appreciable in the high-PO_2 region in the specimens containing more than 5 mol% Sb_2O_3.

Figure 3 shows the PO_2 dependence of the conductivity for 5 mol% Sb_2O_3-doped β-Bi_2O_3 at several temperatures. As temperature increased, regions showing the p-type or n-type PO_2 dependence were extended. No morphological changes were found after a direct current of 1 mA was passed through the specimens for several hours. Such change would be expected if transport of

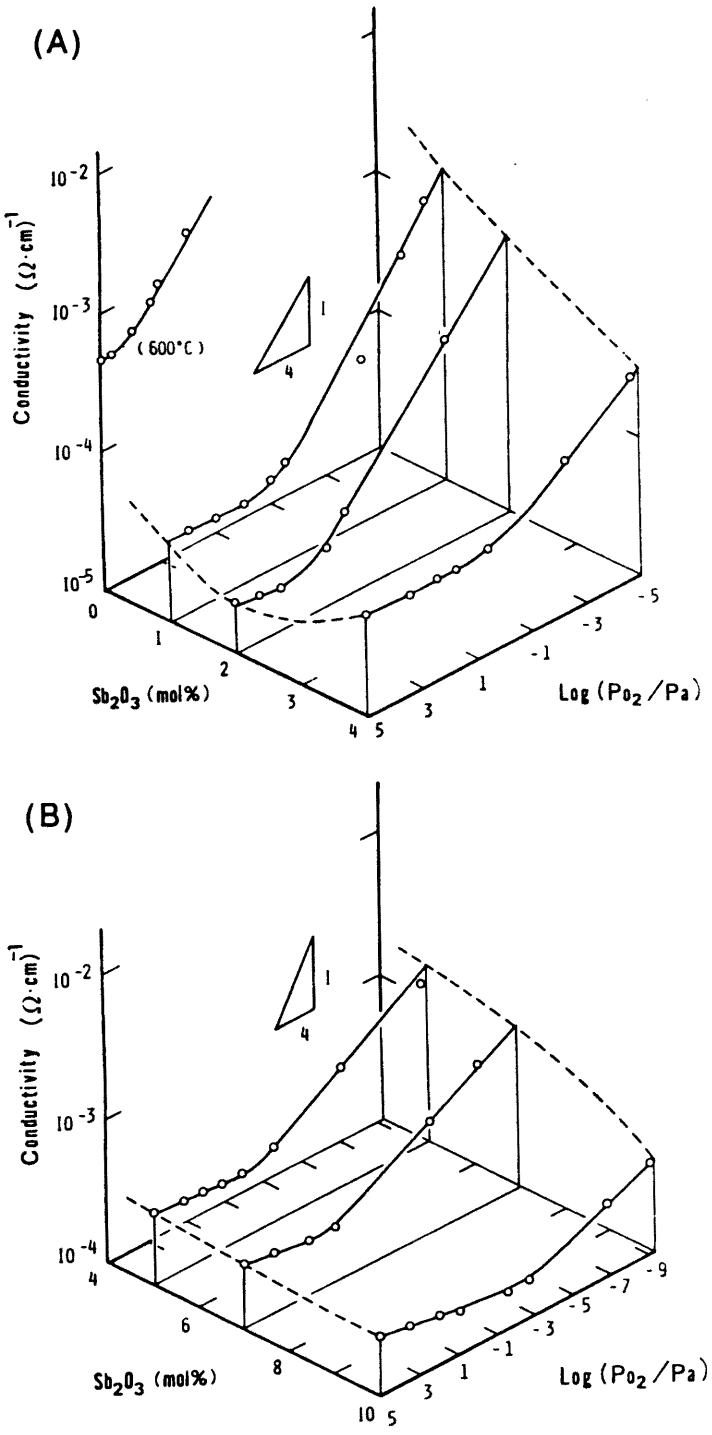

Fig. 3.3-2.
Dependence of conductivity at 500°C on PO_2 and Sb_2O_3 content for β-Bi_2O_3 doped with (A) 0 - 4 mol% Sb_2O_3 and (B) 4 - 10 mol% Sb_2O_3. For metastable pure β-Bi_2O_3, data obtained at 600°C are shown because of polymorphic transformation.

cations occurs. Accordingly, the major contribution to the ionic conductivity is attributed to the transport of oxygen ions.

Ionic transference numbers in 4 to 10 mol% Sb_2O_3-doped β-Bi_2O_3 are shown in Fig.4. Since oxygen gas and air were used correspond to the average transference number for PO_2 between $10^{5.01}$ and $10^{4.33}$Pa. The transference number decreased with an increase in temperature and Sb_2O_3 content. These changes are similar to that expected form the PO_2 dependence of the total conductivity in the high-PO_2 region shown in Figs.2 and 3, if the oxygen-ion conductivity is independent of PO_2 over the measured PO_2 range.

Using the ionic transference numbers and total conductivity in air, the oxygen-ion conductivity can be calculated. The oxygen-ion conductivity at 500°C, its activation energy between 400℃ and 600℃, and the preexponential term are plotted vs the Sb_2O_3 content in Fig.5. The Oxygen-ion conductivity showed a maximun at 4 mol% Sb_2O_3, whereas the activation energy was almost constant although rather lower than that in pure β-Bi_2O_3. The slight difference in activation energy of the total conductivity seems to be due to the contribution of electronic conduction. The ratio of lattice parameters of the tetragonal unit cell (c/a) is also shown in Fig. 5. The tetragonal unit cell of β-Bi_2O_3 is known to be distorted ($c/a > \frac{1}{\sqrt{2}} = 0.707$) [10,14], but the decrease of c/a in Fig. 5 indicates a decrease of this distortion with an increase in Sb_2O_3 content.

Takahashi[17] reported that when a pentavalent cation M^{5+} is substitutedfor Bi^{3+} in the cubic δ form, the oxygen-ion vacancy concentration decreases with the $M_2^2O_5^5$ content according to the expressions:

$$Bi_{2(1-x)}M_{2x}O_{3+2x}V_{1-2x} \qquad (1)$$

where V is the oxygen-ion vacancy. The present authors also found that more than 75% of the antimony atoms were valenced as Sb^{5+} in β-Bi_2O_3 and that excess oxygen atoms were introduced by the oxidation of Sb^{3+} in the specimens. Therefore, the oxygen

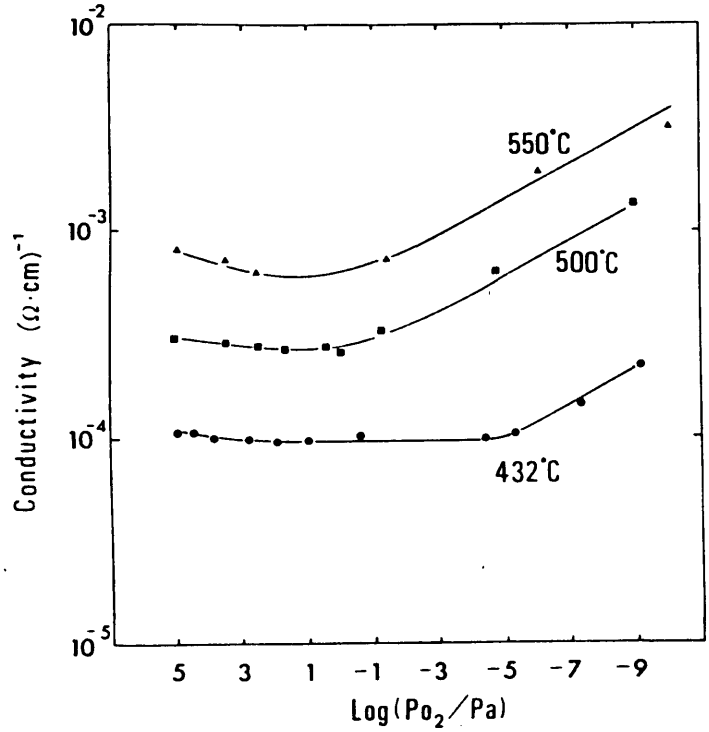

Fig. 3.3-3

Osygen partial pressure dependence of conductivity for β-Bi_2O_3 doped with 5 mol% Sb_2O_3.

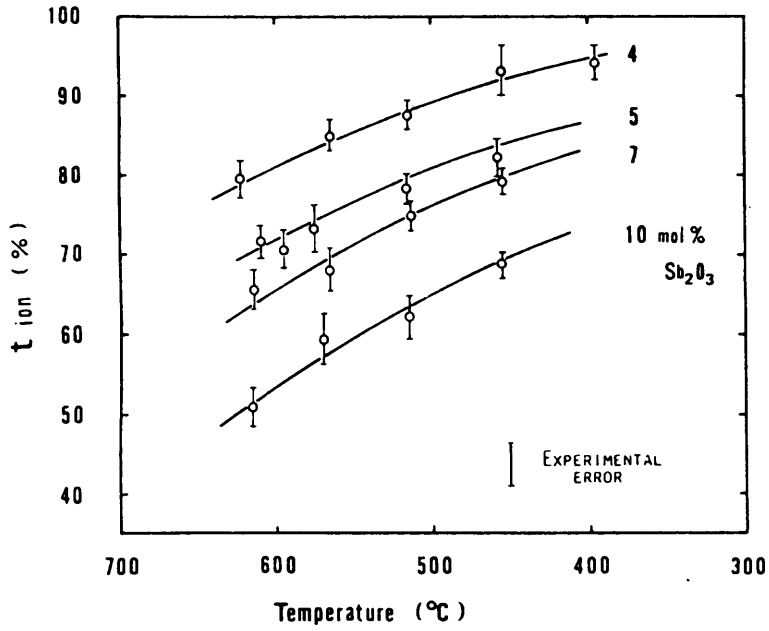

Fig. 3.3-4

Ionic transference numbers in β-Bi_2O_3 doped with 4 - 10 mol% Sb_2O_3 determined from emf of the concentration cell.
[$PO_2" = 10^{5.0}$ Pa, $PO_2' = 10^{4.3}$ Pa]

vacancy concentration should decrease in the tetragonal β-Bi_2O_3 as the antimony concentration increases. When all antimony atoms are oxidized to Sb^{5+} in a 10 mol% Sb_2O_3-doped specimen, the oxygen vacancy concentration must decrease from 25 to 20% of the anion sites. Probably, the introduced oxygen atoms would decrease the distortion in the tetragonal structure.

When the cubic δ form is stabilized by doping with trivalent or pentavalent metal oxides, reportedly the activation[19] energy increases [17-19] or the preexponential term decreases as the dopant content increases.[18] These changes are considered to be due to the association between the substituted cations and the mobile oxygen ions[17,18] or the short-range ordering in "the substituted cation-oxygen coordination units.[14.26] In the tetragonal β form, the decreased structural distortion decreases the activation energy and compensates the effects of the accociation or the ordering. As a result, the apparent activation energy remains unchanged in the stabilized range. Since substantial concentration of the oxygen-ion vacancy is supposed to be decreased not only by the introduced oxygen atoms but by the association or ordering, the preexponential term and the ionic conductivity would be expected to decrease above 4 mol% Sb_2O_3.

To confirm the contribution of oxygen-ion, hole, and electron conduction, the Seebeck coefficient was measuredd as a function of PO_2. The sign of the Seebeck coefficient changed from plus to minus at $10^{-0.5}$Pa for a 5 mol% Sb_2O_3 specimen and at $10^{1.7}$Pa for a 10 mol% Sb_2O_3 specimen, as shown in Fig.6 These PO_2 values agreed with the PO_2 at which the total conductivities of the respective specimens show the minimun in Fig 2. Therefore, this result proves that a change of major charge carrir from positive oxygen vacancy or hole to electron in the β-Bi_2O_3 occurs with decreasing PO_2.

Generally free electrons in oxygen-ion conductors are generated by the following defect equilibrium:

$$O_O^* = 1/2\ O_2 + V_O^{\cdot\cdot} + 2e' \qquad (2)$$

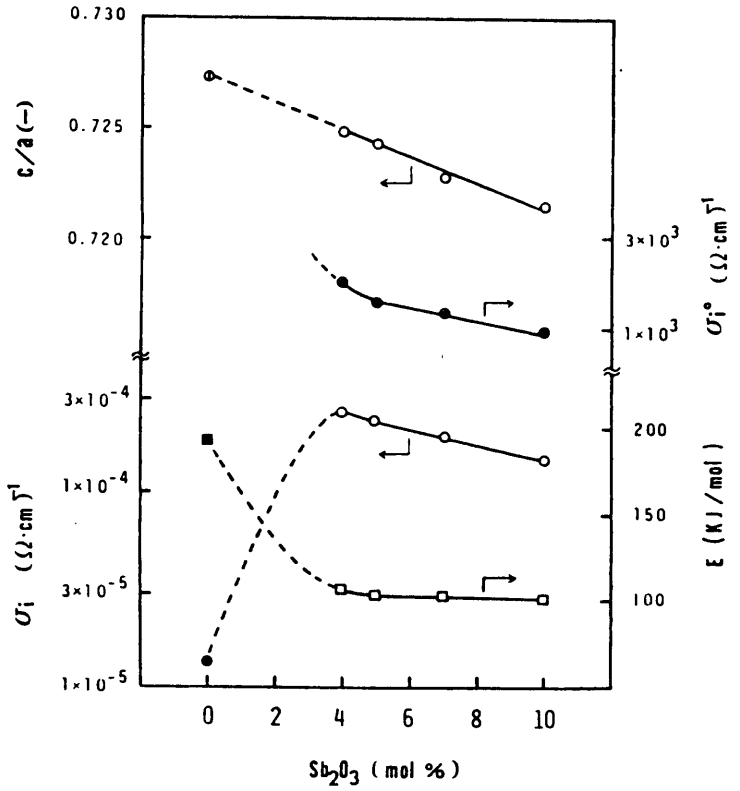

Fig. 3.3-5.
Composition dependence of (○) c/a, (○) oxygen ion conductivity σ_i at 500°C, (●) preexponential term $\sigma_i°$, and (□) activation energy E.

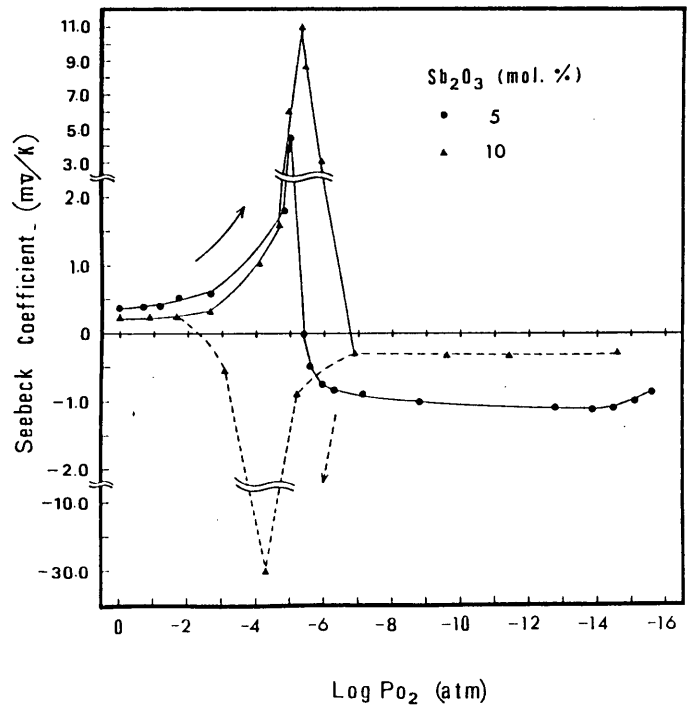

Fig. 3.3-6
Oxygen partial pressure dependence of Seebeck coefficient for β-Bi_2O_3 doped with (●)5 mol% and (▲)10 mol% Sb_2O_3.

In the presence of many oxygen vacancies, the mass action law gives the $PO_2^{-1/4}$ dependence for electron conductivity. Equation 2 seems to be reasonable for the specimen with a law antimony concentration due to the $PO_2^{-1/4}$ dependence of conductivity in the low-PO_2 region. However, as the Sb_2O_3 content increased, electron conductivity and its PO_2 dependence decreased in spite of decreassing ionic conductivity at more than 4 mol% Sb_2O_3, suggesting a change in defect equilibrium.

Wet chemical analysis showed that the concentration of Sb^{5+}vs the total antimony atoms were 92 - 94% and 71 - 73% in the 10mol% Sb_2O_3-doped specimen after annealing at 500°C under a PO_2 of $10^{4.33}$Pa (air) and 10^{-9}Pa, respectively.

These results can be understood if the following equilibrium is applied, together with Eq.3 in the low-PO_2 region for the specimen with a high antimony concectration:

$$Sb_{Bi}^{\cdot\cdot} + 2e' = Sb_{Bi}^{*} \qquad (3)$$

where Sb_{Bi}^{*} and $Sb_{Bi}^{\cdot\cdot}$ are trivalent and pentavalent antimony ions substituted for trivalent bismuth ions, respectively. Equation 3 corresponds to the consumption of the electrons for partial reduction of the pentavalent antimony ions. After sintering in air, most of antimony ions are pentavalent as demonstrated by wet chemical analysis. It is probable that, as the antimony concentration increases, electrons generated by reaction 2 at a low PO_2 would be more freely consumed by reaction 3, resulting in a decreae in electron conductivity. If equilibria 2 and 3 shift to the right equivalently at any PO_2, the electron concentration remains cnstant.

On the other hand, the hole conductivity appeares to increase slightly with increasing antimony concentration. However, the increase in hole conductivity is too small in the measured PO_2 region to give an obvious interpretation.

CONCLUSIONS in II-3

(1) The metastable β form of Bi_2O_3 was obtained by doping Sb_2O_3. The solubility of antimony was 4 to 10 at% in β form, where more than 75 % of antimony atoms were valenced at 5+. The doped form was stable up to 600°C but transformed into α and δ forms at high temperatures.

(2) The total conductivity in pure- and Sb_2O_3-doped β-Bi_2O_3 showed the behavior of mixed conduction, where electron conductivity was predominant below 10^{-2}Pa.

(3) The total conductivity σ_t in pure β-Bi_2O_3 was expressed by next equation ;

$$\sigma_t = \sigma_n^\circ (PO_2/10^5Pa)^{-1/4} + \sigma_p^\circ (PO_2/10^5Pa)^{1/4} + \sigma_i$$

where σ_i, σ_n° and σ_p° are oxygen ion, electron and hole conductivities at 10^5Pa, respectively. Activation energy for the ion and electron conduction was 182 and 111 kJ/mol, respectively. The oxygen partial pressure Pθ, at which the ion and electron conductivities are equal, was

$$\log(P\theta/Pa) = (1.56\times10^4/T) - 14.7 \quad .$$

(4) The β form doped with 4 mol% Sb_2O_3 showed the highest oxygen-ion conductivity of 2.5×10^{-4} $\Omega^{-1}cm^{-1}$ at 500°C, which was more than one order of magnitude higher than that of pure β form. The activation energy for the ionic conduction in the doped β form was about 100 kJ/mol. The structural distortion (a/c) decreased with increasing Sb_2O_3 content. It is assumed that this decrease in distortion bring about smaller activation energy than that in pure β form. The preexponential term σ_i° decreased

with increasing Sb_2O_3 content. It is probably due to excess oxygen atoms introduced by oxidation of Sb^{3+}.

(5) The electron conductivity and its PO_2 dependence in doped β form decreased with increasing Sb_2O_3 content. In contrast, the hole conductivity slightly increased with Sb_2O_3 content. The decrease of Sb^{5+} concen-tration in heavily doped β form at low PO_2 (10^{-9} Pa) was confirmed by wet chemcal analysis. Electrons are assumed to be consumed by partial reduction of Sb^{5+} at low PO_2.

REFERENCES in **II**-3

1. E.M. Levin and R.S. Roth, J. Res. Natl. Bur. Stand., Sect. A, 68, 189 (1964).
2. R. Matsuzaki, H. Masumizu and Y. Saeki, Denki Kagaku, 42, 578 (1974).
3. H.A. Harwig and A.G.Gerards, Thermochim. Acta, 28, 121(1979).
4. M. Miyayama, M. Takata and H. Yanagida, Yogyo Kyokai Shi, 87, 536 (1979).
5. G. Gattow and H. Schroeder, Z. Anorg. Allg. Chem., 318, 176 (1962).
6. G. Gattow and D. Schuetze, ibid., 328, 44 (1964).
7. E.M. Levin and R.S. Roth, J. Res. Natl. Bur. Stand., Sect. A, 68, 197 (1964).
8. T. Takahashi, T. Esaka and H. Iwahara, J. Appl. Electrochem., 7, 31 (1977).
9. F. Hund, Z. Anorg. Allg. Chem., 333, 248 (1964).

10. B. Aurivillius and G. Malmros, Trans. R. Inst. Technol., Stockholm, 1972, No.291, pp.545.
11. J. W. Medernach and R. L. Snyder, J. Am. Ceram. Soc., 61, 494 (1978).
12. A. Vogel, "Text Book of Quantitative Inorganic Analysis" 4th ed., Longman, London (1978) pp.223.
13. P.S. Gopalakrishnan and H. Manohar, Pramana, 3, 277 (1974).
14. H.A. Harwig, Z. Anorg. Allg. Chem., 444, 151 (1978).
15. H.A. Harwig and J.W. Weenk, ibid., 444, 167 (1978).
16. L.G. Sillen, Ark. Kemi. Mineral. Geol., 12A, 1 (1937).
17. T. Takahashi, H. Iwahara and T. Esaka, J. Electrochem. Soc., 124, 1563 (1977).
18. M. J.Verkerk and A. J. Burggraaf, J. Electrochem. Soc., 128, 75 (1981).
19. H.T. Cahen, T.G.N. Van Den Belt, J.H.W. De Wit and G.H.J. Broers, Solid State Ionics, 1, 411 (1980).
20. H. A.Harwig and A. G. Gerards, J. Solid State Chem., 26, 265 (1978).
21. H. Schmalzried, Z. Elektrochem., 66, 572 (1962).
22. T. H. Etsell and S. N. Flengas, J. Electrochem. Soc., 119, 1 (1972).
23. J.M. Wimmer, I. Bransky, "Electrical Conductivity in Ceramics and Glass", Part A, Marcel Dekker, New York (1974) pp.290.
24. T. Takahashi, H. Iwahara and T. Arao, J. Appl. Electrochem., 5, 187 (1975).
25. T. Takahashi, T. Esaka and H. Iwahara, ibid., 7,31 (1977).
26. A. J.Burggraaf, T. van Dijk and M. J. Verkerk, Solid State Ionics, 5, 519 (1981).

II - 4. Ionic and mixed conduction in bcc γ - Bi_2O_3

4-1. Nonstoichiometric γ- $6Bi_2O_3 \cdot SiO_2$

INTRODUCTION

Among the four polymorphs of pure Bi_2O_3, body-centred cubic (γ) form is metastable but can be stabilized by the addition of small amounts of dopant oxides to form the sillenite group of compounds $6Bi_2O_3.MO_2$.[1-4] The bcc $6Bi_2O_3.SiO_2$, a typical sillenite compound, is stable up to 900°C (melting point)[2] and is known to show strong piezoelectric and electro-optic effects and high photoconductivity[5-7]. Hence it is expected to be well suited for photographic and optical wave guide devices.

The electrical conduction of bcc $6Bi_2O_3.SiO_2$ single crystal is reported to be p-type electronic at room temperature and to have very little contribution from oxygen ionic trasport at high temperatures[5,8]. However, The conduction mechanism for sintered or nonstoichiometric bcc $6Bi_2O_3.SiO_2$ is not clear. It is of interest in view of the ionic conduction which is known to be significant for cubic Bi_2O_3 solid solutions[9,10].

In this section, the electrical conductivity and ionic

transference number of sintered bcc $6Bi_2O_3.SiO_2$ was measured, and the conduction mechanism was discussed on the basis of deviation in cationic composition.

EXPERIMENTAL

The raw materials were Bi_2O_3 and SiO_2 (both 99.99% pure). The powders were mixed with a molar ratio of 6:1, melted at 1000 °C in a platinum crucible and quenched to room temperature in air. The quenched sample was subsequently anneald at 700 °C for 2 h and furnace-cooled[11]. Powder X-ray diffraction analysis showed the single phase to be the cubic δ form for the quenched sample and the bcc γ form for the annealed sample, respectiely. The lattice parameter of the bcc γ form was 1.010nm, which was in good agreement with the reported 1.0106nm [8].

The samples for the electrical measurements were made by pressing the bcc form powder into pellets or rods under a pressure of 52MPa and sintering in air at 820°C for 2 h. The apparent density of the sintered specimens was about 86 to 88% of the theoretical value. Preparing sintered specimens by a conventional method without the melting stage gave a minor second phase in the bcc form. Polymorphic transformations were examined by differential thermal analysis (DTA).

Electrical conductivity measurements were performed by a four-probe d.c. method using baked platinum paste as electrodes. Ionic transference numbers were determined by a d.c. polarization method. The experimental set-up is shown in I-3. The Seebeck coefficient was measured by the method described in II-3-2. Cationic composition in the compound was determined by atomic absorption spectroscopy of nitric sample solutions and by spectrophotometry using colouration of molybdosilicic acid with silicon[12].

RESULTS AND DISCUSSION

The DTA curves for the quenched sample showed a large exothermic peak at about 380 °C on heating. This peak is attributed to a transformation of the cubic δ form to the bcc γ form. The γ form was retained after cooling from 800 °C to room temperature. Electrical conductivity of bcc $6Bi_2O_3.SiO_2$ against the reciprocal of the absolute temperature is shown in Fig.1. Data for a single crystal[8] are also shown in Fig.3. The conductivity of the sintered specimen is higher than that of the single crystal and shows an abrupt increase above 700 °C. A similar phenomenon was presented for the bcc $6Bi_2O_3.PbO$ compound [8]. Probably this abrupt increase of condctivity would be due to the highly conductive cubic δ form partially transformed from the bcc γ form, as in the case of $6Bi_2O_3.PbO$.

The dependences of conductivity on oxygen partial pressure (PO_2) for bcc $6Bi_2O_3.SiO_2$ at several temperature are shown in Fig. 2. The PO_2 dependence showed a behaviour of mixed conduction where the n-type PO_2 dependence in the low PO_2 region was $PO_2^{-1/4}$. The contributions of p-type and n-type electronic conduction increased with increasing temperature.

Ionic transference numbers measured by the polarization method are shown in Fig.3. In the present study, the applied voltage was controlled to change the oxygen activity at the blocking electrode to give an activity ratio across the specimen of 1/10 (30 to 43 mV) so that the measured transference numbers correspound to the average value for Po_2 between $10^{4.33}$ (air) and about $10^{3.3}$Pa. The transference number decreased with increasing temperature, which is a similar tendency to that expected from the PO_2 dependences of the conductivity in the high PO_2 region. After the polarization measurements, morphological changes in the specimens were not found; those would be expected if charge transport by cations occurred.

The PO_2 dependence of the Seebeck coefficient at 700°C is

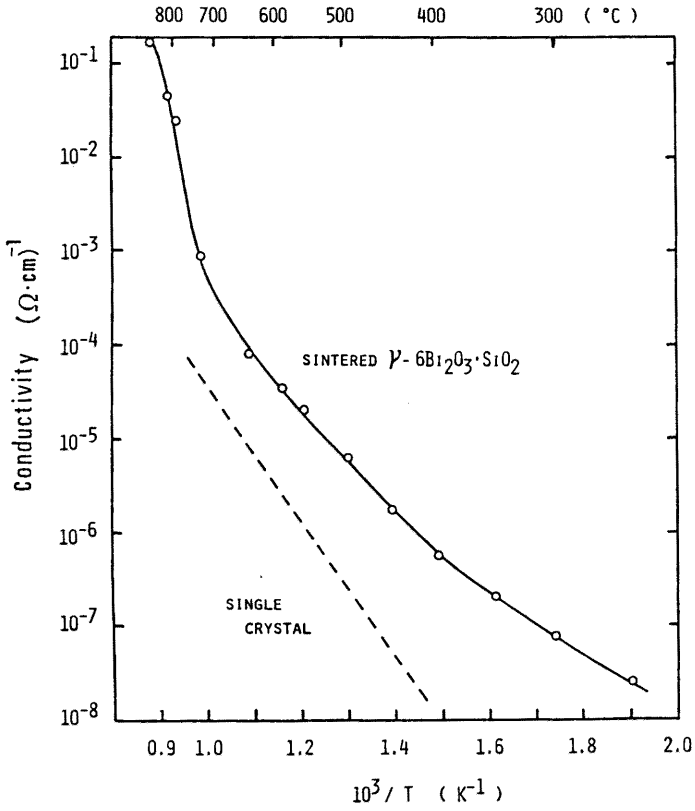

Fig.4.1-1
Conductivity in air for sintered- and single crystal γ-$6Bi_2O_3 \cdot SiO_2$.

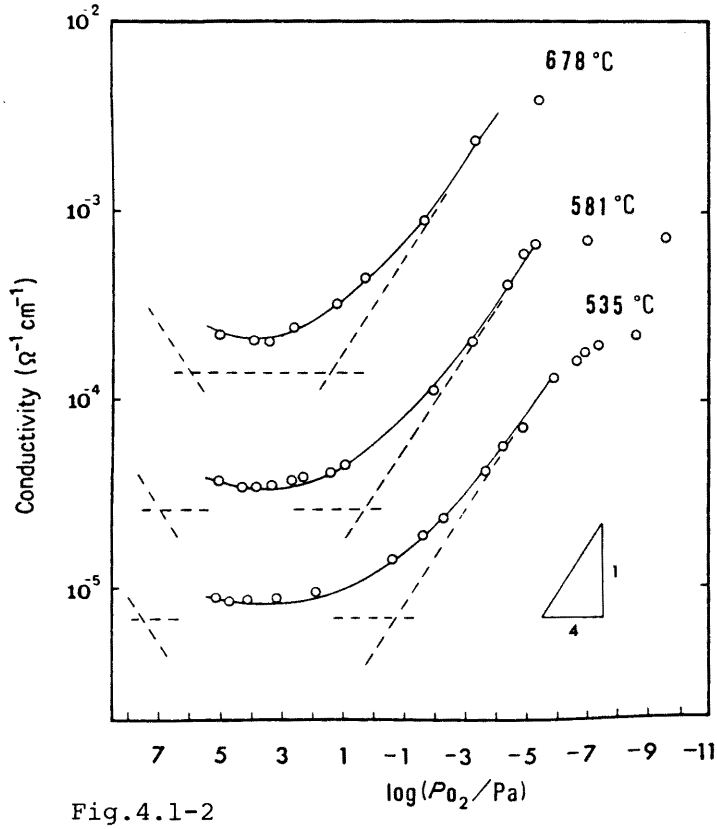

Fig.4.1-2
PO_2 dependence of conductivity for sintered γ-$6Bi_2O_3 \cdot SiO_2$.
----- : separate ion, hole and electron conductivity,
——— : sum of the conductivity.

shown in Fig. 4. The sign of the Seebeck coefficient changes from plus to minus at 10^3 Pa., Which is very close to the PO_2 at the minimum of the conductivity shown in Fig. 2. Therefore, this result proves the change of the major charge carrier from the positive hole or oxygen vacancy to the electron with decreasing PO_2.

Composition analysis in the sintered spesimens showed that the bismuth concentration was almost equal to the theoretical value, whereas the silicon concentration was slightly less than the theoretical value. The atomic ratio Si/Bi (theoretical value 1/12) was $(0.95 \pm 0.02)/12$ from atomic absorption spectroscopy and $(0.93 \pm 0.01)/12$ from spectrophotometry. These deviations are assumed to be caused by adsorbed water in the starting SiO_2 powder or to imperfect reaction of SiO_2 with Bi_2O_3. When SiO_2 is left unreached in the specimens it cannot be detected due to its insolubility in acid water. Probably, the partial polymorphic transformation above 680°C shown in Fig.1 would aries from this deviation in composition.

Generally, holes and electrons in oxygen ion conductrs are generated by the following defect equilibriums;

$$1/2\ O_2 + V_O^{\cdot\cdot} = O_O^{*} + 2h^{\cdot} \qquad (1)$$

$$O_O^{*} = 1/2\ O_2 + V_O^{\cdot\cdot} + 2e' \qquad (2)$$

When the concentration of oxygen vacancy is fixed by a charge compensation for introduced impurities or a devitation in cationic composition, such as $2[V\ddot{o}]=4[V_{Si}''''']$ for a neutrality condition, the mass action law gives the PO_2 dependences of $PO_2^{1/4}$ and $PO_2^{-1/4}$ for hole and electron conductivity, respectively. Even if holes are generated according to the following equilibrium:

$$1/2\ O_2 = O_i'' + 2h^{\cdot} \qquad (3)$$

where O_i'' is an interstitial oxygen ion, hole canductivity would show the $PO_2^{1/4}$ dependence in the presence of oxygen vacancies with a fixed concentration[13], since an equilibrium between interstitial oxygen ions and oxygen vacancies must also be

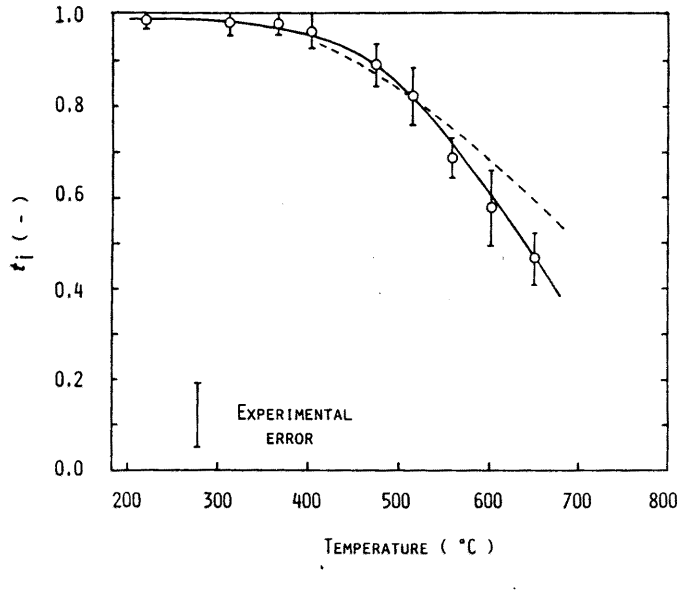

Fig.4.1-3
Temperature dependence of ionic transference number at PO_2 of $10^{4.33}$ (air) to $10^{3.3}$ Pa. Dashed line is calculated value from Eqs. 6 to 8.

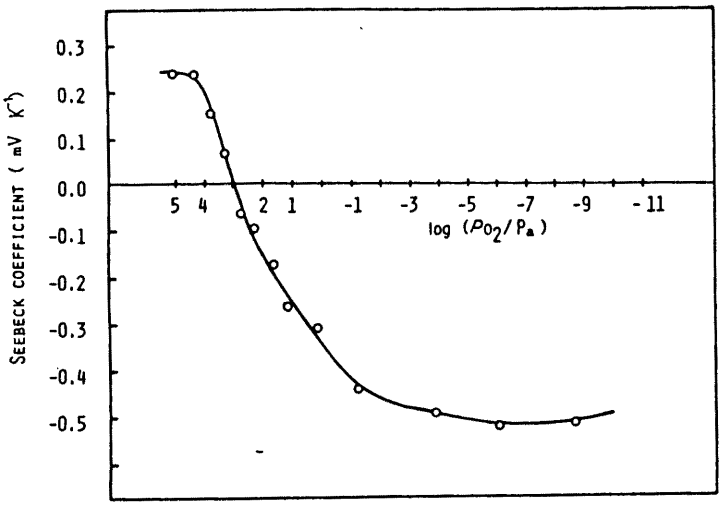

Fig.4.1-4
PO_2 dependence of Seebeck coefficient at 700°C for bcc $6Bi_2O_3 \cdot SiO_2$.

satisfied such that

$$O_O^* = V_O^{\cdot\cdot} + O_i'' \qquad (4)$$

The electron conductivity in the bcc $6Bi_2O_3.SiO_2$ was proportional to $PO_2^{-1/4}$ as shown in Fig.2. This indicates the ionic conductivity independent of PO_2 and the hole conductivity proportional to $PO_2^{1/4}$, and hence total conductivity can be expressed as;

$$\sigma_t = \sigma_i + \sigma_p^\circ (PO_2/10^5 Pa)^{1/4} + \sigma_n^\circ (PO_2/10^5 Pa)^{-1/4} \qquad (5)$$

where σ_i is the oxygen ion conductivity and σ_p° and σ_n° are the hole and electron conductivity at a PO_2 of 10^5 Pa, respectively. The oxygen ion, hole and electron conductivity at a PO_2 of 10^5Pa, which are separeted from the total conductivity so as to satisfy Eq.5, are shown in Fig.5. Each conductivity can be exprssed in $\Omega^{-1}cm^{-1}$ unit as ;

$$\sigma_i = 4.04\times10^3 \exp[-135(kJ/mol)/RT] \qquad (6)$$

$$\sigma_p^\circ = 1.50\times10^6 \exp[-185(kJ/mol)/RT] \qquad (7)$$

$$\sigma_n^\circ = 6.73\times10^5 \exp[-195(kJ/mol)/RT] \qquad (8)$$

where R and T have their ordinary meanings. The ionic transference numbers calculated using Eqs. 6 to 8 at a PO_2 of 10^5 Pa are also shown in Fig.3. The measured tranference numbers are in good agreement with the calculated numbers although the measured values are somewhat smaller. The polarization method used in the present study assumes that leakage currents and electrode-gas conductance are negligibly small[14]. Actually, those effects cannot be eliminated perfectly and hence these may cause the lower value of the measured transference numbers.

The conductivity of the bcc $6Bi_2O_3.SiO_2$ single crystal measured in air presentd by Kilner et al.[8] is also shown in Fig.5. It has values and an activation energy close to the hole conductivity of the sintered specimens. Kilner et. al. also determined the diffusion coefficient of oxygen using the ^{18}O tracer diffusion profile in the single crystal. An estimated

oxygen ion conductivity from the diffusion coefficient was approximately 3×10^{-10} ($\Omega^{-1}cm^{-1}$) at 500°C, which is much lower than that in the present study.

Since Bi^{3+} ions (0.111nm) are too large to be situated at tetrahedrally coordinated Si^{4+} (0.026nm) sites [15], it is expected from the diviation in cation atomic ratio that silicon vacancies are present in the sintered specimen. Craig and Stephenson[16] have performed X ray analysis on the bcc compounds of $ZnO-Bi_2O_3$ or $Fe_2O_3-Bi_2O_3$ systems and suggested that pentavalent bismuth ions substitute on the tetrahedral sites leaving the electron population constant on each tetrahedral site. However, it is difficult to explain the much increased oxygen ion conductivity either by the substitution of Bi^{5+} ions at tetrahedral sites or by oxygen diffusion through grain boundaries. Furthermore, if the anion sub-lattice is occcupied perfectly, silicon vacancies would dissociate and generated holes, resulting in an increase of hole conductivity. Therefore, Schottky-type defects may be present in the nonstoichiometric specimens and the increased oxygen ion conductivity would be attributed to the silicon and oxygen ion vacancies. Probably the dominant neutrality condition for the defect equilibriums is $2[V_O^{\cdot\cdot}]=4[V_{Si}^{''''}]$, as expected from the PO_2 dependences of conductivity. The existence of silicon and oxygen ion vacancies is proposed also in the single crystals on the basis of optical measurements [17].

Oxygen partial pressures $P_{\oplus}$ and $P_{\ominus}$, at wihch the hole and electron conductivity are equal to the oxygen ion conductuvity, respectively, can be obtained from the PO_2 dependences of conductivity. They are expressed as a function of absolute temperature as;

$$\log(P_{\oplus}/Pa) = (8.50\times10^3/T) - 3.04 \qquad (9)$$

$$\log(P_{\ominus}/Pa) = (-10.8\times10^3/T) + 12.81 \qquad (10)$$

are shown in Fig.6. Fig.6 is also a semiquantitative diagram of dominant conduction mechanisms in the nonstoichiometric bcc $6Bi_2O_3.SiO_2$ in the present study.

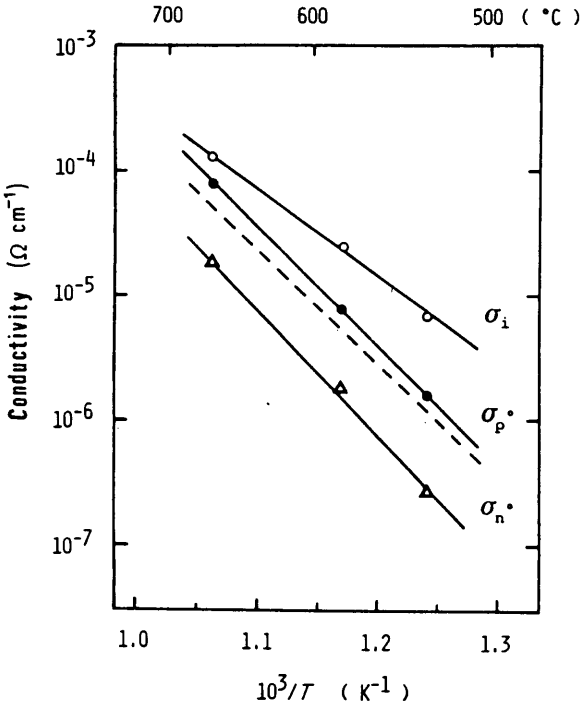

Fig.4.1-5
Temperature dependences of oxygen ion (σ_i), hole ($\sigma_p°$) and electron ($\sigma_n°$) conductivity at PO_2 of 10^5 Pa. Dashed line shows electronic conductivity in single crystal in air.8)

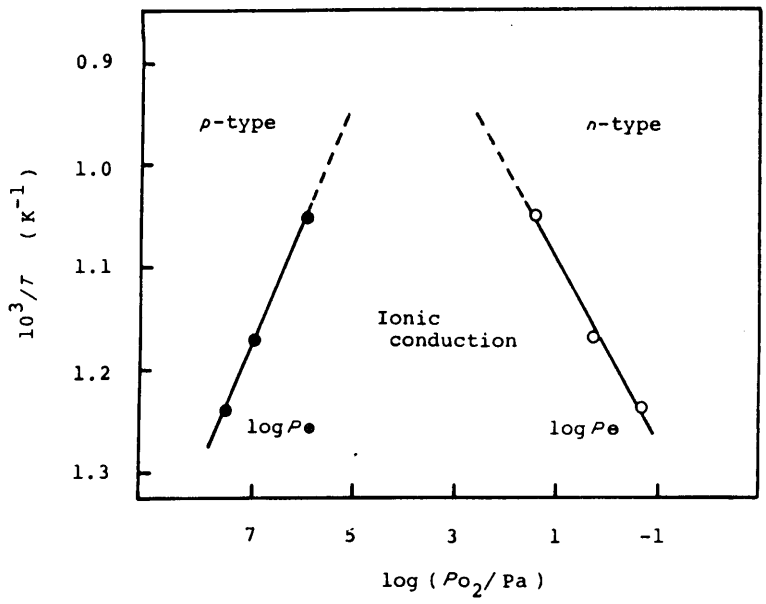

Fig.4.1-6

Log $P_⊕$ and log $P_⊖$ against 1/T for sintered $6Bi_2O_3 \cdot SiO_2$.

4 - 2. Sb_2O_3-doped γ - Bi_2O_3

INTRODUTCION

The electrical conduction of bcc $Bi_{24}Si_2O_{40}$ single crystal is reported to be P-type electronic. However, $Bi_{24}Pb_2O_{38}$ and the nonstoichiometric $Bi_{24}Si_2O_{40}$ sintered specimen show much higher oxygen ionic conductivities resulting in a mixed conduction behaviour as described in the last section. Harwig and Gerards[18] also suggested that the oxygen ionic conduction is predominant in the pure γ-Bi_2O_3 based on the frequency dispersion of impedance. However, details of electrical conduction of the pure and doped γ-Bi_2O_3 are not clear.

In II-3-1, it was described that the γ-form sintered specimen can be obtained at room temperature by doping a few mol% of Sb_2O_3. In the present section, the electrical conduction in γ-Bi_2O_3 doped with Sb_2O_3 was examined.

EXPERIMENTAL

The raw materials were α-Bi_2O_3 and Sb_2O_3 (both 99.99% pure). The powders were mixed, calcined in air at 730°C for 2h in a platinum crucible, finely ground, and pressed into pellets (10mm in diameter 3mm in depth) or rods (5 × 3 × 10 mm) under 54MPa. The pressed bodies were sintered at 800°C for 5h in

air and furnace-cooled.

Polymorphic forms and lattice constants were determined by X-ray diffraction (XRD). Polymorphic transformation were examined by high-temperature XRD and differential thermal analysis (DTA). The concentration of Sb^{3+} and Sb^{5+} ions in γ-Bi_2O_3 were determined by wet chemical analysis.

Electrical conductivity was measured by a complex impedance method at 5 to 13 MHz and a four-probe d.c. method. The 4-probe d.c. method was used for the determination of the oxygen partial pressure (PO_2) dependence of conductivity. No significant deviation in conductivity was observed for both methods. Ionic transference number was determined by a d.c.polarization method.

RESULTS AND DISCUSSION

Samples of bccγ-Bi_2O_3 were obtained by doping with 1 to 3 mol% Sb_2O_3. Minor monoclinic XRD peaks were detected only in the 1 mol% specimens. The apparent density of the sintered specimens was 88 to 92 % of the theoretical value.

The lattice constant decreased with an increase of Sb_2O_3 content as shown in Fig.1. This indicated that Sb_2O_3 dissolved into γ-Bi_2O_3 in the present composition. Wet chemical analysis showed that more than 80% of antimony ions are pentavalent in 2 mol% Sb_2O_3 doped γ-Bi_2O_3. The DTA curves and high-temperature XRD patterns indicated that the γ form transforms into α form at about 560°C and then into δ form at about 710°C on increasing temperature. On cooling, the δ form transformed directly into the γ form.

Fig.2 shows typical impedance plots of γ-Bi_2O_3 doped with 3 mol% Sb_2O_3 at 356 and 452°C. One semicircle in contact with the zero point at high frequencies and a section of semicircle at low frequencies can be observed. The low frequency region can be explained by electrode impedance.[19] There was no semicircle

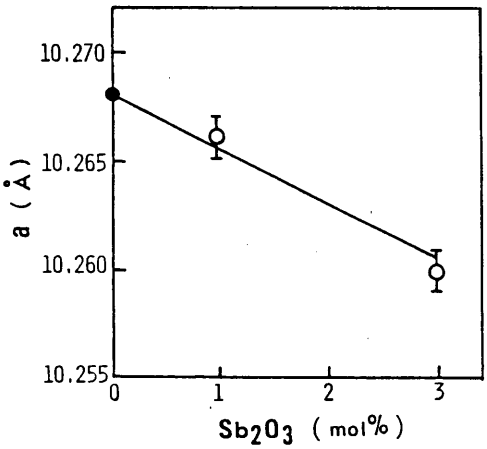

Fig.4.2-1

Lattice constant of γ-Bi_2O_3 doped with Sb_2O_3.
(● : ref 4)

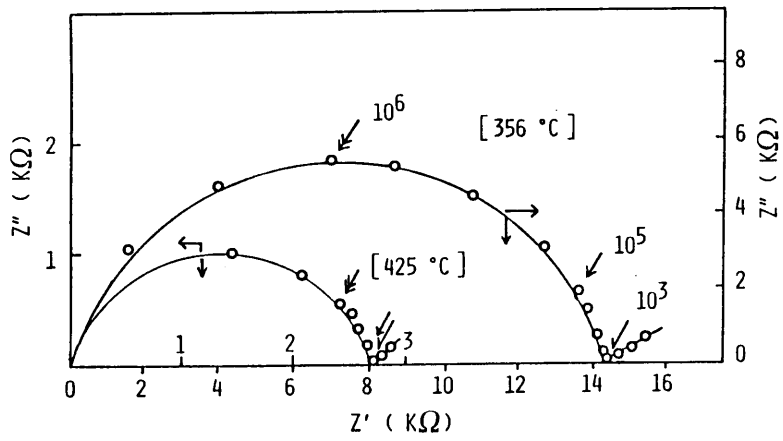

Fig.4.2-2

Complex impedance plots of γ-Bi_2O_3 doped with 3 mol% Sb_2O_3 at 356 and 425°C. Indicated numbers are the measuring frequency (Hz).

associated with the grain boundary, which often appears in middle frequency region for oxygen ionic conductors such as stabilized zirconia.[19] It is not clear whether this is due to the very small grain-boundary impedance or to the identical time constants in grain and grain-boundary impedances, which prevents the spliting of both contributions in the impedance plot. However, in the present study, the end-point of the first semicircle was taken as the bulk resistance to calculate conductivity.

The temperature dependences of the conductivity for Sb_2O_3 doped Bi_2O_3 on heating are shown in Fig.3. The polymorphic transformations into the α and δ forms are accompanied by abrupt conductivity changes. The composition dependence of the conductivity in the γ form will be discussed later.

Ionic transference numbers in the Sb_2O_3 doped Bi_2O_3 are shown in Fig.4. The applied voltage was controlled to be below 50mV. Accordingly, the measured transference numbers correspond to the average value under a PO_2 of between $10^{4.33}$ (air) and $10^{2.7}$Pa. The transference numbers were almost 1 in the bcc γ form (below 550°C) and fcc δ form (above 720°C), whereas they were almost zero in the monoclinic α form. After the polarization, morphological changes in the spacimens were not found; those would be expected if charge transport by cations had occurred.

The dependence of conductivity on PO_2 for γ-Bi_2O_3 doped with 1 to 3 mol% Sb_2O_3 at 500°C are shown in Fig. 5. The conductivities were kept constant under the PO_2 of 10^5 - 10^{-9} Pa. The results for the ionic transference number and PO_2 dependence of conductivuty demonstrate that the γ-Bi_2O_3 doped with 1 to 3 mol% Si_2O_3 is an oxygen ionic conductor in the wide range of PO_2.

Fig.6 shows the dependence on Sb_2O_3 content of conductivity σ, activation energy E and pre-exponential term σ_o, when they are expressed as $\sigma = \sigma_o \exp(-E/kT)$ where k and T have their usual meanings. Theconductivity showed a maximun at 2.5 mol% Sb_2O_3. The activation energy remained almost unchanged and hence it is clear that the change of σ_o is due to that of σ .

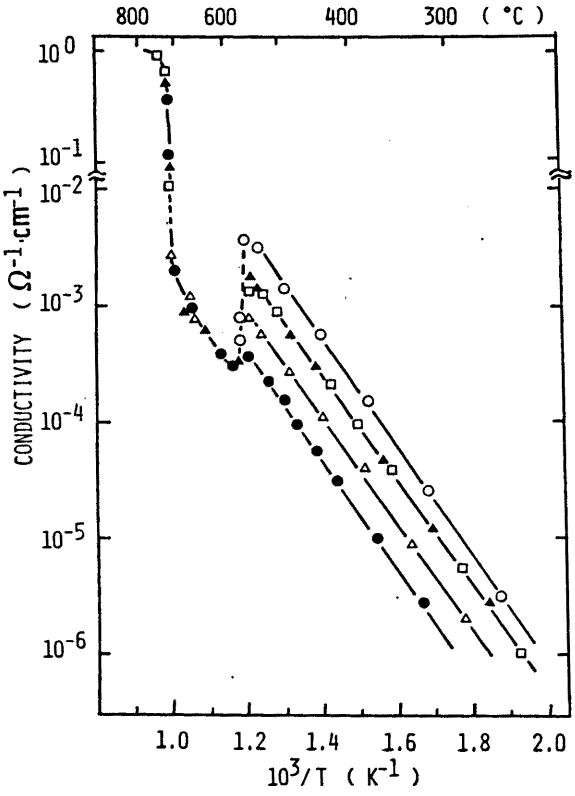

Fig.4.2-3
Temperature dependence of conductivity of γ-Bi_2O_3 doped with Sb_2O_3; (●) 1, (△) 1.5, (▲) 2, (○) 2.5, (□) 3 mol%.

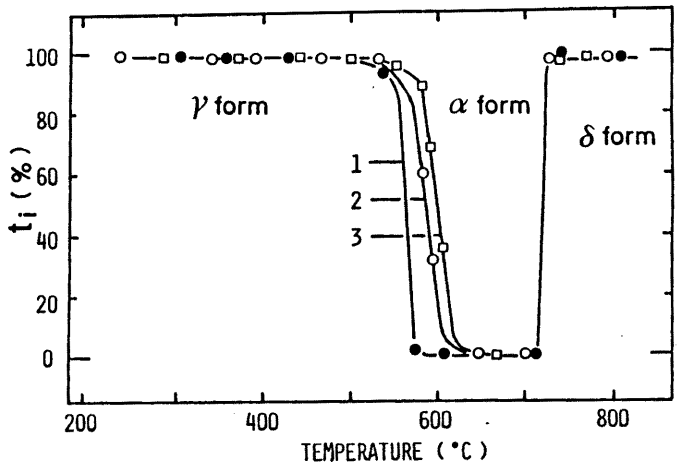

Fig.4.2-4
Ionic transference numbers in Sb_2O_3-doped Bi_2O_3.
Indicated numbers show Sb_2O_3 content (mol%).

It is proposed that pure γ-Bi_2O_3 contains $Bi_{26}O_{39}$ or $Bi^{3+}Bi^{5+}O_{40}$ in the unit cell.[1,16,20] However, if the oxygen sublattice is completely occupied, γ-Bi_2O_3 would not show such a high conductivity. In fact, estimated oxygen ionic conductivity. at 500 C in $Bi_{24}Si_2O_{40}$ and non-stoichiometric $Bi_{24}Si_{2-x}O_{40-2x}$(x = 0.1 to 0.14) are reported to be 3×10^{-10} and 4×10^{-5} $\Omega^{-1}cm^{-1}$, respectively.[8] Those are much lower than that of γ-Bi_2O_3 doped with Sb_2O_3. In addition, the reported density of pure γ-Bi_2O_3, 9.21 $g.cm^{-1}$ [20], is smaller than the calculated density of 9.29 for $Bi_{26}O_{39}$ and 9.315 $g.cm^{-3}$ for $Bi_{26}O_{40}$(using 1.0268nm as the lattice constant), but larger than 8.575 $g.cm^{-3}$ for $Bi_{24}O_{36}$ assuming that all tetrahedrons are vacant. Accordingly, it is assumed that the oxygen sublattce in pure γ-Bi_2O_3 is only partially occupied and consequently the large vacancy concentration brings about a high oxygen ionic conductivity. However, it is not clear whether those vacancies are caused only by Bi^{3+} occupation at tetrahedral Si^{4+} sites or by some Shottky-type defects of Bi^{3+} (or Bi^{5+}) and oxygen vacancies.

As shown in Fig.6, the pre-exponential term σ_o increased with increasing Sb_2O_3 content up to 2.5 mol%. This indicates an increase in the oxygen vacancy concentration effective for ionic conduction, as demonstrated in Chap.I-2. Reported ionic radii (6-coordinated) are 0.103 and 0.076 nm for Bi^{3+} and Bi^{5+}, 0.076 and 0.060 nm for Sb^{3+} and Sb^{5+}, and 0.040 nm for Si^{4+}, respectively , based on 0.140 nm for O^{2-}. [15] The oxygen vacancies in γ-Bi_2O_3 must be bound or orderded around Bi^{3+} (or Bi^{5+}) at tetrahedral sites, which are too large to occupy those sites. The incorporated smaller Sb^{5+} ions would probably substitute preferentially at the tetrahedral sites and subsequently the concentration of the bound vacancies would be decreased resulting in an increase in σ_o.

On the other hand, the bcc lattice approachs the perfect structure as the oxidized Sb^{5+} ions and corresponding oxygen ions are further incorporated. When incorporated Sb_2O_3 content is 3.85

mol%, composition becomes stoichimetric $Bi^{3+}(Bi^{3+}Sb^{5+})O_{40}$, although its presence is not yet confirmed. Accordingly, the decreases in σ_o and σ at above 2.5 mol% Sb_2O_3 shown appear to be due to a decrease in the total oxygen vacancy concentration.

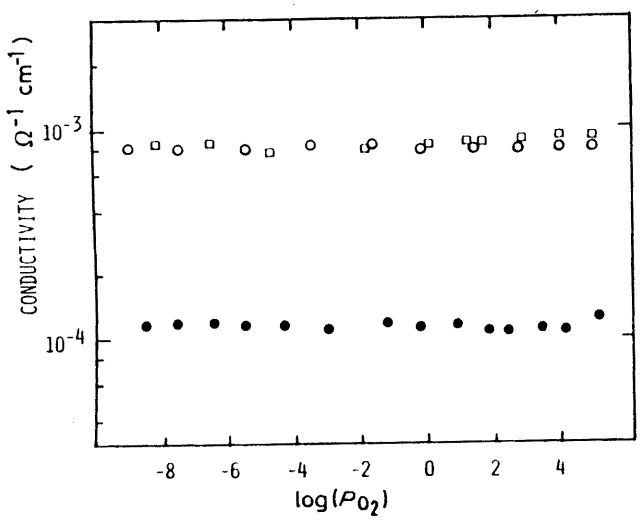

Fig.4.2-5

PO_2 dependence of conductivity at 500°C for γ-Bi_2O_3 doped with Sb_2O_3; (●) 1, (○) 2, (□) 3 mol% Sb_2O_3.

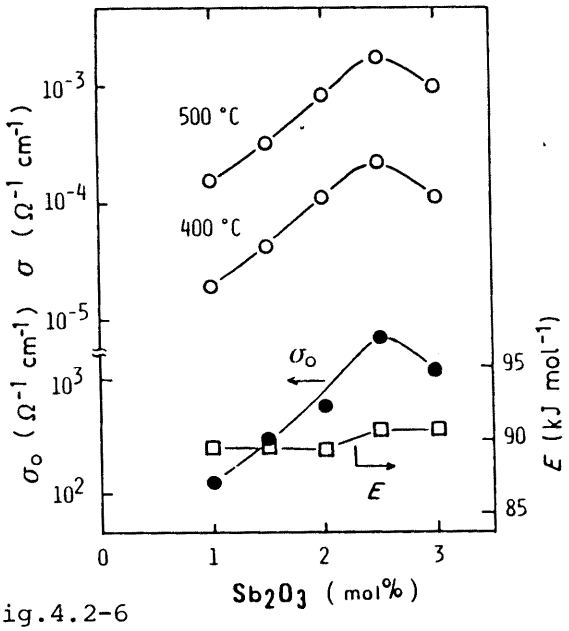

Fig.4.2-6

Sb_2O_3 content dependences of conductivity σ (at 400 and 500°C), activation energy E and pre-exponential term σ_o.

CONCLUSIONS in II-4

(1) The sintered bcc $6Si_2O_3.SiO_2$ was found to be a mixed conductor, in which elctron conductivity was proportional to $PO_2^{-1/4}$ and predominant below 10^{-1} Pa. The activation energy at a Po_2 of 10^5 Pa was found to be 135,185, and 191 kJ mol^{-1} for oxygen ion, hole and electron conduction, respectively, at 535 to 678°C.

(2) Silicon concentration in the sintered $6Bi_2O_3.SiO_2$ was slightly less than the theoretical value, resulting in cation atomic ratio Si/Bi of 0.93 to 0.95/12 (theoretically 1/12).

(3) Schottky-type defects of silicon an oxygen vacancies were proposed to explain a much higher oxygen ion conductivity in the sintered $6Bi_2O_3.SiO_2$ when compared with the reported value in single crystals.

(4) Body centred cubic γ-Bi_2O_3 doped with 1 to 3mol% Sb_2O_3 was stable up to 550°C but transformed into monoclinic α and fcc δ-Bi_2O_3 at high temperatures.

(5) In the Sb_2O_3 doped γ-Bi_2O_3, the oxygen ionic conduction was predominant in the PO_2 range of 10^5 to 10^{-9}Pa. As the Sb_2O_3 content increased, oxygen ionic conductivity inceases up to 2.5 mol% Sb_2O_3 reaching a maximum of 1.8×10^{-3} $ohm^{-1}cm^{-1}$ at 500°C and then decreased. However, the activation energy for ionic conduction remained almost unchanged.

(6) It was confirmed that more than 80% of antimony ions are pentavalent in γ-Bi_2O_3. Those Sb^{5+} ions appear to affect the concentration of oxygen vacancies effective for ionic conduction.

REFERENCES in **II**-4

1. L.G. Sillen, Ark. Kemi. Mineral. Geal. 12A,1 (1937).
2. E.M. Levin, and R.S. Roth, J. Res. Nat.Bur. Stand. Sect. A 68,197 (1964).
3. S.C. Abrahams, P.B. Jamison, and J.L. Bernstein, J.Chem. Phys. 47, 4043 (1967).
4. H.A. Harwig, Z. Anorg. Allg. Chem. 444,151, (1978).
5. R.E. Aldrich, S.L. Hou, and M.L. Hervill, J. Appl. Phys. 42, 493 (1971).
6. S.L. Hou, R.B. Lauer, and R.E. Aldrich, J. Appl.Phys. 44, 2652 (1973).
7. H. Shhweppe, and P.Quadflieg, IEEE Trans. Sonics Ultrasonics SU-21, 56 (1974)
8. J.A. Kilner, J. Drennan, P. Dennis, and B.C.H. Steele, Solid. State Ionics 5, 527 (1981).
9. T.Takahashi, H.Iwahara, and T. Esaka, J.Electrochem.Soc. 124,1563 (1977).
10. M.J. Verkerk, and A.J. Burggraaf, ibid.128, 75 (1981).
11. Ho-Knu Kim, T.Kokubo, S. Ito, and M. Tashoro, Yogyo kyokai Shi 90,348 (1982).
12. O.H. Hill, and J.C. Brice, J, Mater.sci. 9, 1252 (1974).
13. M.F. Lasker and R.A. Rapp, Z. physik.Chem.Neue Folge B49 198 (1966)
14. R.W. Vest, and N.M. Tallan, J. Appl. Phys. 36, 543 (1965)
15. R.D. Shannon, and C.T. Prewitt, Acta Cryst.B25, 925 (1969)
16. D.C.Craig, and N.C.Stephenson, J. Solid State Chem., 15, 1 (1975)
17. M.Peltier, and F.Micheron, J. Appl.Phys. 48.3683 (1977).
18. H.A. Harwig, and A.G. gerards, J. Solid state chem. 26, 265 (1978).
19. J.E. Bauerle, J.Phys.Chem.Solid 30,2657 (1969).
20. W.C.Schumb andE.S.Rittner, J. Am. Chem. Soc.65, 1055 (1943).

II - 5. Ionic conduction in fcc δ - Bi_2O_3 doped with rare-earth oxides

INTRODUCTION

Among oxygen-ion conductors, fcc Bi_2O_3 (δ form) stabilized by doping of rare-earth oxides is known to show the highest conductivity. Relations between dopant species, their amounts and the conductivity, reported up to now, are summarized as follows ;
(1) The conductivity decreases with increasing dopant-concentration in spite of a constant concentration of oxygen vacancy. Accordingly, the maximum conductivity is obtained at the lowest dopant-concentration needed for the stabilization of the δ form.[1-4]
(2) At a fixed dopant-concentration, the conductivity slightly increases with increasing cation radius of dopant.[3-5]
(3) The minimum dopant-concentration needed for the stabilization is smaller for a dopant having smaller cation radius, except for Yb_2O_3.[3,4] Accordingly, the top data of conductivity is shown in Er_2O_3-doped δ-Bi_2O_3.

Although there were many investigations on conduction behavior of fcc δ-Bi_2O_3, factors to stabilize the δ form and to determine the conductivity are still obscure. In section 3, it was described that changes in lattice consant affect the ionic

conduction in doped β form. However, the relation between conductivity and lattice constant in the δ form has not been investigated. In the present section, factors for stabilization and conduction mechanism were investigated for δ-Bi_2O_3 doped with rare-earth oxides R_2O_3 (R = Dy, Er, Tm, Yb, Dy+Yb). The co-doping of Dy+Yb was selected because their average cation radius is almost equal to that of Er.

EXPERIMENTAL

Rare-earth oxides were obtained by thermal decomposition of reagent grade $Dy_2(C_2O_4)_3.xH_2O$, $Er_2(C_2O_4)_3.xH_2O$, $Tm_2(C_2O_4)_3.xH_2O$ and $Yb_2(CO_3)_3.xH_2O$ at 700 to 760°C. Bismuth oxide (99.99 %) and rare-earth oxides were mixed in a desired ratio, calcined at 800 °C for 5 h in a Pt crucible and ground. The resulting powder was pressed into rectangular bars (5 by 5 by 15 mm) at 130 MPa, sintered for 5 h and cooled at the rate of 100°C/h. Sintering temperature was 900 to 1000°C, which was raised as R_2O_3 content increased. In order to confirm the phase stability, annealing at 550°C for 50 h was conducted for some specimens.

Phase identification was performed by X-ray diffraction. Lattice constants were calculated using the least-square method and Si as an internal standard. Conductivity was measured by the complex impedance method at frequencies of 5 Hz to 13 MHz. Platinum electrodes were applied by sputtering.

RESULTS

Specimens having composition $(Bi_2O_3)_{1-x}(R_2O_3)_x$ are denoted as R_x hereafter. The $(Dy+Yb)_x$ corresponds to the $(Bi_2O_3)_{1-x}$-$(Dy_2O_3)_{x/2}(Yb_2O_3)_{x/2}$. Some specimens with low R concentration (small x) showed minor peaks of second phases (probably rhombo-

hedral phase) in the X-ray diffraction. After annealing, amount of the second phases further increased.

Temperature dependence of conductivity of $R_{0.2}$ (R = Dy, Er, Yb, Dy+Yb) is shown in Fig.1. For specimens containing second phases such as $Yb_{0.2}$ and annealed $Dy_{0.2}$, the conductivities were more than half order of magnitude lower than those of others. The stability of the δ forms, judged from the X-ray diffraction pattern and the conductivity, were summarized in Table.1.

Figure 2 shows the relation between lattice constant of fcc phase and composition (in as-sintered specimens). In all system, lattice constant decreased with increasing dopant-concentration, obeying the Vegard's rule except for $R_{0.16}$ specimens. At a given concentration, the larger the ionic radius of rare-earth element R, the larger the lattice constant.

Figure 3 shows conductivities at 430°C plotted against ionic radius of R. The conductivity increases with increasing ionic radius of R, and the minimum dopant-concentration for the fcc phase(x_{min}) decreases with decreasing ionic radius of R down to 1 A. In addition, it is also found that co-doping of Dy and Yb gives almost same conductivity and x_{min} (about 20 mol%) to those of Er-doped specimens.

Composition dependences of activation energy E and pre-exponential term σ_o are shown in Figs. 4 and 5, respectively.

Table I-5-1. Stabilization of δ-Bi_2O_3

symbol	as-sintered	annealed
●	pure δ	pure δ σ const
◑	pure δ	δ + minor phase σ const
○	pure δ	mixed phase σ lowered
x	mixed phase σ lowered	——

dopant \ mol%	30	25	20	16
Dy	●	○	○	—
Dy + Yb	●	●	◑	x
Er	●	●	◑	x
Tm	—	◑	—	—
Yb	●	○	x	—

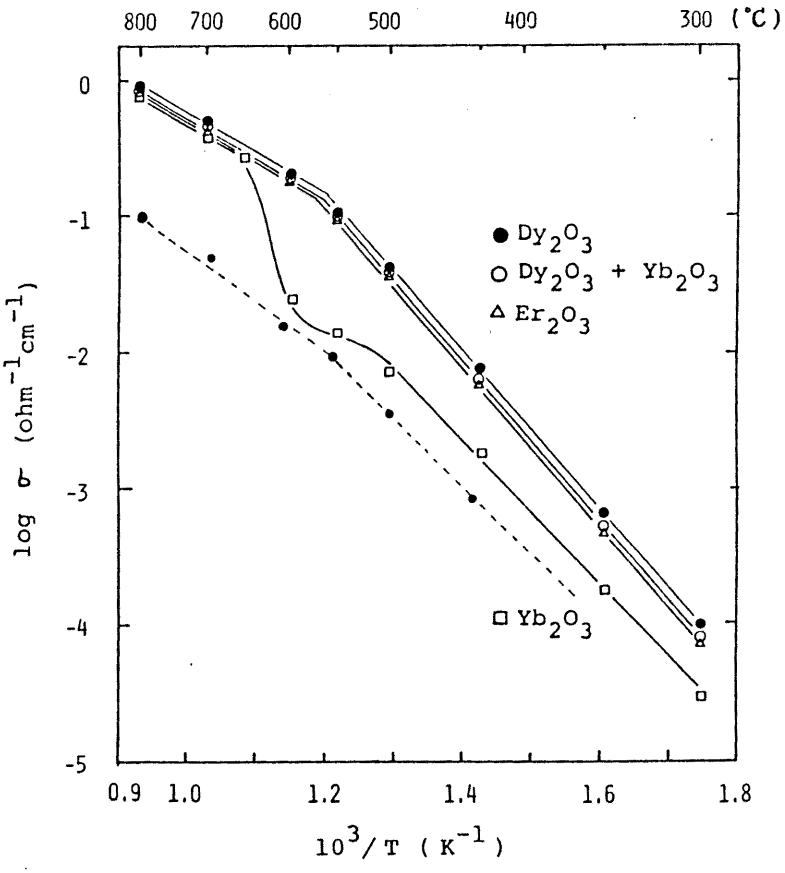

Fig.5-1

Temperature dependence of conductivity of $(Bi_2O_3)_{0.8}(R_2O_3)_{0.2}$.

——— : as-sintered, - - - - : annealed.

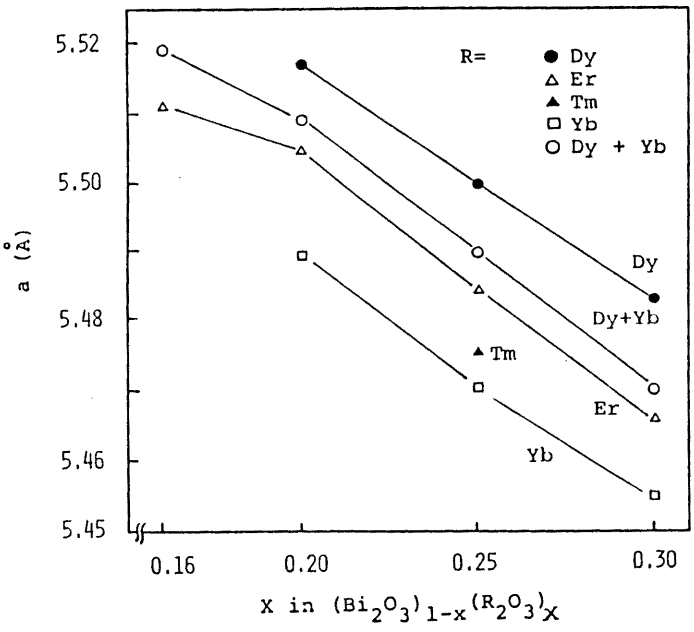

Fig.5-2

Lattice constants in $(Bi_2O_3)_{1-x}(R_2O_3)_x$.

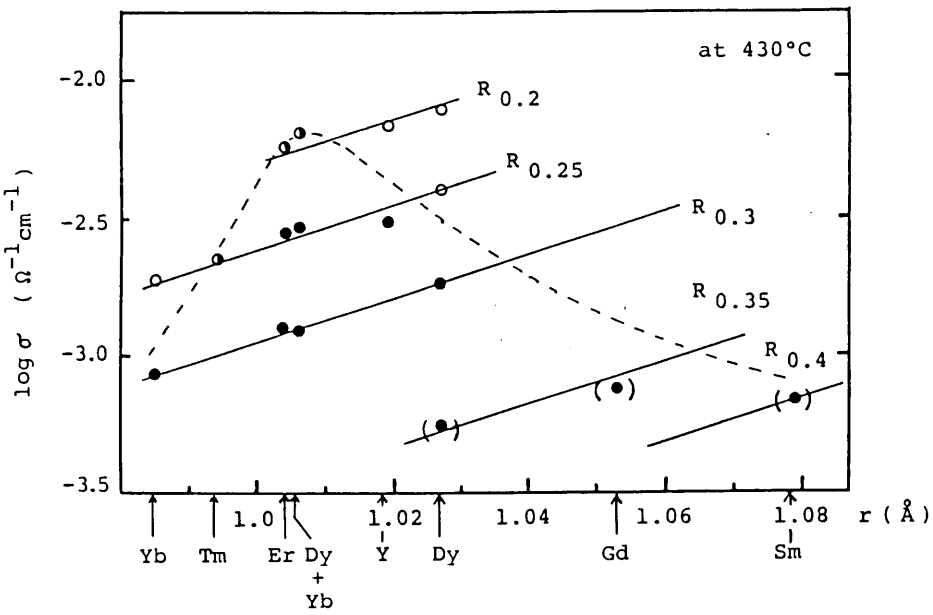

Fig.5-3

Conductivity at 430°C vs. R-ion radius. Symbils are same with Table 1, (●) from ref.4. Dashed line indicates stabilized region.

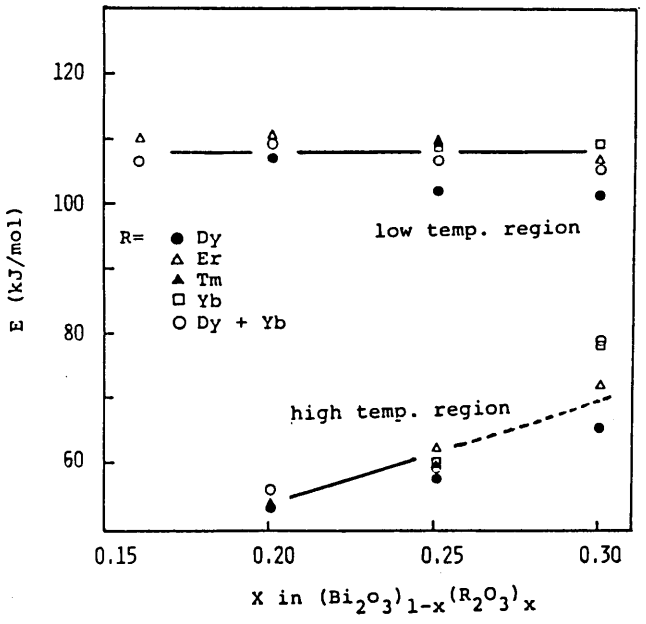

Fig.5-4

Composition dependence of activation energy E.

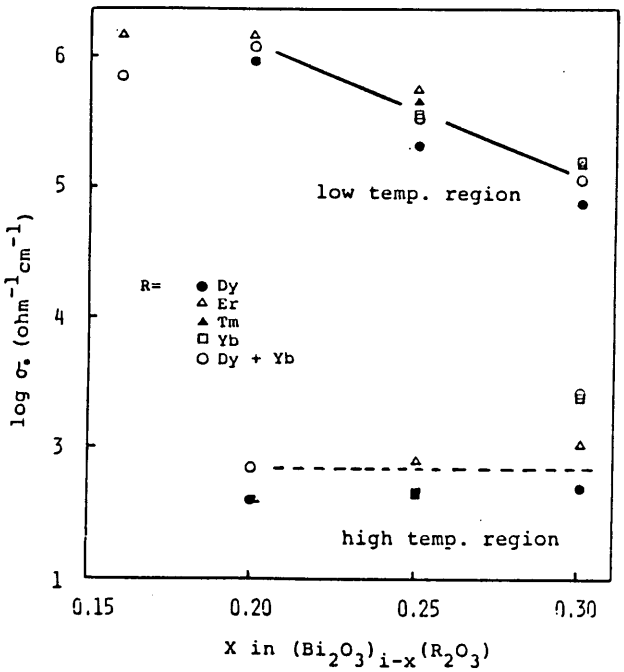

Fig.5-5

Composition dependence of pre-exponential term σ_0.

There were two defferent dependences for high (> 550°C) and low (< 550°C) temperature regions ; E increases with increasing dopant-concentration and σ_o is kept constant in the high T region, in contrast, σ_o decreases with increasing dopant-concentration but E is almost independent on it in the low temperature region.

DISCUSSION

(1) Factors for stabilization

As described previously, x_{min} decreases with decreasing ionic radius of R except for Tm and Yb. Lattice constant also decreases with the ionic radius. However, the lattice constant at x_{min} is different for dopant species R, i.e. 5.49-5.50 A for Er and Dy+Yb, below 5.47 A for Yb and above 5.515 A for Sm. Accordingly, lattice constant cannot be a direct indication for stabilization of the fcc phase.

In the ideal fluorite structure with lattice constant **a**, cationic radius r_m and anionic radius r_o, next equations must be set up,

$$r_m + r_o = (\sqrt{3}/4)\mathbf{a} \qquad (1)$$

$$r_m/r_o = \sqrt{3} - 1 \qquad (2)$$

where eq.1 is derived from an assumption of contacts of adjacent cation and anion in the normal positions, and eq.2 from ideal 8-coordination of a cation with anions. (Actually, the 8-coordination can be realized in the range of $\sqrt{3} - 1 \leq r_m/r_o < 1$.)

Assuming a constant value of r_o in eq, 1, lattice constant **a** can be expressed by

$$\mathbf{a} = (4/\sqrt{3})r_m + C \qquad (3)$$

where C is constant(= $(4/\sqrt{3})r_o$). Figure 6 shows lattice constant vs. arithmetical-mean caion radius $\bar{r}_m$ in doped fcc phase. Shannon's ionic radii[6] (8-coordinated) were used for the calcula-

tion of $\bar{r}_m$. The measured **a** situated near the dashed line $\mathbf{a} = (4/\sqrt{3})\bar{r}_m + 2.881$, although deviations were large. In comparison with Fig.3, the fcc phase seems to be stabilized at r_m below 1.134 A except for Tm- and Yb-doped specimens. Apparent oxygen ion radius can be estimated from the dashed line to be 1.2475 A, which is smaller than the standard value of 1.38 A (4-coordinated)[6]. Covalency of Bi ion and a large amount of oxygen vacancy may be a cause of the somewhat smaller oxygen ion radius.

In order to understand the stabilzation crystallographically next estimation was conducted. The ideal r_m and r_o in fluorite structure can be obtained from eqs.1 and 2, as

$$r_m = (\sqrt{3} - 1)\mathbf{a}/4 \ , \quad r_o = \mathbf{a}/4 \qquad (4)$$

The difference Δr between actual $\bar{r}_m$ and ideal r_m means misfitness of ionic radius for a fluorite lattice having lattice constant a. Figure 7 shows Δr vs. dopant concentration x. The Δr decreased linealy with increasing x for each R species and it was found that the fcc phase is stabilized at Δr below 0.126 A except for Tm- and Yb-doped specimens.

Following structural data are reported for the stabilized fcc Bi_2O_3 on the basis of refined X-ray and neutron diffraction analysis[7-9] : In the fcc Bi_2O_3 with low dopant concentrations, cations occupy the normal positions (000) but oxygen ions are displaced from the normal positions$(\frac{1}{4},\frac{1}{4},\frac{1}{4})$. This displacement is not a function of temperature. At high temperatures oxygen ions are distributed statistically around the normal position$(\frac{1}{4}+d,\frac{1}{4}+d,\frac{1}{4}+d)$, but they are bound at one position keeping the displacement at low temperatures. The displacement parameter d decreases with increasing dopant concentration from 0.066 (pure Bi_2O_3)[7] to 0 (32mol% Gd_2O_3-doped Bi_2O_3)[9].

A decrease in the displacement parameter appears to correspond to a decrease in the misfitness of cation and anion sizes in fluorite lattice as shown in Fig.7. From these results, Bi ion is assumed to be too large to constract fluorite lattice with oxygen ions, and hence a decrease in mean-cation radius due

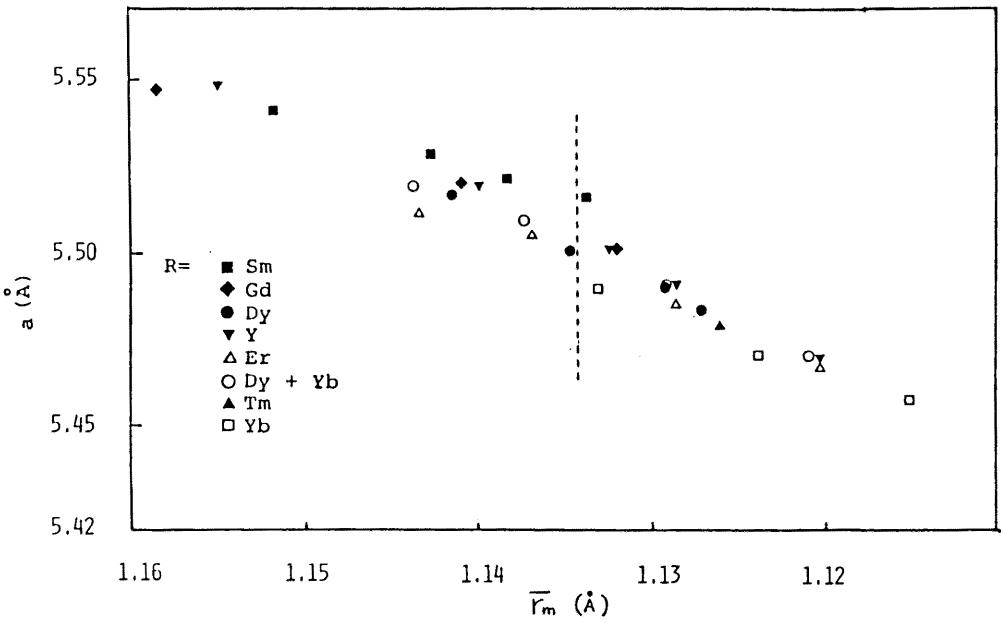

Fig.5-6. Lattice constant vs. mean cation radius.

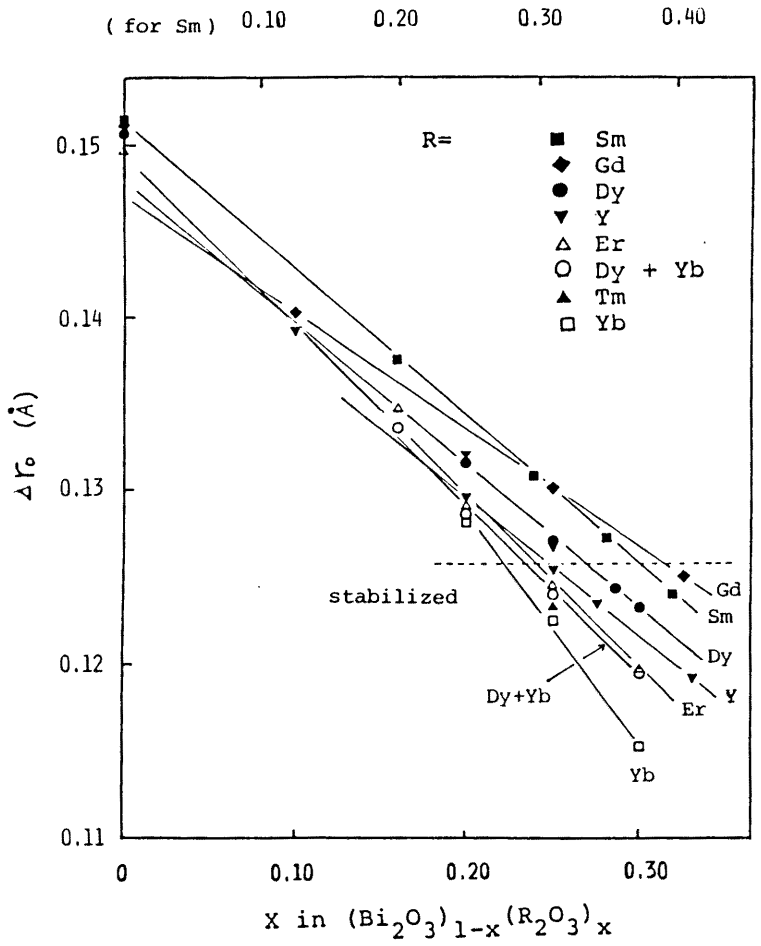

Fig.5-7. Misfitness of cation radius in $(Bi_2O_3)_{1-x}(R_2O_3)_x$ for fluorite lattice.

to introduction of smaller R ions brings about a decrease in misfit, resulting in the stabilization of fluorite structure.

The Tm- and Yb-doped specimens were not stabilized even when $\bar{r}_m$ < 1.134 A and r < 0.126 A. Since r_o would be changeable in Bi_2O_3, the condition for 8-coordination of R ions with oxygen ions is tentatively given by eqs.1 and 2 as

$$r_R \geqq (\sqrt{3} - 1)a/4 \qquad (5)$$

This condition is not satisfied in Bi_2O_3 containing Yb_2O_3 below 30 mol% and Tm_2O_3 below 25 mol%, because of small ionic radius of Yb (0.985 A) and Tm (1.002 A).

(2) Conduction mechanism

Figure 8 shows conductivities at 700 °C and 430 °C vs. lattice constant. Since lattice constant **a** is dependent on R-ion radius and concentration x, both factors on conductivity can be observed. the conductivity at 430 °C increased with increasing a (increasing R-ion radius and decreasing x). In contrast, the conductivity at 700°C depended on x but was independent on R-ion radius. Figure 9 shows activation energy E vs. lattice constant in high and low temperature region. The E value in the low T region decreased slightly with increasing **a** (increasing R-ion radius), being independent on x. The E value in the high T region depended only on x. From the results of Figs. 4,5,8 and 9, conduction characteristics can be summarized as in Table 2.

Table I-5-2. Effects of cation radius and concentration of dopant on conductivity

High T

	r_m ↑	x ↑
σ	-	⇊
E	-	⇈
σ_o	-	-

Low T

	r_m ↑	x ↑
σ	↑	⇊
E	↓	-
σ_o	-	⇊

(r_m : ion radius of dopant,
x : concentration of dopant,
↑ : increased
↓ : decreased
- : independent)

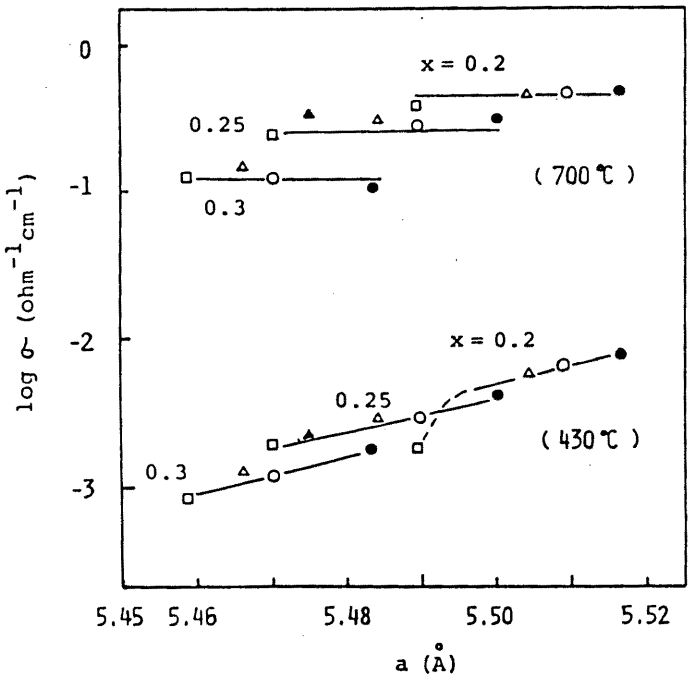

Fig.5-8

Conductivity (at 430 and 700°C) vs. lattice constant.
Indicated numbers (x) are R_2O_3 concentrations.
Symbols are same with those in Fig.5-9.

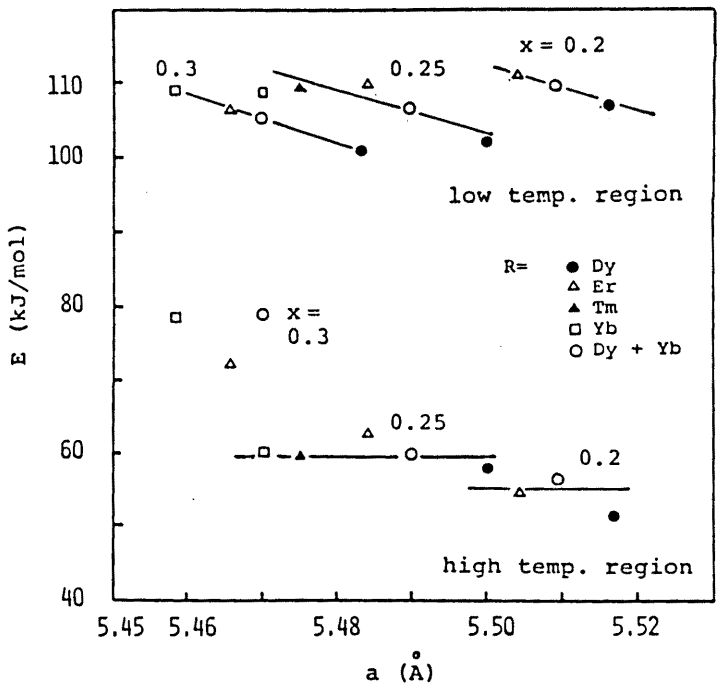

Fig.5-9

Activation energy vs. lattice constant.
x are R_2O_3 concentration.

Figure 10 shows a schematic diagram indicating migration of an oxygen ion. Migration of an oxygen ion from one tetrahedron to the next empty one involves breaking of the Bi-O or R-O bond and passage through Bi_3, (Bi_2R) or (BiR_2) triangular planes. The mesh-radius of the plane is determined by lattice constant and ionic radii of Bi and R. Figure 11 shows the mesh-radius of (Bi_2R) plane and of the plane consisting of three cations having mean-cation radius. It is found that the mesh-radius of the (Bi_2R) plane is independent on the dopant species but decreases with increasing dopant concentration. This composition dependence is just the same to that of activation energy at high temperatures. However, it is difficult to explain the lowest activation energy in pure fcc Bi_2O_3.

Another possible explanation for a change in activation energy is a change in polarization energy, involved in total energy for migration through a tetrahedron plane. The values of polarizability are 3.6 A for Pb^{2+}, 3.3 A for Bi^{3+} (estimated from Pb^{2+} and Tl^{+}(3.9 A)), 1.01-0.8 A for Gd^{3+}-Yb^{3+}, and 3 A for O^{2-}.[8,10] It is reported that the activation energy of Bi_2O_3-PbO solid solution at >600 °C is equal to that of pure Bi_2O_3.[11] Introduction of the less polarizable R ions results in a less negative value of the polarization energy, and hence it is expected that the energy for passage through the tetrahedon plane is increased.

The pre-exponential term σ_o of conductivity in high T region was independent of composition. The value of σ_o estimated using eq.3-7 in Chap.I-2 was about 3×10^3 $(ohm.cm)^{-1}$, which is approximately in agreement with the measured values of $0.5\text{-}1\times10^3$ $(ohm.cm)^{-1}$. This suggests that all oxygen ions take part in the conduction process in the high T region.

The R-O bond will be stronger than the Bi-O bond because the stability of c-type R_2O_3, which is structurally related to the dificient fluorite, is larger than that of Bi_2O_3. The fact that an oxygen ion is bound at one position with some displacement at

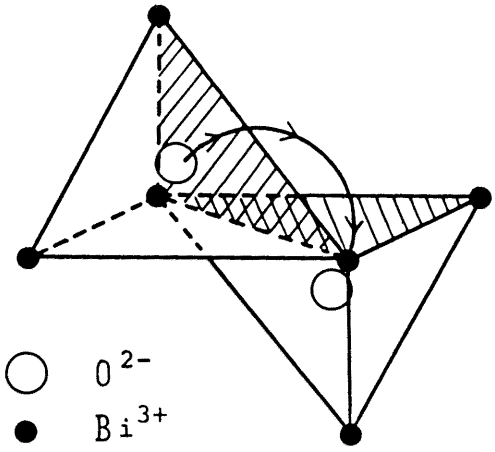

Fig.5-10

Schematic view for the migration of an oxygen ion in the fluorite lattice.

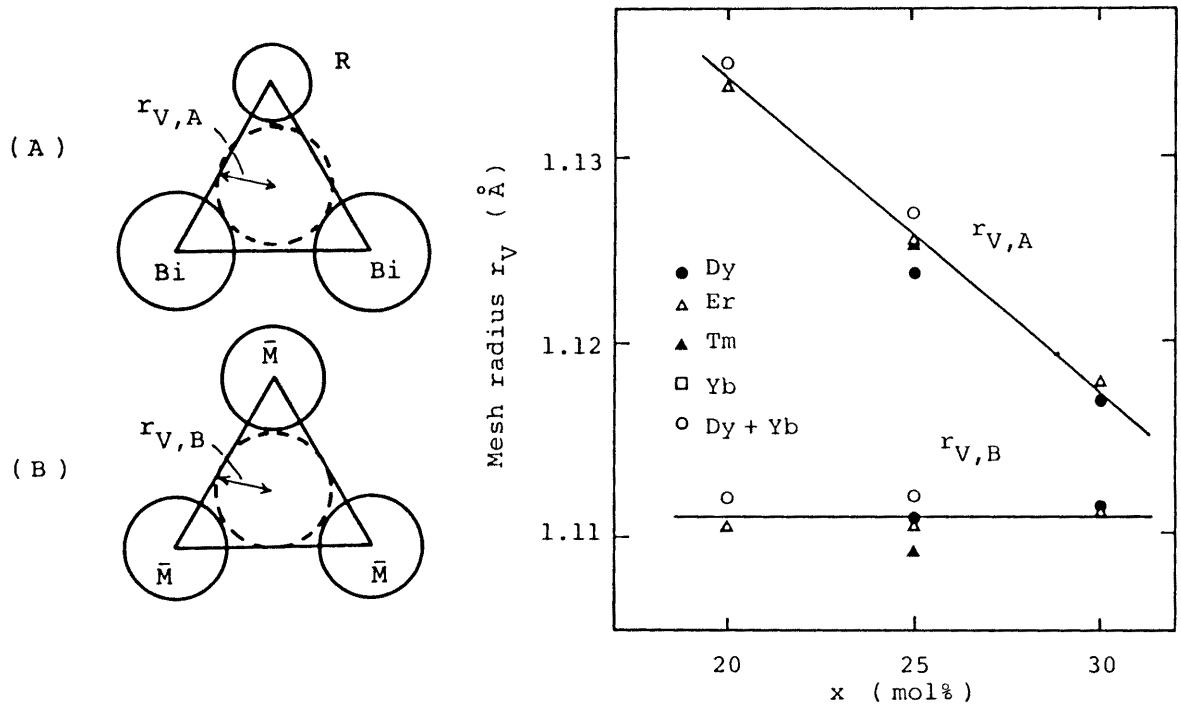

Fig.5-11

Mesh radius r_V of (Bi_2R) plane in model (A) and (B).

low temperatures would be due to this strong R-O bond and small R-ion radius. The strength will be slightly different for the different R ions. The activation energy E in the low T region decreased with increasing R-ion radius, being independent on dopant concentration, as shown in Fig.9 and Table 2. This fact would suggest that the strength of R-O bond is the predominant factor for determining E in the low T region.

At more than 25 mol% R_2O_3, (Bi_2,R_2) tetrahedra exist together with (Bi_3,R) tetrahedra. The oxygen ions in the (Bi_2,R_2) tetrahedra are bound to two R ions and much larger energy will be needed for breaking the R_2-O bond. It is likely that the contribution of oxygen ions in the (Bi_2,R_2) tetrahedra to conductivity is negligibly small. Accordingly, an increase of R_2O_3 concentration will result in an increase of oxygen ions in the (Bi_2,R_2) tetrahedra and then a decrease in the pre-exponential term (the effective concentration of mobile oxygen ions).

CONCLUSION in **II**-5

(1) The fcc Bi_2O_3 co-doped with an equal amount of Dy_2O_3 and Yb_2O_3 (mean R^{3+} radius: 1.006 A) showed almost same lattice constant and conductivity to Er_2O_3-doped Bi_2O_3 (Er^{3+}: 1.004 A).

(2) The misfitness between lattice constant **a** and mean cation radius r_m in the fluorite structure can be an indication for the stabilization of the fcc Bi_2O_3 doped with rare-earth oxides, R_2O_3. In addition, R^{3+} ion radius (r_R) must satisfy the condition of 8-coordination with oxygen ions. As a result, next conditions were proposed ;

$$\Delta r = r_m - (\sqrt{3}-1)a/4 > 0.126$$

$$r_R \geqq (\sqrt{3}-1)a/4$$

(3) At high temperatures, all oxygen ions contribute to ionic conduction. The activation energy is assumed to be determined by the average polarization energy of Bi^{3+} and R^{3+} or by the mesh width of (Bi_2R) plane.

(4) At low temperatures, the strength of R-O bond determines the activation energy. The concentration of mobile oxygen ions decreases with increasing R_2O_3 content, probably due to an increase in oxygen ions bound in (Bi_2R_2) tetrahedra.

REFERENCES in II-5

1. T. Takahashi, H. Iwahara and T. Arao, J. Appl. Electrochem., 5, 187 (1975).
2. M.J. Verkerk, K. Keizer and A.J. Burggraaf, J. Appl. Electrochem., 10, 81 (1980).
3. M.J. Verkerk and A.J. Burggraaf, J. Electrochem. Soc., 128, 75 (1981).
4. H. Iwahara, T. Esaka, T. Sato and T. Takahashi, J. Solid State Chem., 39, 173 (1981).
5. H.T. Cahen, T.G.M. Van Den Belt, J.H.W. De Wit and G.H.J. Broers, Solid State Ionics, 1, 411 (1980).
6. R.D. Shannon, Acta Cryst., A32, 751 (1976).
7. H.A. Harwig, Z. Anorg. Allg. Chem., 444, 151 (1978).
8. M.J. Verkerk, G.M.H. van de Velde, A.J. Burggraaf and R.B. Helmholdt, J. Phys. Chem. Solids, 43, 1129 (1982).
9. K. Koto, H. Mori and Y. Ito, Solid State Ionics, 18&19, 720 (1986).
10. C.S.G. Phillips and R.J.P. Williams, Inorganic Chemistry (Part 1), Oxford, 1965, p.176.
11. P. Demonchy, D. Conflat, J.C. Boivin and D. Thomas, C. R. Acad. Sci. Ser. C, 289, 317 (1979).

II - 6. Conclusion in Chapter II

(Relation between crystal structure and ionic conduction in Bi_2O_3)

In Chapter II, relationship between crystal structure and oxygen-ion conduction was discussed for Bi_2O_3 polymorphs.

Figure 1 shows oxygen-ion conductivities in pure δ and β forms and the highest conductivities in systems of doped β (Sb), γ (Sb,Si) and δ (Er) forms, reported in sections 1-5. Among those forms, fcc δ forms show higher conductivities. The oxygen -ion conduction cannnot be detected in α form.

Figure 2 shows unit cell volume converted to the fluorite-structure unit (containing two Bi_2O_3) for each polymorphs. The unit cell volume was in the order of $\delta > \beta > \gamma > \alpha$ form. The interatomic distances of Bi-O bond in each form are presented in Fig.3. The ideal Bi-O distance (the sum of ionic radii of Bi^{3+} and O^{2-}) is also presented for comparison.

(1) δ form

The δ form has an almost constant Bi-O distance, even if the short-range ordering is taken into consideration. The value is close to the ideal distance. This brings about equivalent oxygen sites and isotropic migration path of oxygen ions, and leads to a high ionic conductivity. However, doping of rare-earth oxide generates interactions between dopant cations and oxygen ions,

and hence the conductivity is decreased.

(2) β form

In the tetragonal β form (a superstructure of the δ form), the distance spreads out in a wide range and only two O atoms maintain the same distance as the δ form has. This spread is due to a long-range ordering of oxygen vacancy and to subsequent distortion in Bi sublattice. Those cause a smaller unit cell volume and unequivalent oxygen sites, resulting in a low mobility of oxygen vacancy (a high activation energy for conduction). The unit cell volume and ionic conductivity do not change very much in Sb-doped(>4 mol%) β form. This would be due to incorporated oxygen atoms and subsequent decrease of the distortion in Bi sublattice.

(3) α form

In the monoclinic α form, two kinds of Bi atom (5- and 6-coordinated with O atoms) are present, and their Bi-6O (or -5O) octahedrons are largely distorted due to assymmetric aarrangements. Accordingly, the unit cell volume is the smallest and Bi-O distances are different for all oxygen sites. These are to reflect covalent nature of Bi atom. In such a structure, vacant oxygen site in the δ- or β form (one-fourth of 8(c) oxygen sites in Fm3m for the δ form) does not work as a position through which oxygen ions can move, and a very low mobility of oxygen is expected.

(4) γ form

In the stoichiometric bcc γ-$Bi_{12}GeO_{20}$, Bi atoms coordinate with 7 O atoms and their Bi-O distances are close to those of Bi_1-O in the α form. Four-coordinated Ge atom has a very small Ge-O distance. Accordingly, oxygen-ion conductivity should be very low like in the α form. However, nonstoichiometric bcc forms (Si- and Sb-doped γ forms in section 4) contain cation

vacancies probably at the Ge site, and hence corresponding oxygen vacancies are present as discussed in section 4. The unit cell volume situates between those of β- and α forms. Accordingly, oxygen ionic conductivity becomes appreciable due to an increase in the oxygen vacancy concentration.

From above consideration, next two factors are found to be important for high oxygen ionic conduction in the fluorite-related structure ;

1. equivalent oxygen sites (low migration energy).
2. high concentration of oxygen vacancy.

For the first factor, a symmetrical cation sublattice and small interaction between dopant cations and oxygen ions are required. Generally, the second factor is achieved by doping of low-valent cation for the ordinal fluorite compounds like ZrO_2. However, it can be achieved by nature if the first factor is satisfied for the fluorite(δ -)Bi_2O_3.

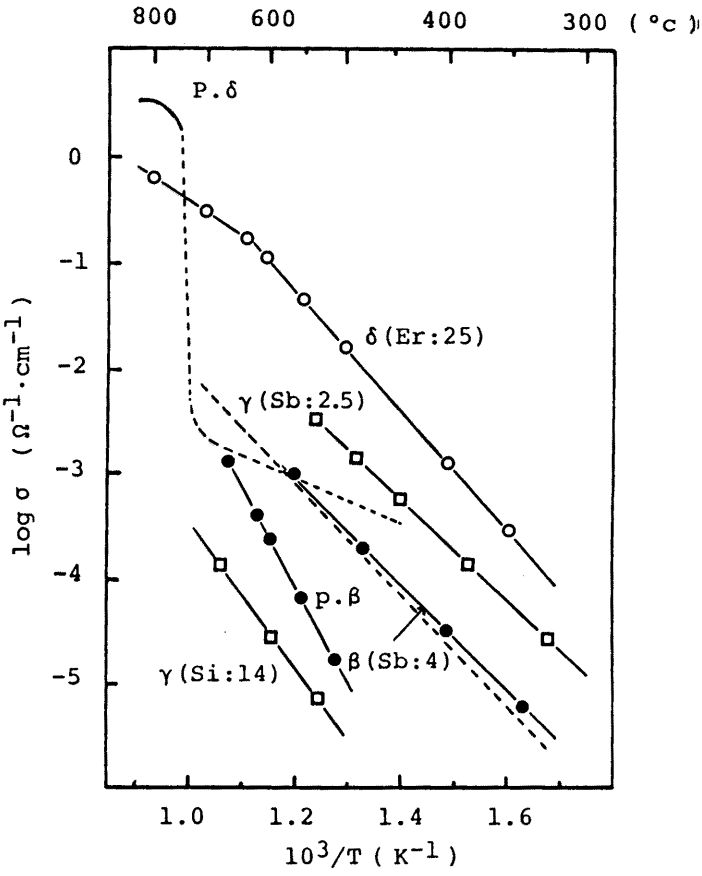

Fig. 6-1.
Oxygen-ion conductivity in pure and doped Bi_2O_3 polymorphs.

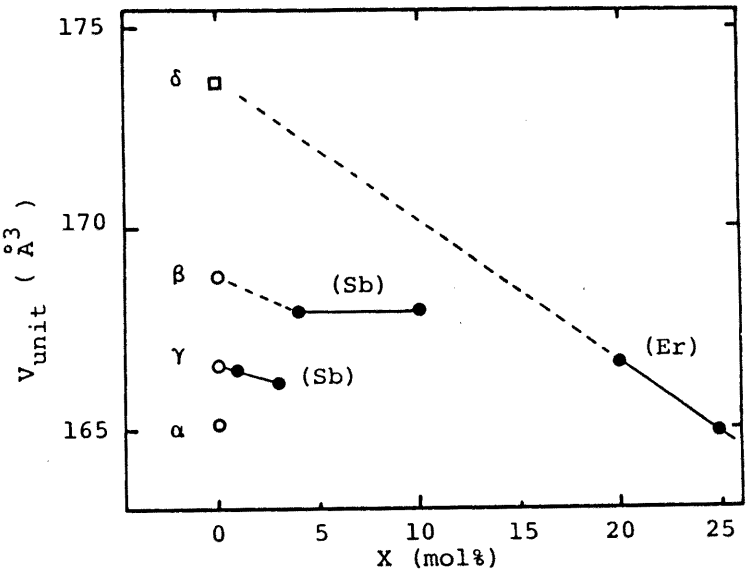

Fig. 6-2.

Unit cell volumes of Bi_2O_3 polymorphs.

● : measured, ○ : reported, □ : estimated.

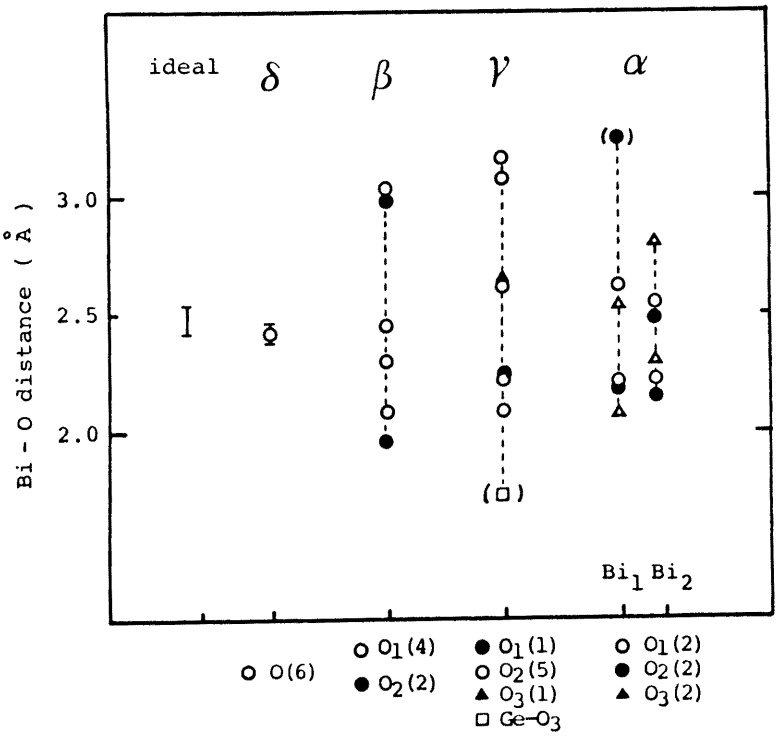

Fig. 6-3.

Interatomic distances of Bi-O bond in each form.
(γ form : $Bi_{12}GeO_{20}$, others : pure Bi_2O_3)

Chapter III

Ionic Conduction in The System Bi_2O_3-ZrO_2 Stabilized with Y_2O_3

III - 1. Conduction mechanism in fcc δ - Bi_2O_3 solid solutions doped with ZrO_2 and Y_2O_3

INTRODUCTION

The fcc δ-Bi_2O_3 can be stabilzed at low temperatures by adding of dopant oxifes such as Y_2O_3, Ln_2O_3 (Ln = Sm - Yb), WO_3, Nb_2O_5 et al..[1-6] The conductivity of these fcc solid solutions is lower than that in the fcc δ form of pure Bi_2O_3, and decreases with increasing dopant concentration. As a result , in the temperature region below 700 ℃, the conductivity has a maximum value at the lower limit of the formation range of the fcc solid solution in each binary system. In contrast, the fcc phase cannot be observed in Bi_2O_3-ZrO_2 system at low temperatures.[7]

For ternary system, Keizer et al. have reported the phase diagram of Bi_2O_3-ZrO_2-Y_2O_3 system.[8] However, precise phase boundary still remains obscure and ionic conduction of the fcc Bi_2O_3 solid solutions in the system has not been investigated. This system is of interest because fcc ZrO_2 and fcc Bi_2O_3, both stabilized with Y_2O_3, have basically same crystal structure and show similar oxygen-ion conduction. Since the melting points are markedly different for Bi_2O_3 (825 ℃) and ZrO_2 (abot 2700°C), simultaneous sintering of three components often gives inhomogeneous distribution of composition in sintered specimens,

resulting in an occurrence of second phases(monoclinic ZrO_2 or tetragonal Bi_2O_3).[8,9]

In this section, fcc Bi_2O_3 solid solutions were prepared by using powders of Bi_2O_3 and ZrO_2 both doped with same amount of Y_2O_3, and their oxygen-ion conduction was investigated.

EXPERIMENTAL

Two systems with different Y_2O_3 concentrations were examined. In system I, Y_2O_3 concentration was kept at 10 mol% in both Bi_2O_3 and ZrO_2: i.e. $(Bi_2O_3)_{0.9}(Y_2O_3)_{0.1}$ and $(ZrO_2)_{0.9}(Y_2O_3)_{0.1}$. In system II, Y concentration was kept at 20 at%: i.e. $(Bi_2O_3)_{0.8}(Y_2O_3)_{0.2}$ and $(ZrO_2)_{0.8}(YO_{1.5})_{0.2}$, which corresponds to 11.1 mol% Y_2O_3 in ZrO_2.

The Y_2O_3-doped Bi_2O_3 (BY) were prepared by calcining mixture of Bi_2O_3 and Y_2O_3 in Pt crucibles. Two calcining (at 800 and 850 °C for 5 h), quenching and grinding procedures were carried out in order to prevent from an occurring of metastable second phases. The Y_2O_3-doped ZrO_2 (ZY) were prepared by mixing ZrO_2 and Y_2O_3 in PSZ ball mills. Purities of the starting materials were all 99.99 %. The BY and ZY powders were mixed in a desired ratio, pressed into rectangular bars (5 by 5 by 15 mm) at 170 MPa, sintered at 930°C for 12 h, and cooled down to room temperature at 100°C/h. For some specimens, annealing at 500°C for 50 h was carried out.

The present phases were identified by X-ray diffraction measurements. Lattice constants were calculated by the least-square method using Si as an internal standard. The densities of the powdered specimens were measured at 25°C by the standard Archimedes method using toluene. Differential thermal analysis was carried out at heating rate of 5°C/min. The thermal expansion was measured with a dilatometer on sintered rods. The conductivity was measured by the complex impedance method at 350 to 800 °C. Platinum electrodes were applied by sputtering.

RESULTS AND DISCUSSION

The X-ray diffraction patterns of BY and ZY powders were of fcc monophases of Bi_2O_3 and ZrO_2, respectively, in both systems I and II. However, the diffraction peaks of BY in system I were somewhat broadened. Table 1 shows detected phases in sintered specimens. Diffraction peaks of fcc ZY were observed for specimens containing more than 14 mol% ZY in system I and 10 mol% ZY in system II, respectively. After annealing at 500°C for 50 h, small peaks of tetragonal Bi_2O_3 conuld be observed in system I. As the ZY concentration increased, lattice constant of fcc BY in system I increased up to 14 mol% ZY, while in system II it decreased up to 10 mol% ZY, as shown in Fig.1. These results imply that fcc solid solutions are formed in as-sintered specimens over those composition ranges, although the fcc phase in system I is not stable. The lattice constant of fcc Bi_2O_3 in Bi_2O_3-Y_2O_3 system is reported to show a monotonic decrease with increasing Y_2O_3 in the range 10-40 mol% Y_2O_3.[1] Also in the present systems, lattice constants in system II ($Y_2O_3 \approx 20$ mol%) were smaller than those in system I (Y_2O_3 10 mol%).

Table Ⅲ -1-1.
The Phases Observed in As-sintered and Annealed Specimens

System	x in $BY_{1-x}ZY_x$ (mole fraction)	Phases	
		as-sintered	annealed
I	0 - 0.14	δ	δ + $\underline{\beta}$
	0.16 - 0.80	δ + F	
II	0 - 0.10	δ	δ
	0.12 - 0.70	δ + F	

δ : fcc BY corresponding to δ-Bi_2O_3,
β : tetragonal BY corresponding to β-Bi_2O_3,
F : fcc ZY, under line indicates minor concentration.

For the fcc phases in Bi_2O_3-Y_2O_3[1] and Bi_2O_3-Er_2O_3[2] systems, it is reported that incorporated cations substitute for the Bi sites and two oxygen vacancies in a unit cell are almost retained; i.e. $Bi_{4(1-x)}M_{4x}O_6V_2$ where M is Y or Er and V is an oxygen vacancy. For the fcc ZrO_2-Y_2O_3 system, it is known that Y ions substitute for the Zr sites and corresponding oxygen vacancies are produced.

Theoretical densities in the present BY-ZY system were calculated from the measured lattice constants assuming the following three cases :

(1) Y and Zr ions substitute for the Bi sites,

(2) Y ions substitute for the Bi sites and Zr ions situate at interstitial sites,

(3) All Y and Zr ions from ZY situate at interstitial sites.

In Fig.2, the calculated densities for each model and the measured densities are plotted against ZY concentration for system I.The measured densities were in a good agreement with the calculated values for model (1) over the whole composition range measured. From this result, the composition at the solubility limit of ZY into BY can be estimated to be

$Bi_{3.30}Zr_{0.27}Y_{0.43}O_{6.13}V_{1.87}$ for system I and

$Bi_{3.03}Zr_{0.17}Y_{0.80}O_{6.08}V_{1.92}$ for system II, respectively.

the complex impedance plots consisted of two sections of semicircles, which were due to bulk resistance and cell capacitance at high frequencies and to electrode impedance at low frequencies. Figure 3 shows temperature dependences of conductivity of $BY_{1-x}ZY_x$ in system I (a) and II (b). In system I, a jump of conductivity at about 550°C was observed, and the activation energy for conduction was 32-36 kJ/mol above 600°C and 80-85 kJ/mol below 500°C. A thermal hysteresis in conductivity was also observed between the heating and cooling process. In system II, there was no jump in conductivity but the activation energy changed at 550°C. they were 49-54 and 108-110 kJ/mol above and below 550°C, respectively. This change in activation energy

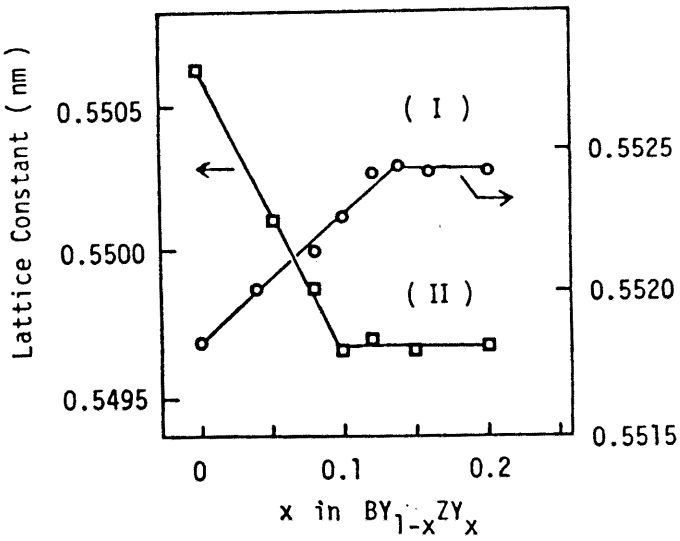

Fig. 1-1

Lattice constants of fcc Bi_2O_3 in systems I and II .

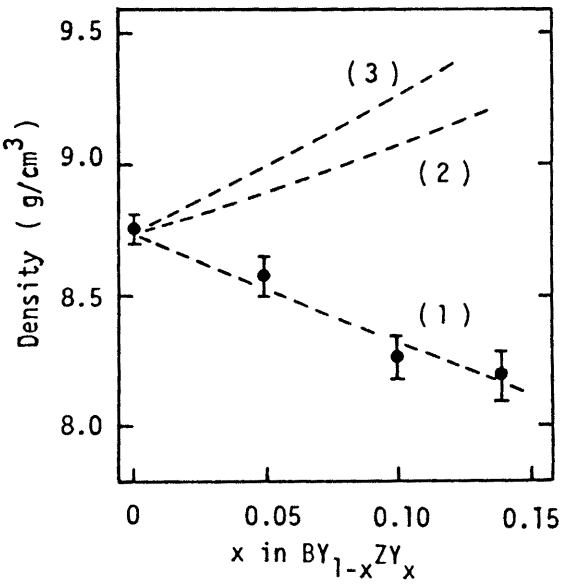

Fig. 1-2

Measured (●) and calculated densities assuming the models (1) - (3) described in the text for system I.

is generally observed in the fcc Bi_2O_3 solid solutions with low substituent concentrations.

The conductivities of $BY_{0.86}ZY_{0.14}$ (I) and $BY_{0.9}ZY_{0.1}$ (II) were independent on PO_2 in the region of 10^5-10^{-7}Pa at 500-800°C. This suggests that the oxygen-ion conduction is predominant in the above PO_2 region.

Composition dependences of conductivity are shown in Fig.4 for system I (a) and II (b). In both systems changes in conductivity above 600°C were small ; only slight decreases of conductivity were noticed in specimens with high ZY concentrations. At below 550°C, as the ZY concentration increased, the conductivity decreased in system II but incresed in system I in spite of decreasing concentration of oxygen vacancy. In specimens containing ZY more than the solubility limits ($BY_{0.86}ZY_{0.14}$ (I) and $BY_{0.9}ZY_{0.1}$ (II)), the conductivity decreased with increasing ZY concentration in both systems. As a result, the highest conductivity at low temperature was achieved in $BY_{1.0}$ in system II and $BY_{0.86}ZY_{0.14}$ in system I.

In the fcc Bi_2O_3 solid solutions with low substituent concentrations, it has been reported that positions of oxygen ions are displaced from the normal tetrahedral sites and distributed statistically around the normal sites.[10,11] the low activation energy at high temperatures in the present systems would be due to this type of disordering of oxygen ions, and hence conductivity would not be changed so much by changes in composition or oxygen vacancy concentration. At low temperatures, oxygen ions are bound at one position with some displacement, where positional disorder is only among the normal sites.[10,11] In this disordering state the conductivity decreases with increasing dopant concentration, as described in Chap.II-5. The conduction behavior in system II at low temperatures is due to such a short-range ordered oxygen sublattice.

Increase in lattice constant(Fig.1) and conductivity at low temperatures(Fig.4) with increasing ZY concentration in system I

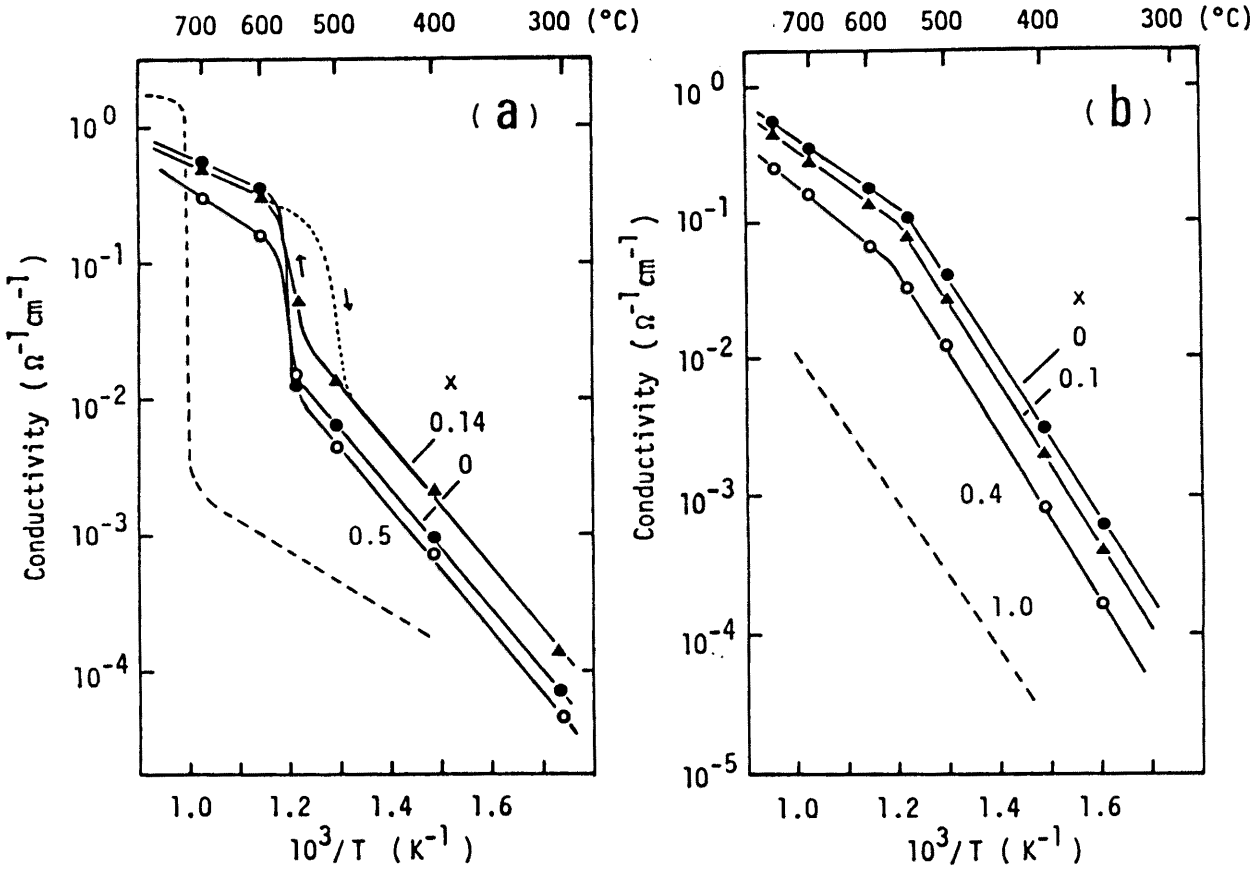

Fig. 1-3.

Temperature dependences of conductivity of $BY_{1-x}ZY_x$ in systems (**a**) I and (**b**) II. The broken line represents the conductivity of (**a**) pure Bi_2O_3 and (**b**) ZY.

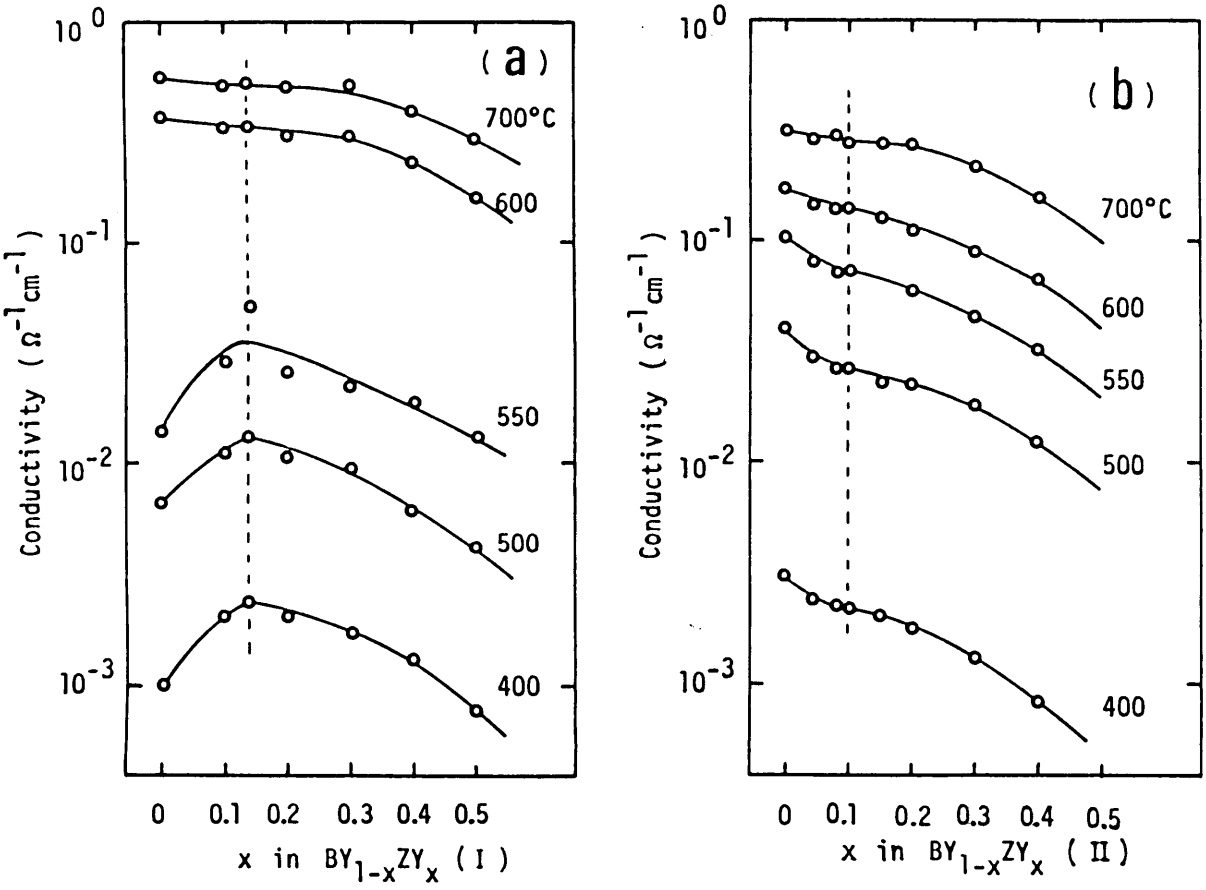

Fig. 1-4.

Composition dependences of conductivity of $BY_{1-x}ZY_x$ in system (**a**) I and (**b**) II . The broken line represents the solubility limit of ZY.

cannot be explained by the order-disorder transition described above. In addition, the jump of conductivity at about 550°C is not due to a simple phase segregation, because the conductivity was further decreased about half order of magnitude after annealing (appearence of tetragonal phase). The volume, measured with a dilatometer in system I, incresed about 0.17 % at 570-600 °C on heating, and decreased about 0.10 % at 460-500°C on cooling. Differential thermal analysis also showed a small endothermic peak at 570 °C on heating. These temperatures almost agree with those of jumps in conductivity. Probably, the fcc structure of Bi_2O_3 solid solution in system I would be distorted tetragonally as a quasi-equilibrium state at low temperatures due to small Y_2O_3 concentration. Broadened diffraction peaks also suggest the distortion of the fcc structure. Accordingly, as the ZY concentration increases, this distortion would be decreased resulting in increases in lattice constant and conductivity.

By comparing the conduction behavior and the composition in systems I and II, ZrO_2 was found to have some contribution to the stabilization of fcc Bi_2O_3 but to be not so effective as Y_2O_3.

CONCLUSION in **III**-1

(1) In Bi_2O_3-ZrO_2-Y_2O_3 system, fcc Bi_2O_3 solid solutions without any second phases can be fabricated by using Y_2O_3-doped Bi_2O_3 (BY) and Y_2O_3-doped ZrO_2 (ZY).

(2) In system with Y concentration of 20 at%, the fcc phase was formed at 0 - 10 mol% ZY and oxygen-ion conductivity decreased with increasing ZY. In system with Y_2O_3 concentration of 10 mol%, metastable fcc phase was formed at 0 - 14 mol% ZY and the conductivity below 600°C increased with increasing ZY in the fcc monophase region but decreased in two-phase (BY and ZY) region.

(3) There was a correlation between lattice constant and conductivity at low temperatures. A high conductivity was obtained in specimen with a large lattice constant in both systems I and II.

(4) Addition of ZrO_2 was found to have some contribution to the stabilization of fcc Bi_2O_3 but it was not so effective as that of Y_2O_3.

REFERENCES in **III**-1

1. T. Takahashi, H. Iwahara and T. Arao, J. Appl. Electrochem., 5, 187 (1975).
2. M.J. Verkerk, K. Keizer and A.J. Burggraaf, J. Appl. Electrochem., 10, 81 (1980).
3. M.J. Verkerk and A.J. Burggraaf, J. Electrochem. Soc., 128, 75 (1981).
4. H. Iwahara, T. Esaka, T. Sato and T. Takahashi, J. Solid State Chem., 39, 173 (1981).
5. H.T. Cahen, T.G.M. Van Den Belt, J.H.W. De Wit and G.H.J. Broers, Solid State Ionics, 1, 411 (1980).
6. T. Takahashi, H. Iwahara and T. Esaka, J. Electrochem. Soc., 124, 1563 (1977).
7. F. Hund, Z. Anorg. Allg. Chem., 333, 248 (1964).
8. K. Keizer, M.J. Verkerk and A.J. Burggraaf, Ceram. Int., 5, 143 (1979).
9. K. Keizer, A.J. Burggraaf and G. De With, J. Mater. Sci., 17, 1095 (1982).
10. M.J. Verkerk, G.M.H. van de Velde, A.J. Burggraaf and R.B. Helmholdt, J. Phy. Chem. Solids, 43, 1129 (1982).
11. K. Koto, H. Mori and Y. Ito, Solid State Ionics, 18 & 19, 720 (1986).

III - 2. Microstructure and conductivity in Bi_2O_3 - ZrO_2 composites

INTRODUCTION

Among oxygen ion conductors, fcc Bi_2O_3 stabilized by doping of Y_2O_3 or rare-earth oxides is known to show the highest conductivity. The conductivity is one or two orders of magnitude higher than that of stabilized ZrO_2 at corresponding temperatures.

In stabilized zirconia, oxygen ionic conduction is predominant (ionic transport number > 0.99) over a wide range of oxygen partial pressure (PO_2) down to about 10^{-15} Pa at 1000°C.[1] In contrast, stabilized Bi_2O_3 is easily reduced under low PO_2 and decomposed into Bi metal at PO_2 of about 10^{-8} Pa at 600°C.[2] Accordingly, stabilized Bi_2O_3 is not suitable for practical use under very low PO_2 at high temperatures such as fuel cells. In addition, the mechanical strength of Bi_2O_3-based materials is not high enough to fabricate complicated-shape devices.

The system of stabilized fcc Bi_2O_3 and fcc ZrO_2 is of interest in vies of improvement of above electrical and mechanical properties. In the last section, it was found that solid solutions and composites, consisting of fcc phases of Bi_2O_3 and ZrO_2, are obtained by using powders of fcc Bi_2O_3 and ZrO_2 both doped with Y_2O_3 as starting meterials.

In the present section, microstructure and electrical conductivity of the composites were investigated, and the observed conductivity was compared with values calculated by using various mixing rules.

EXPERIMENTAL

In the present system, Yttrium concentration was kept constant at 20.0 ca.% i.e. $(Bi_2O_3)_{0.8}(Y_2O_3)_{0.2}$ (denoted as BY) and $(ZrO_2)_{0.8}(YO_{1.5})_{0.2}$(ZY), respectively (system **II** in the last section).

The powders of BY and ZY were prepared as described in**III**-1. Particle size distribution of the resulting powders were measured with a centrifugal particle size analyzer. Two kinds of powders were mixed in a desired ratio, pressed into rectanglar bars at 170 MPa, and sintered at 930°C for 12 h in air. For ZY-rich (>50 mol% ZY) specimens with low sinterbility, hot-pressing was performed at 900°C under 10 MPa for 6 h in air on pre-sintered (800°C) specimens.

The present phases in the samples were identified by X-ray diffraction. The microstructure of the sintered samples were examined with the scanning electron microscope (SEM) and electron probe micoanalysis (EPMA).

The electrical conductivity was measured by the method described in III-1.

RESULTS AND DISCUSSION

More than 60 % of powder particles before final sintering were 1-7 μm in size for BY and 1-5 μm ZY, and average particle sizes were estimated to be 3.3 μm for BY and 2.2 μm for ZY, respectively.

Figure 1 shows the X-ray diffraction patterns of $BY_{0.9}ZY_{0.1}$, $BY_{0.45}ZY_{0.55}$ (mole fraction), and ZY. Diffraction peaks of fcc BY and fcc ZY monophses were observed in the composition range $x \geqq 0.90$ and $x \leqq 0.02$ for BY_xZY_{1-x}, respectively. In the range of $0.02 < x < 0.90$, both BY and ZY peaks were observed and there were no peaks of second phases other than the fcc phases.

In the monophasic region, lattice constant of fcc BY decrease with increasing ZY concentration as shown in Fig.III-1-1. Lattice constant of fcc ZY increased by adding of BY from 0.5142 nm (0 mol% BY) to 0.5154 nm (2 mol% BY). In the two-phase region, the lattice constants of BY and ZY were almost constant. As a result, specimens BY_xZY_{1-x} in the composition range of $0.02 < x < 0.90$ can be regarded as composites consisting of two fcc phases of $BY_{0.9}ZY_{0.1}$ (BY_{ss}) and $BY_{0.02}ZY_{0.98}$(ZY_{ss}).

Porosities were 6-13 % in normal-sintered specimens with $x > 0.6$ and 1-6 % in hot-pressed specimens. Normal-sintering at high temperatures $> 1100°C$ also gave dense spesimens even at $x > 0.5$, but tetragonal β-Bi_2O_3 appeared as a second phase.

Figure 2 shows a polished surface of $BY_{0.7}ZY_{0.3}$ and $BY_{0.2}ZY_{0.8}$, and relative X-ray intensities of Bi and Zr. The dark particles are found to correspond to ZY_{ss}. The ZY_{ss} particles, 1-3 μm in size, were observed to be dispersed in BY_{ss} matrix. In monophasic specimens as $BY_{0.9}ZY_{0.1}$, Bi, Zr and Y atom were distributed homogeneously.

Most of the impedance plots consisted of two sections of semicircle due to grain and electrode impendence . A small semicircle in middle frequency region, which is associated with grain boundary, appeared only in the plots for specimens containing more than 40 mol% ZY below 500°C. Since the contribution of the grain-boundary impendance did not exceed 4 % of total impedance, the end-point of the first semicircle was taken as the resistance to calculate conductivity in the present study.

The temperature dependence of conductivity σ in typical specimens in the BY-ZY system are shown in Fig.3. Conductivity

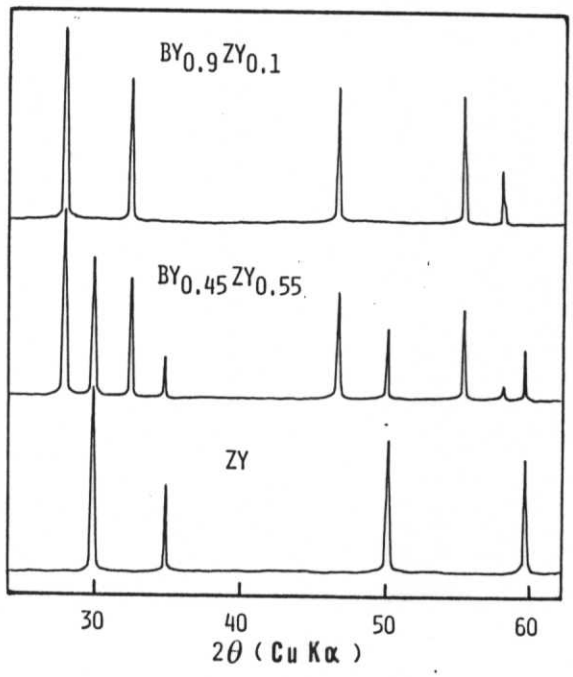

Fig. 2-1.

X-ray diffraction patterns of $BY_{0.9}ZY_{0.1}$, $BY_{0.45}ZY_{0.55}$ and ZY.

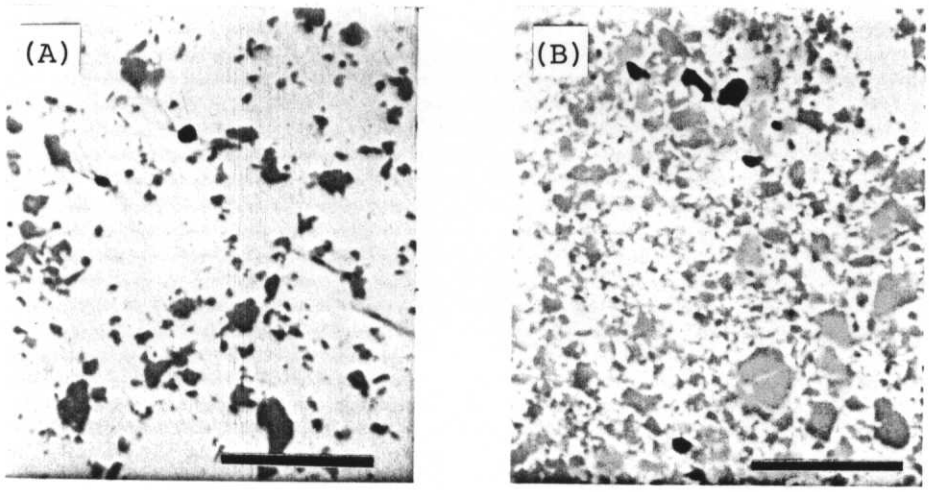

Fig. 2-2.

Scanning electron micrograph of polished surface of (A) $BY_{0.7}ZY_{0.3}$, (B) $BY_{0.2}ZY_{0.8}$ (bars = 10 μm).

(continued)

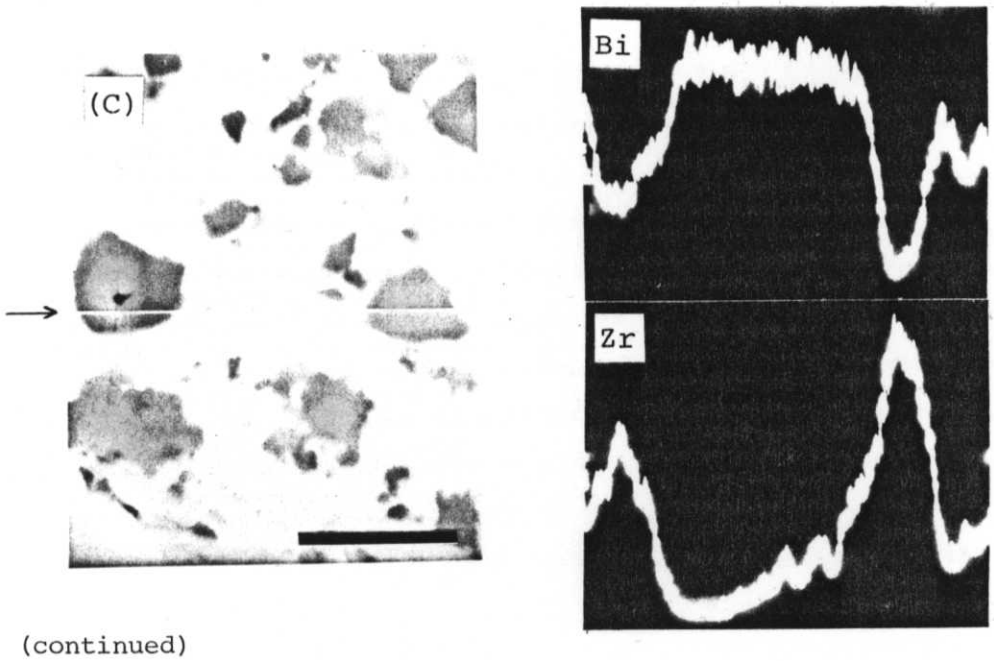

(continued)

(C) $BY_{0.45}ZY_{0.55}$ (bar = 5 μm) and relative X-ray intensities of Bi and Zr on line indicated in (C).

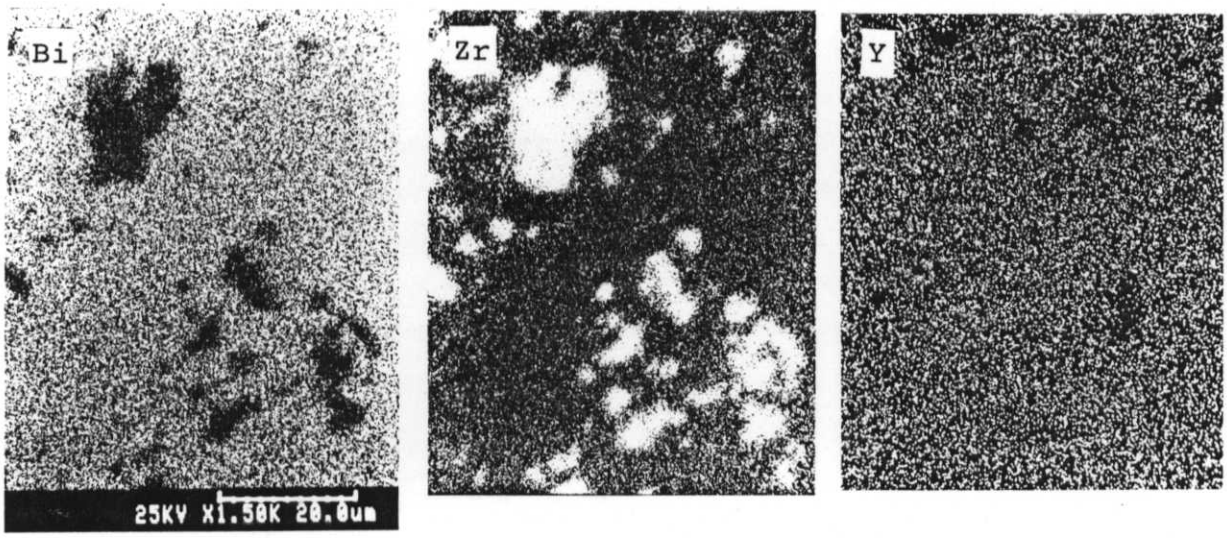

(D) Distributions of Bi, Zr and Y in $BY_{0.7}ZY_{0.3}$.

(Some aggregates are observed)

of ZY was of specimen sintered at 1500°C for 5 h. A bend in the Arrhenus plot (a change in activation energy) at about 550°C was observed in all specimens except for ZY solid solutions. Appearence of this change in activation energy indicates that there is no marked change of conduction mechanism in BY solid solutions and in individual BY_{ss} particles of composites.

Figure 4 shows the composition dependence of conductivity in the BY-ZY system. Both in the solid solution and composite region, conductivity decreased as the ZY concentration increased.

The dependence of conductivity on PO_2 for $BY_{1-x}ZY_x$ with x = 0, 0.1 and 0.4 at 800°C are shown in Fig.5. The conductivities were kept constant under the PO_2 between 10^5 and about 10^{-7} Pa, indicating oxygen conduction to be dominant. The conductivities decreased at PO_2 below 10^{-7} Pa. Specimens annealed at the low PO_2 contained β-Bi_2O_3ss, and Bi metal was precipitated on surface of the specimens. For the macroscopically homogeneous composites as in the present study, applicable PO_2 range for solid electrolyte was confirmed to be determined by the dissociation PO_2 of BY_{ss} component.

Numerous equations have been derived in an attempt to calculated the effective conductivity of heterogeneous materials, in general for two-phase systems.

Maxwell derived an expression for the effective conductivity of a solid consisting of sperical particles of one phase dispersed in a continuous matrix phase :

$$\sigma = \sigma_1 \frac{\sigma_2 + 2\sigma_1 + 2V_2(\sigma_2-\sigma_1)}{\sigma_2 + 2\sigma_1 - V_2(\sigma_2-\sigma_1)} \qquad (1)$$

where subscript 1 refers to the matrix, subscript 2 to the dispersed phase, and v's are their volume fractions.[3] In this equation, it is generally assumed that the perturbation of the electric field around one particle dose not influence the field around the other particles. This requires that the particles are well separated, and as a result the equations are applicable only

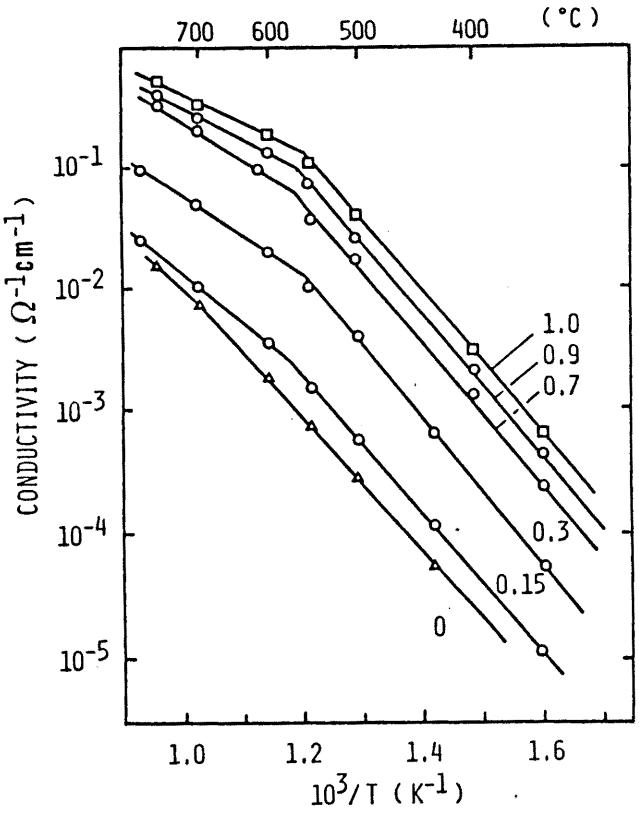

Fig. 2-3.
Temperature dependence of conductivity in BY_xZY_{1-x}.
Numbers indicate x.

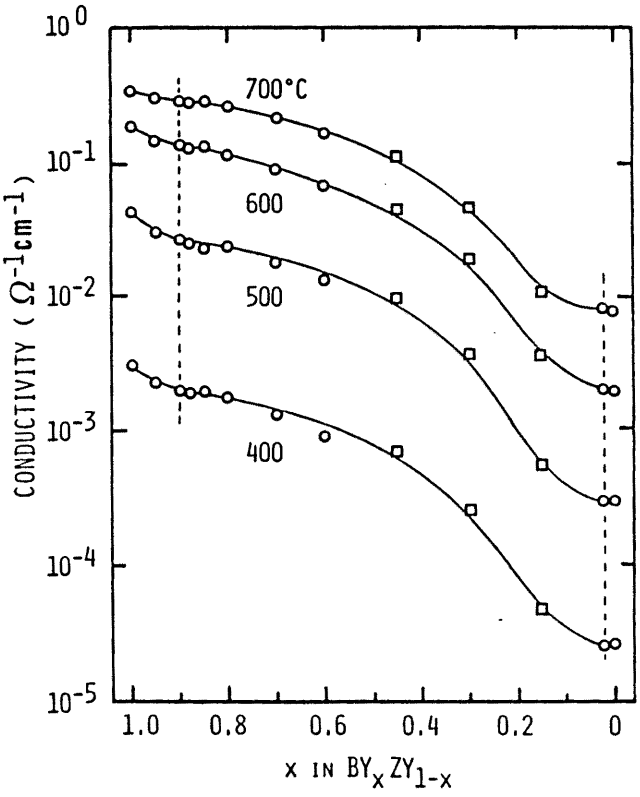

Fig. 2-4.
Composition dependence of conductivity in BY_xZY_{1-x} measured for normal-sintered (●) and hot-pressed (■) specimens. Dashed lines indicate solubility limits.

up to a particle volume fraction v_2 <0.15. This equation is often used for the porosity-correction of conductivity.

In order to expand the applicable region of valume fraction, the effective-medium theory was proposed by Landauer[4]. This theory is assumed that each additional particlesis dispersed in a medium of some effective conductivity determined by the amount of dispersed phase already present. Landauer derived an equation in the case where there is no correlation betweenn the positions of the two types of particles, as

$$\sigma = \frac{1}{4}\left\{(3V_1-1)\sigma_1 + (3V_2-1)\sigma_2 + \left[\left\{(3V_1-1)\sigma_1 + (3V_2-1)\sigma_2\right\}^2 + 8\sigma_1\sigma_2\right]^{1/2}\right\} \quad (2)$$

where subscripts 1 and 2 mean just two types of the phases.

Another method, percolation theory, can be used in the system consisting of conducting particles and insulting particles. Electrical current can flow through the system only when there is a sompleted path of adjacent conducting particles crossing the system. Kirkpatrick[5] and Pike et al.[6] calculated the effective canductivity of such random resistive networks statistically using Monte Carlo techniques :

$$\sigma(V) = A(V - V_c)^t \quad (3)$$

where v is the volume fraction of the conductive phase and V_c is the critical volume fraction enable to make a completed conduction path and A and t are constants (t = 1.5-1.6)

For the case of a macroscopically homogeneous and isotropic two-phase material, Hashin et.al derived expressions for the upper and lower bounds of the effective conductivity, σ_u and σ_l [7] as

$$\sigma_u = \sigma_B + \frac{V_A}{[1/(\sigma_A-\sigma_B)] + (V_B/3\sigma_B)} \quad (4a)$$

$$\sigma_l = \sigma_A + \frac{V_B}{[1/(\sigma_B-\sigma_A)] + (V_A/3\sigma_A)} \quad (4b)$$

where $\sigma_A < \sigma_B$. Although derived in an entirely independent manner, Eqs.4a and 4b are just the same with the Maxwell's equation 1 for the two case ; component A dispersed in B (σ_u) and B in A (σ_l).

Figure 6 shows conductivities at 500°C in the composite region ($0.02 < x < 0.9$) plotted against the volume fraction of ZY_{ss} (V_{ZY}). The volume fractions were calculated from composition and unit-cell volumes of BY_{ss} and ZY_{ss}. In order to eliminate the porosity effct, porosity correction was being made on conductivity in normal-sintered specimens using the Maxwell's equation with $\sigma_2 = 0$ for pores. In Fig. 6, calculated conductivities by using Eqs. 1-4 are also presented for comparison. The calculated conductivity P was that obtained by applying the tentative values $V_c = 0.1$, $t = 1.55$ and $A = 3.6 \times 10^{-2}$ into Eq.3.

The measured conductivities were situated between the upper and lower bounds, and approximately agreed with the values of the effective-medium theory and the percolation theory suggesting that a correlation between the positions of the two kinds of particles is small. However, the measured values were a little higher than the calculated values in specimens with ZY > 50 mol%.

The V_c value (the minimum volume fraction for a completed conduction path) in Eq.3 is reported to be dependent on the arrangement of particles, and has been calculated statistically to be 0.3 for single cubic and 0.2 for fcc lattice arrangements.[5] The obtained V_c value of 0.1 in the present system is smaller than those theoretical values. This suggests that conductive BY_{ss} particles are well-connected than in the case of random distribution. On SEM observation (Fig.2.b), BY_{ss} appeares to be well-connected than ZY_{ss} particles. Probably, the preferential arrangement of BY_{ss} would be a cause for a little higher conductivity than that of effective-medium approximation. However, it is not clear whether this preferential arrangement is due to a low melting point of BY or to hot-pressing.

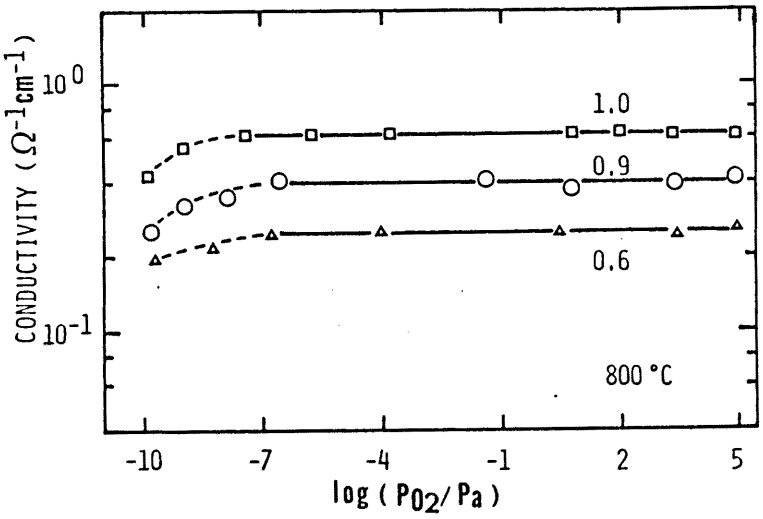

Fig. 2-5.

PO_2 dependence of conductivity in BY_xZY_{1-x}. Numbers indicate x.

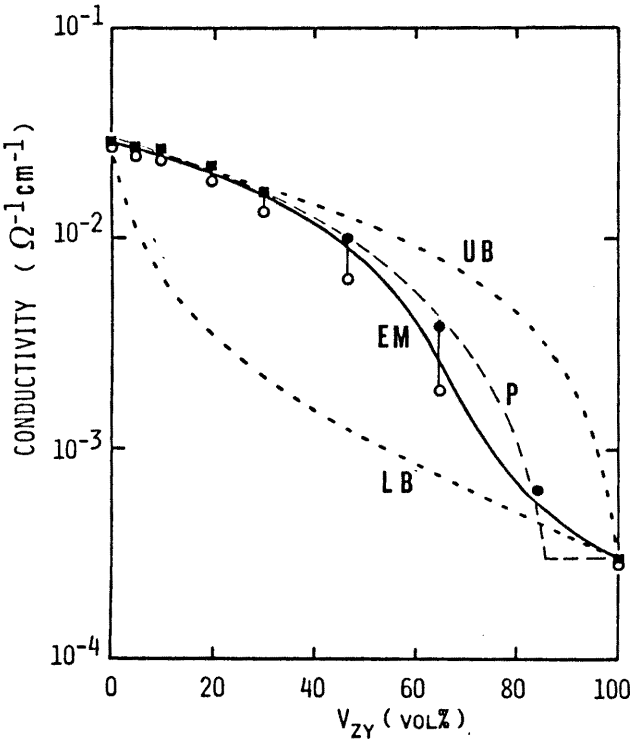

Fig. 2-6.

Conductivity in composites at 500°C vs. volume fraction of ZY_{SS}; ○ ,● measured for normal-sintered and hot-pressed specimens, and ■ porosity-corrected. Lines UB and LB are calculated upper and lower bounds, EM by effective-medium theory, and P by percolation theory.

CONCLUSION in III-2

(1) In the system fcc Bi_2O_3 (BY) - fcc ZrO_2 (ZY) stabilized with Y_2O_3 (Y : 20 at%), composites appeared in the range of $0.02 < x < 0.90$ for BY_xZY_{1-x} (mole fraction).

(2) The conductivity decreased with increasing ZY concentration. The composition dependence could be explained by using an effective-medium theory, suggesting a random distribution of the two kinds of particles. However, BY particles seemed to be well-connected than ZY particles in ZY-rich region.

(3) The PO_2 range, in which the composite shows oxygen ionic conduction, was almost same to that of Bi_2O_3 solid solutions.

REFERENCES in III-2

1. T.H. Etsell and S.N. Flengas, J. Electrochem. Soc., 119, 1 (1972).
2. T. Takahashi, T. Esaka and H. Iwahara, J. Appl. Electrochem., 7, 303 (1972).
3. J. C. Maxwell, in "Treatise on Electricity and Magnetism, Vol.1" 3rd ed. (Clarendon Press, London, 1892).
4. R. Landauer, J. Apple. Phy., 23, 779 (1952).
5. S. Kirkpatrick, Rev. Mod. Phys., 45, 574 (1973).
6. G.E. Pike, W.J. Camp, C.H. Seager and G.L. McVay, Phys. Rev. B, 10, 4909 (1974).
7. Z. Hashin and S. Shtrikman, J. Appl. Phys., 33, 3125 (1962).

III - 3. Conclusion in Chapter III

The Y_2O_3-stabilized fcc Bi_2O_3 (BY) and fcc ZrO_2 (ZY) have basically same crystal structure but they have some different characteristics ; the BY has a high oxygen-ion conductivity and good sinterbility (low m.p. 825°C), and the ZY has good stability under low PO_2 and high temperatures (m.p. $\simeq$ 2700°C) and a high mechanical strength. In Chapter III, the ionic conduction behavior in solid solutions and two-phase mixed composites in the BY-ZY system were investigated. Results can be summarized as follows ;

(1) By using stabilized BY and ZY powders, it was succeeded to fabricate solid solutions and BY-ZY composites without any second phases.

(2) The solubility limit of ZY into BY depended on Y_2O_3 concentration : 14 mol% ZY for BY with 10 at% Y, and 10 mol% ZY with 20 at% Y. In the solid solutions, incorporated Zr and Y ions substituted for the Bi ion sites.

(3) In the system with 20 at% Y, composites appeared in the range of $0.02 < X < 0.90$ for BY_xZY_{1-x}, which consisted of particles

with the end compositions.

(4) the oxygen-ion conductivity decreased with increasing ZY content in both solid solutions and composites. However, only for BY solid solutions with 10 at% Y, the conductivity increased at low temperatures due to stabilization of fluorite structure by doping of ZY.

(5) In the composites, it was suggested that two-kinds of particles are randomly distributed and the both contribute to the ionic conduction without marked interference at interfaces.

(6) The PO_2 range , in which the composite shows oxygen-ion conduction, was determined by that of BY.

In the present study, the conduction behavior was investigated only for a macroscopically homogeneous composite. However, artificially-designed composites, i.e. a composite consisted of layers with different composition or a composite in which the composition changes continuously, would be possible to be fabricated on the basis of the present fabrication process and the fundamental conduction behavior. Although mechanical properties bave not been examined in the present study, an improvement or control of electrical and mechanicl properties would be achieved in such a structure-controlled composites.

Chapter IV

Grain-Boundary Resistivity in Y_2O_3-Stabilized ZrO_2

IV - 1. Dependence of grain-boundary resistivity on grain-boundary density

INTRODUCTION

There have been many investigations of the contribution of grain boundaries to ionic condition in stabilized zirconia ceramics; this contribution is known to become important at lower tempetures, where it often causes practical problems in their use. Grain boundaries cause not only an increase in the overall resistivity but also introduce undesirable time responses in the emf of zirconia oxygen monitors[1] and large increases in resistivity after annealig.[2]

Recent progress in the preparation of zirconia powders, such as the alkoxide method and the precipitation method, makes it easy to obtain dense, pure stabilized-zirconia ceramics with small grain sizes. However, these methods do not necessarily lead to low grain-boundary resistivity.

The influence of microstructure, especally grain size, on grain-boundary resistivity has been reported by several workers.[3-8] Ioffe et al.[4] found that the overall grain-boundary resistivity at 450°C decreases by more than an order of magnitude when the grain size is increased from 0.2 to 18 μm in ZrO_2-5,7mol% Y_2O_3 prepared by alkoxide synthesis. These workers also

indicated a decrease in the resistance per square centimeter of grain-boundary surface with increasing grain size above 2.4 μm. Verkerk et al.[7] have reported that, for high-purity $(ZrO_2)_{0.836}$-$(YO_{1.5})_{0.164}$ and $(ZrO_2)_{0.86}(YO_{1.5})_{0.14}$ containing > 0.1 wt% Ca and Ti, the grain-boundary resistivity decreases linearly with grain size for small grain sizes (0.3 to 4 μm) and is constant for larger grain sizes up to 13.5 μm.

However, overall resistivity and resistance per unit grain-boundary area depend strongly on composition, impurity concentration and preparation method; hence, the influence of microstructure on grain-boundary resistivity has not yet been interpreted coherently. In the present section, the influence of grain-boundary density on the grain-boundary resistivity and resistance per square centimeter of grain-boundary surface of Y_2O_3-stabilized ZrO_2 films was investigated, and the origin of grain-boundary resistivity was discussed.

EXPERIMENTAL

Zirconia films were made by a modified doctor blade method.[9,10] A mixture containing (in mol%) 92 ZrO_2, 8 Y_2O_3, and 0.5 $FeSO_4.7H_2O$, and an aqueous solution containing 5.0 mol% $Al(NO_3)_3\ 9H_2O$ were ground and calcined at 1400°C for 6 h. The resultant powders were dispersed in an aqueous solution containing 5 wt% methylcellulose and ground for 1 h in an agate mill. Green sheets were made on a glass plate with an applicator for thin-layer chromatography. A film, 200 to 300 μm thick, was obtained after drying. Disks 6 mm in diam. cut from the sheet were heated to 300°C at a rate of 75°C/h and held for 1 h to decompose and evaporate the organic binder. The resultant powder was pressed at 20 MPa onto a polystyrene film. The compacted granular film on the polystyrene was placed in a Pt container and heated to 400°C for 1 h, followed by sintering at 1700°C for 2 to

5 h. Final composition can be estimated as

$Zr_{0.825}$-$Y_{0.140}$-$Al_{0.050}$-$Fe_{0.005}$-$O_{1.9025}$.

The grain-boundary density was used to characterize the microstructure of specimens.[11,12] The grain-boundary density, D, (number of grain boundaries per unit length) was determined from N/nL, where N is the total number of intersections of grain boundaries with grid lines drawn perpendicular to the film surface for each 5 μm on micrographs of the fracture surfaces, n the number of grid lines, and L the length of the grid lines (the film thickness). The D values were estimated from more than 300 grid lines for each sample.

Alternating-current resistivity was measured for sintered films and thin plates of commercial single-crystal ZrO_2-8 mol% Y_2O_3 at 300-500°C. Silver electrodes were placed on both surfaces of the films by vacuum evaporation, and Ag lead wires were baked on with Ag paste. High-power X-ray diffraction analysis showed that the specimens had the fluorite structure and there was no peaks of second phase. Microstructure was examined with scanning electron microscope and electron prove microanalysis.

RESULTS AND DISCUSSION

Figure 1 shows a fracture surface, film surface, and electron probe micrographs which indicate the Al and Fe ditributions. The films were 100 μm thick. Grain size was 10 to 70 μm. It can be observed that Al is enriched at grain boundareis.

Figure 2 shows typical imdepence plot for the sintered films and single-crystals and a postulated equivalent circuit.[3.6.7.] Comparison of the impedance plots indicates that the second semicircle in the plot for the sintered films is associated with grain-boundary dispersion.

The resistivities of the grain (ρ_b) and grain boundary (ρ_{gb}) were calculated from

$$\rho_b = R_3 S/L \qquad (1)$$

$$\rho_{gb} = R_2 s/L \qquad (2)$$

where S is the electrode area. The activation energy of the resistivity, given by Arrhenius plot at 300 to 500 °C, was 92 - 95 kJ/mol for the grain and 113 - 124 kJ/mol for the grain boundary.

Figure 3 shows the grain and grain-boundary resistivities at 400 C as a function of the grain-boundary density D. Both resistivities are almost independent of D. The resistance per square centimeter of grain-boundary surface (R_{gb}) was calculated from

$$R_{gb} = \rho_{gb}/D \qquad (3)$$

and shown in Fig.4. The R_{gb} value decreased with increasing D.

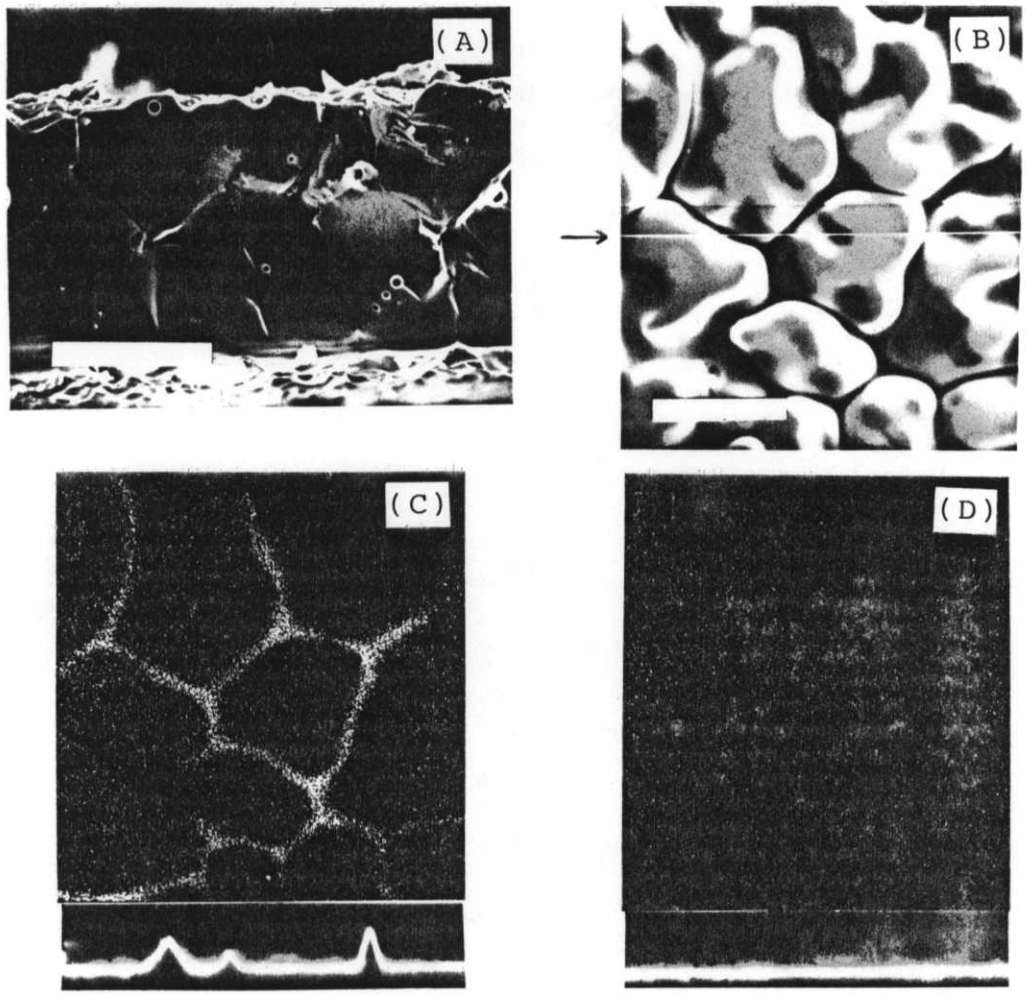

Fig.1-1.

Scanning electron micrographs of (A) fracture surface (bar = 50 μm) and (B) film surface (bar = 20 μm) and electron probe micrographs of (C) Al and (D) Fe distribution on surface (B) and relative intensity of Al and Fe on line shown in (B).

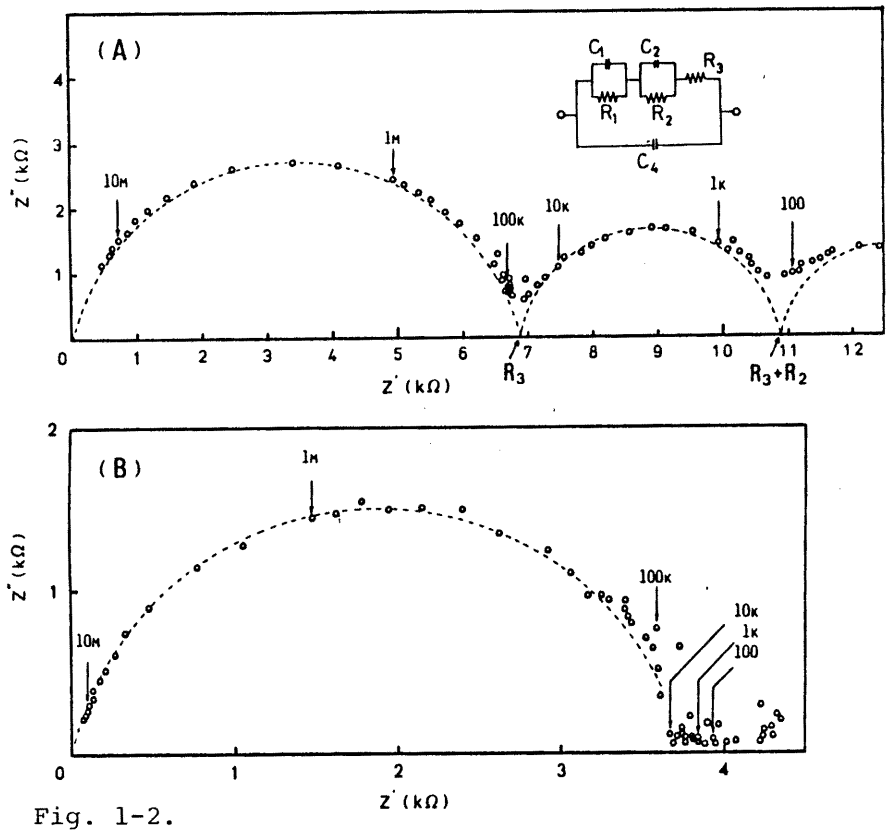

Fig. 1-2.
Impedance plots for (A) sintered specimen and (B)single crystal and an equivalent circuit. R and C are resistances and capacitances ; R_1,C_1:electrode, R_2,C_2:grain boundary, R_3:grain, C_4:cell capacitance.

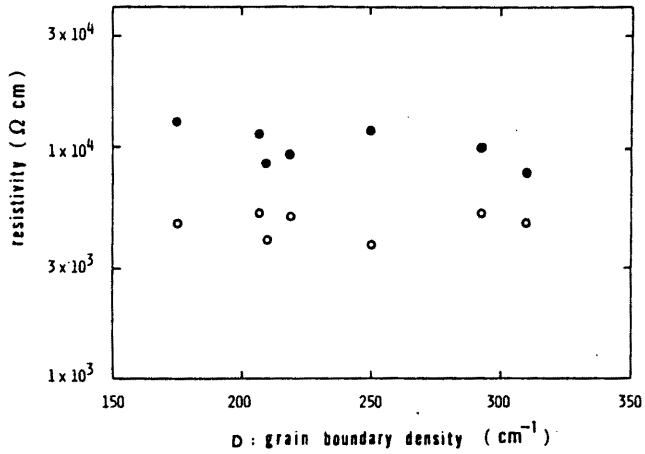

Fig. 1-3.
(●)Grain and (o)grain-boundary resistivity vs. grain-boundary density at 400°C.

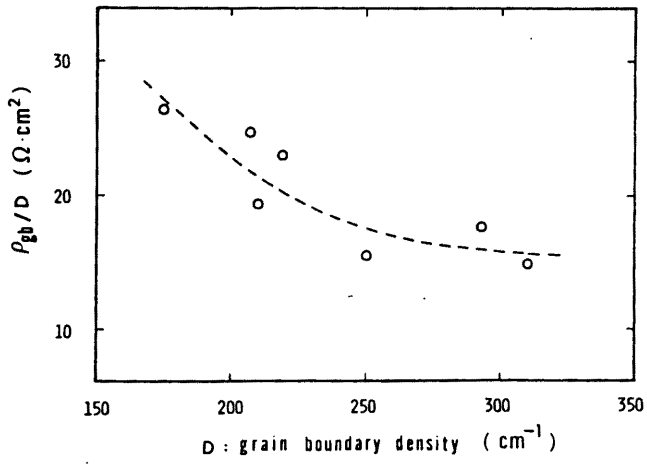

Fig. 1-4.
Resistance per cm^2 of grain-boundary surface vs. grain-boundary density at 400°C.

It is known that Fe_2O_3 increases the resistivity of stabilized zirconia.[13,14] Alumina was reported to have the same effect[14.15] or no effect.[16,17] The solubility limits of Fe_2O_3 and Al_2O_3 in YSZ are reported to be 1.1 mol% at 1142 - 1172°C[14] and 4.35 mol % at 1400°C[13] for Fe_2O_3, and 0.1 mol% at 1300°C for Al_2O_3.[14] For the specimens in the present study, the Al_2O_3 concentration far exceeded the solubility limit, and the grain boundaries were found to be enriched in Al, as shown in Fig. 1.C.

The grain-boundary resistivities at 400°C, obtained in the present study and reported in literature[4,7], were summarized in a log-log plot as shown in Fig.5. Two regions can be observed, i.e. R_{gb} is independent of D in the low-D region and increases with increasing D in the high-D region. The grain-boundary resistivities for samples containing impurities seem to be higher than those for pure samples in the low-D region. Figure 6 shows the D dependance of R_{gb} at 400°C. The R_{gb} decrease with increasing D in the low-D region and are independent of D in the high-D region.

The fundamental origin of grain-boundary resistivity in stabilized zirconia has not yet been clarified, although many theories have been discussed, e.g. decrease of concentration and mobility of oxygen vacancies caused by space charges, segregation of impurities or components, and formation of second phases.[3,5-6,14,16] If space charges resulting from the irregularity of the lattice can account for the resistance of the grain-boundary surface, the R_{gb} value should be constant, i.e. independent of D. Also, in the case of the segregation of principal components, e.g. Y^{3+} and Zr^{4+}, this effect would not change very much with D. In such cases, the grain-boundary resistivity is determined only by the number of grain blundaries and hence increases with increasing D. The D dependences of σ_{gb} and R_{gb} in the high-D region in Figs.5 and 6 probably can be explained by these intrinsic effects of space charges and segregation of the principal components at grain boundaries. Differences in the R_{gb} values at a fixed D in the high-D region are assumed to be due to

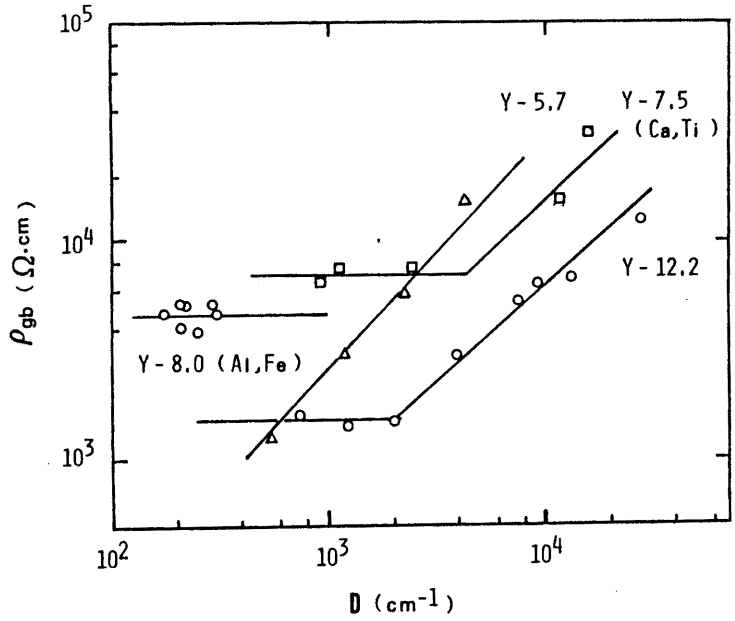

Fig. 1-5.

Grain-boundary resistivity as a function of grain-boundary density in Y_2O_3-stabilized ZrO_2 at 400°C. Numbers indicate Y_2O_3 content (in mol%) and elements in ( ) main impurities.
● , ■ from ref.7, ▲ ref.4.

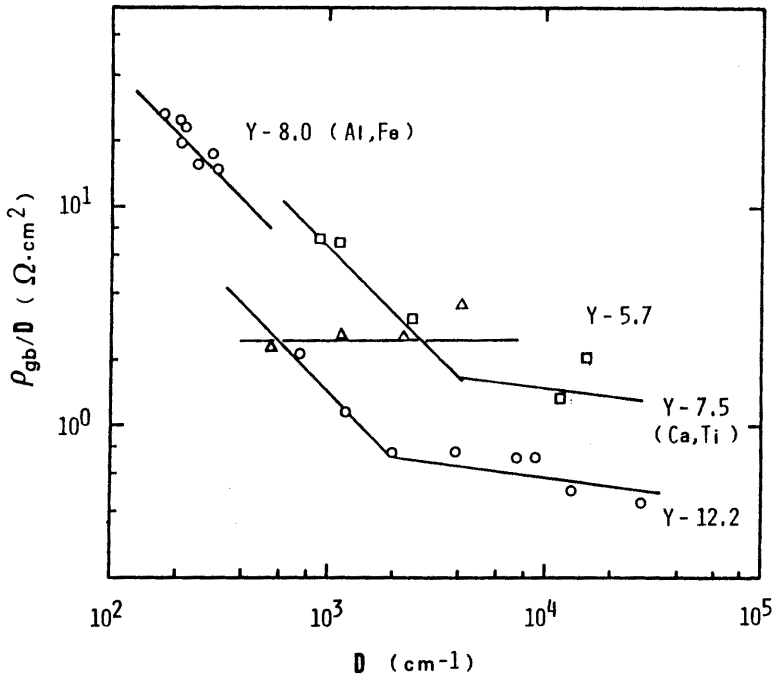

Fig. 1-6.

Resistance per cm^2 of grain-boundary surface as a function of grain-boundary density at 400°C.

differences in composition and preparation method.

In contrast, when segregation of impurities or second phases dominate the resistance of the grain-boundary surface, they should be affected by a change in D. Since the total amount of impurities in a unit volume is constanat, it is expected that the concentration of impurities per square centimeter of grain-boundary surface will decrease as D increases. The decreasing R_{gb} with incerasing D in the low-D region shown in Fig. 6 could be explained by an extrinsic effect, i.e. changes in segragation state or second phase volume and subsequent changes in space charge, associated with a decrease in the concentration of impurities at a grain boundary.

From these results, it is suggested that low grain-boundary resistivity can be achieved in stabilized zirconia ceramics with high purity and low grain-boundary density.

CONCLUSION in **IV**-1

(1) For the stabilized zirconia films using Al_2O_3 as a sintering agent, it is indicated by electron probe analysis that the Al concentration was preferentially enriched near grain boundaries, although only cubic zirconia was detected by X-ray diffraction.

(2) In the ZrO_2 films containing Al_2O_3, the grain and grain-boundary resistivity were independent of the grain-boundary density D. However, the resistance per square centimeter of grain-boundary surface decreased with increasing D in the range 170 to 310 cm^{-1}.

(3) The log-log plot using reported data showed that the grain-boundary resistivity increased with increasing D in the high-D region but was independent of D in the low-D region. These results were interpreted in terms of intrinsic effects such as

lattice irregularity in the high-D region and extrinsic effects such as impurity segregation in the low-D region.

REFERENCES in **IV**-1

1. B.C.H. Steel, J. Drennan, R.K. Slotwinski, N. Bonanos and E.P. Butler ; pp.286-309 in Advances in Ceramics, Vol.3. Edited by A.H. Heuer and L.W. Nobbs. The American Ceramic Society, Columbus, OH, 1981.
2. F.K. Moghadam and D.A.Stevenson, J. Am. Ceram. Soc., 65, 213 (1982).
3. J.E. Bauerle, J. Phys. Chem. Solids, 30, 2657 (1969).
4. I. Ioffe, M.V. Inozemtsev, A.S. Lipilin, M.V. Perfilev, and S,V, Karpachov, Phys. States Solidi A, 30, 87 (1975).
5. S.H. Chu and M.A.Seitz,J. Solid State Chem.,23, 297 (1978).
6. T. van Dijk and A.J. Burggraaf, Phys. Status Solidi A, 63, 229 (1981).
7. M.J. Verkerk, B.J. Middelhuis, and A.J. Burggraaf, Solid States Ionics, 6, 159 (1982).
8. C.K. Chiang, J.R. Bethin, A.L. Dragoo, A.D. Franklin, and K.F.Young, J. Electrochem. Soc., 129, 2113 (1982).
9. M. Nagai and H. Yanagida, Ceramurgia Int., 2, 145 (1976).
10. H. Yanagida,M.Takata, and M. Nagai, J. Am. Ceram. Soc., 64, C-34-35 (1981).
11. C.S.Smith,and L. Guttman,J. Met. 5, 81 (1953).
12. M.I.Mendelsson, J. Am. Cerm. Soc., 52, 443 (1969).
13. R.V. Wilhelm, and D.S. Howarth, Am. Ceram. Soc. Bull., 58, 228 (1979).
14. M.J. Verkerk, A.J.A. Winnubst, and A.J. Burggraaf, J. Mater. Sci., 17, 3113 (1982).
15. K.C.Radford,and R.J. Bratton,J. Mater. Sci., 14, 59(1979).
16. N.M. Beekmans and L.Heyne,Electrochim. Acta, 21, 303(1976).
17. E.P.Bulter, and J.Drennan, J. Am. Ceram. Soc., 65, 474(1982).

IV - 2. Effects of Al_2O_3 adittions on microstructure and resistivity

INTRODUCTION

Stabilized zirconia is a well-known oxygen ionic conductor which acts over a wide range of oxygen partial pressure. Since zirconia has a high melting point (2680°C), temperatures in excess of 1600 °C are generally required for traditional fabrication techniques. Sintering agents and/or fine zirconia powders are required for producing dense, impermeable and mechanically strong stabilized zirconia ceramics.

However, in most cases, sintering agents have a negative effect on the conduction behavior of stabilized zirconia. Small additions of SiO_2 are particulrly effective for the densification of CaO-stabilized ZrO_2 (CSZ),[1] but they cause a large increase in resistivity of Y_2O_3 -stabilized ZrO_2 (YSZ) at low temperatures.[2,3] Additions of TiO_2 to CSZ, [1,4] and of Fe_2O_3[5,6] and Bi_2O_3 [6-8] to YSZ, are also reported to aid densification and cause moderate increases in resistivity.

The effect of Al_2O_3 on the resistivity of stabilzed zirconia is rather complicated. Reported effects of Al_2O_3 additions are summarized in Table 1. Beekmans and Heyne reported that additions of Al_2O_3 did not influence the impedance behavior of CSZ.[9]

Bernard reported that Al_2O_3 additions not only assist sintering but lower the overall and grain-boundary resistivity of YSZ.[10] This effect was also evident in CSZ containing impurities such as SiO_2.[4] In contrast,it is also reported that Al_2O_3 additions increase the bulk and grain-boundary resistivity in high-purity YSZ[6,11]. According to Bernard, there was no evidence for liquid phase formation during sintering at 1300°C, and the Al_2O_3 was present principally as second phase particles. The estimated solubility limit of Al_2O_3 was 0.1 mol% at 1300°C. Butler et al. have examined Al_2O_3 particles in $(Y,Yb)_2O_3$ -stabilized ZrO_2 and suggested that the Al_2O_3 acts as a scavenger for SiO_2 located at grain boundaries, resulting in a reduced resistivity.[12]

Grain growth in CSZ and YSZ is reported to be affected by the Al_2O_3 additions,[1,11] and it is well known that grain-boundary resistivity depends on the microstructure (e.g. grain size) and impurity concectration,[6,13,14] as described in the last section. Accordingly, when examining the effect of Al_2O_3 addition on resistivity, microstructural changes have to be taken into account. However, such a systematic investigation has not been undertaken up to now. The present section describes the effect of Al_2O_3 additions on the microstructure, and the grain and grain-boundary resistivity of dense YSZ ceramics.

EXPERIMENTAL

The raw materials used were ZrO_2 (>99.95% pure), Y_2O_3 and Al_2O_3(both 99.99%), having mean particle sizes of 0.8, 3.8, and 1.5 μm, respectively. A mixture containing 92 ZrO_2, 8 Y_2O_3 (in mol%) and ethanol was ground in PSZ ball mills for 1 h, dried and calcined in a Pt crucible at 1400°C for 3 h. The ZrO_2 aggregates were mixed with the desired amount of Al_2O_3 and ground in PSZ ball mills for 120 h. The resulting powders were subsequently pressed into pellets(10 mm in diam. by 3 mm thick) at 125 MPa,

Table I. Reported Effects of Al_2O_3 Additions on Microstructure and Resistivity of Stabilized Zirconia

Ref.	Stabilizer	Al_2O_3 concentration (mol%) and other impurities	Sintering temperature, T_s (°C)	Microstructural* change	Location of Al_2O_3	Resistivity and† activation energy
9	≃17 mol% CaO	0.2–13 (SiO_2:0.7)	1780		Second phases	No effect
10	9 mol% Y_2O_3	0.44–1.33	1300	Assisted sintering	Second-phase particles	$\rho_g \rightarrow$, $E_g \rightarrow$ $\rho_{gb} \downarrow$, $E_{gb} \rightarrow$
1, 4	10 mol% CaO	1, 2 (SiO_2+MgO ≃3 wt%)	1480	r.d. 84→93% g.s. 35→12 μm	Concentrated at grain boundary	ρ_t < ρ_t (2 mol%) (1 mol%)
11	9 mol% Y_2O_3	1.0	2000	r.d. 97→99% g.s. 27→45 μm		$\rho_g \uparrow$ $\rho_{gb} \uparrow$
6	9.3 mol% Y_2O_3	0.78	1190	g.s. 0.7→0.8 μm T_s is lowered		$\rho_g \uparrow$, $E_g \rightarrow$ $\rho_{gb} \uparrow$, $E_{gb} \uparrow$
12	≃8 mol% Y_2O_3/Yb_2O_3	1.0 (SiO_2:0.6) 2.7 (SiO_2:0.3)	1600		α-Al_2O_3 particles containing inclusions	

*r.d.=relative density, g.s.=average grain size. †ρ_g, ρ_{gb}, ρ_t=grain, grain-boundary, and total resistivity; E_g, E_{gb}=activation energy for ρ_g and ρ_{gb}, respectively; ↑, ↓, →= increased, decreased, and unchanged, respectively.

Table II. Apparent Density, Grain-Boundary Density, and Average Grain Size of Y_2O_3-Stabilized ZrO_2 with Al_2O_3 Additions

Al_2O_3 (mol%)	Apparent density (%)*	Grain-boundary density (cm^{-1})	Grain size† (μm)
0	97	1.42×10^3	7.1
0.2	96	7.63×10^2	13.1
0.4	96	3.61×10^2	27.7
0.6	96	2.84×10^2	35.2
0.8	95	2.78×10^2	35.9
1.0	96	3.98×10^2	25.1

*Estimated from theoretical densities (calculated from lattice constants). †Mean linear intercept.

sintered at 1700°C for 3 h. Heating and cooling rate was 220°C/h.

Some of the sintered specimens were ground again and subjected to X-ray diffraction measurements. Lattice constants were calculated using the least-squares method and Si as an internal standard. The grain-boundary density D was determined from scanning electron micrographs of surfaces of as-sintered specimens, using a linear intercept technique.[15] The D values were estimated from more than 200 grid lines (of 90 μm length) per specimen. Some sintered specimens were examined by an electron probe microanalyzer, in order to information on Al distribution.

Alternating-current resistivity was measured in air at 400 - 600 °C. Platinum electrodes were applied by baking platinum paste at 1000 °C. At least four specimens were used to obtain resistivity data at each composition. Average values of measured resistivity are presented in the following section.

RESULTS AND DISCUSSION

About 70% of powder particles before sintering were 0.3-2.0 μm in size. Average particle size was estimated to be 0.7-0.9 μm for all compositions. Apparent dinsities, grain-boundary densities and average grain sizes in sintered specimens are given in Table 2. The mean linear intercepts were adopted as the average grain sizes.[16] The apparent densities were similar, however, as the Al_2O_3 concentration increased, the grain-boundry density decreased (grain size increased), reaching a minimum at 0.8 mol% Al_2O_3, and then increased at 1.0 mol% Al_2O_3.

Figure.1 shows scanning electron microgrhphs of YSZ powder before sinteringand surfaces of as-sintered YSZ containing Al_2O_3 concentrations of 0, 0.6, and 1.0 mol%. Second phase particles can be observed as bright or dark spots in YSZ containig 0.6 and 1.0 mol% Al_2O_3, although the amount of them is very small in YSZ containing 0.6 mol% Al_2O_3. They were 0.5 to 2.5 μm in size and

situate both inter- and intragranularly. Relative X-ray intensity of Al for specimens containing 0.6 and 1.0 mol% Al_2O_3 are shown in Fig. 2. Most of the particles showed high Al concentrations, but some of the bright particles showed an equal concentration to that in grains(a particle at the right side on the line in Fig. 2(B)). Apparent enrichment of Al at grain boundaries was not observed.

By XRD analysis (40 kV-100mA), only cubic zirconia was detected. There wewe no diffraction peaks of second phase for all compositions. Lattice constant decreased with increaseing Al_2O_3 concentration up to 0.5 mol%, as shown in Fig. 3. This decrease will be due to substitution of smaller A^{3+} ions (0.53 10^{-10}m) for Zr^{4+} ions (0.84×10^{-10}m)[17] in the ZrO_2 structure. The solubility limit of Al_2O_3 can be estimated to be 0.5 mol% in the material sintered at 1700°C and cooled at the rate of 220°C/h. Because of this cooling process, the present system may be not in equilibrium, and hence the solubility limit of 0.5 mol% may be that at a lower temperature than 1700°C.

From the results of X-ray microanalysis and lattice constants, most of the second phase particles shown in Fig. 1 and 2 can be concluded to be precipitated Al-rich compound or residual Al_2O_3.

It has been suggested that the Al_2O_3 particles in Al_2O_3 containing YSZ, being situated intergranularly, prevent grain growth by boundary pinning and permit elimination of most pores.[12] In the present system, in contrast, grain size increased at 1.0 mol% Al_2O_3. This result would also support that a certain amount of Al_2O_3 has dissolved into these YSZ but the solubility limit is slightly larger than 0.5 mol% (probably 0.6-0.8 mol%) at 1700°C.

As described in I-3, the ac impedance of polycrystalline stabilized zirconia contains contributions from the grains, the grain can boundaries and the electrolyte/electrode interface, and can be represented by three semicircles in the complex inpedance

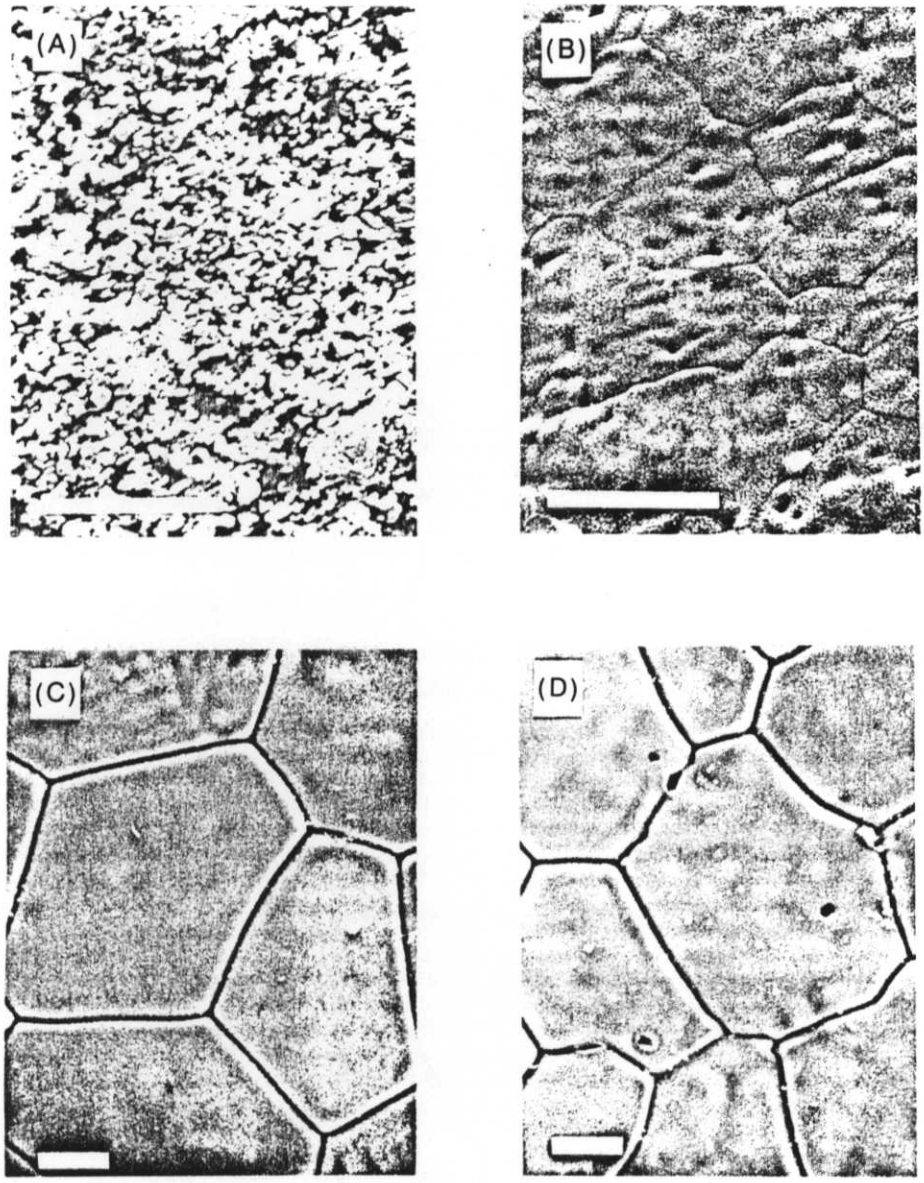

Fig. 2-1.

Scanning electron micrographs of (A)ball-milled Y_2O_3-stabilized ZrO_2 (YSZ) powder, (B)surface of as-sintered YSZ compact, (C)surface of sintered YSZ compact containing 0.6 mol% Al_2O_3, and (D)surface of sintered YSZ compact containing 1.0 mol% Al_2O_3.

(bars = 10 μm)

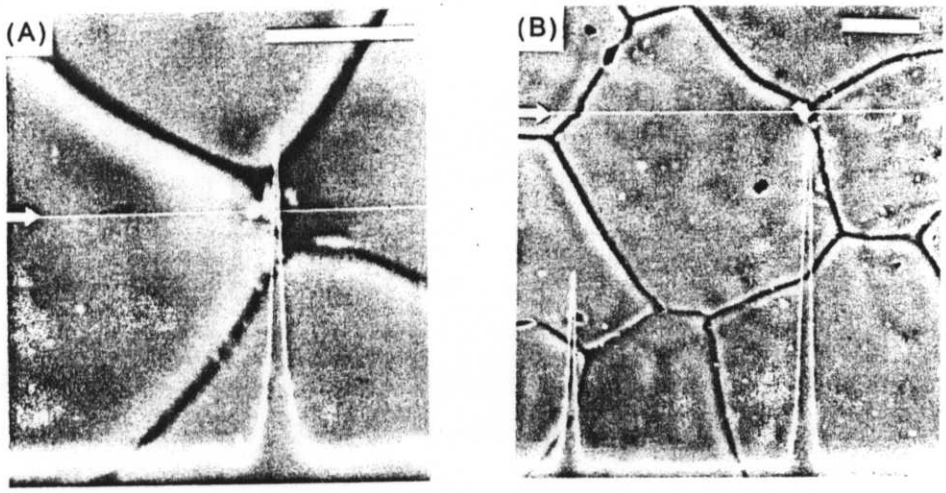

Fig. 2-2.

Relative Al X-ray intensity on line indicated for Y_2O_3-stabilized ZrO_2 containing (A) 0.6 mol% and (B) 1.0 mol% Al_2O_3.

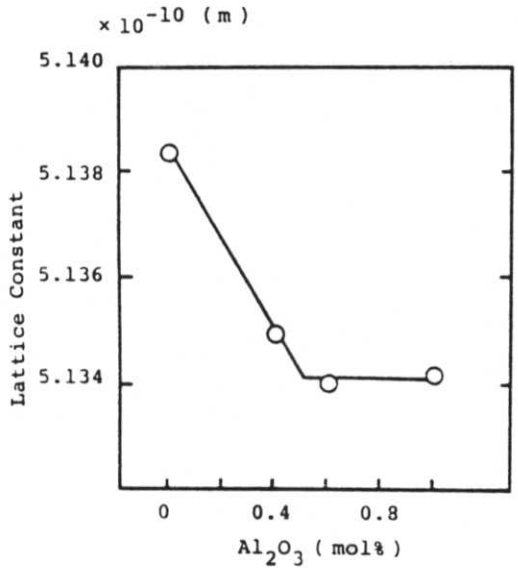

Fig. 2-3.

Lattice constant of Y_2O_3-stabilized ZrO_2 vs. Al_2O_3 concentration.

plots[13,14,18]. The grain (R_g) and grain boundary (R_{gb}) resistances were determined from chord lengths of the first and second semicircles at high frequencies in the impedance plots. The grain (ρ_g) and grain boundary (ρ_{bg}) resistivities were calculated from

$$\rho_g = R_g S/L \quad (1)$$

$$\rho_{gb} = R_{gb} S/L \quad (2)$$

where S is the electrode area and L specimen thickness.

Figure 4 shows ρ_g and ρ_{gb} for specimen compositions 0, 0.4, and 0.8 mol% Al_2O_3 as a function of temperature. No deviations from linearity were observed in the Arrhenius plots between 400 and 600 °C. The Al_2O_3 concentration dependences of ρ_g, ρ_{gb} along with that of the total resistivity ρ_t (= $\rho_g + \rho_{gb}$) at 400 and 600°C are shown in Fig. 5 (A) and (B), with error bars indicating the range of deviation in the resistivity measurement. The grain resistivity increased slightly with increasing Al_2O_3 concentration up to 0.6 mol% and then saturated, whereas grain-boundary resistivity showed a maximum at 0.4 mol%Al_2O_3. There is no marked difference in the dependence with temperature in Fig.5 A and B.

Activation energy, E, and preexponential term, ρ_o, for grain and grain-boundary resistivity were calculated from

$$\rho = \rho_o \exp(E/kT) \quad (3)$$

where K and T have their usual meanings. The values are plotted against Al_2O_3 concentration in Fig. 6. The preexponetial terms of grain (ρ_{og}) and grain-boundary resistivity (ρ_{ogb}) were almost constant. In contrast, the activation energies both increased initially with increasing Al_2O_3 concentration, but they appear to saturate or slightly decrease above 0.6 mol% Al_2O_3.

It is known that the activation energy in YSZ increases with increasing Y_2O_3 content in the fluorite structure region due to association or ordering of defects.[19] If Al_2O_3 dissolves into YSZ substitutionally in the same way as Y_2O_3, increases of E_g and E_{gb} will be expected. A linear increase in E_g of 44-50 kJ/mol was reported when the Y_2O_3 content increased from 10 to 20 mol%,[20] which corresponds to an increase in E_g of 2.2-2.5 kJ/mol for each

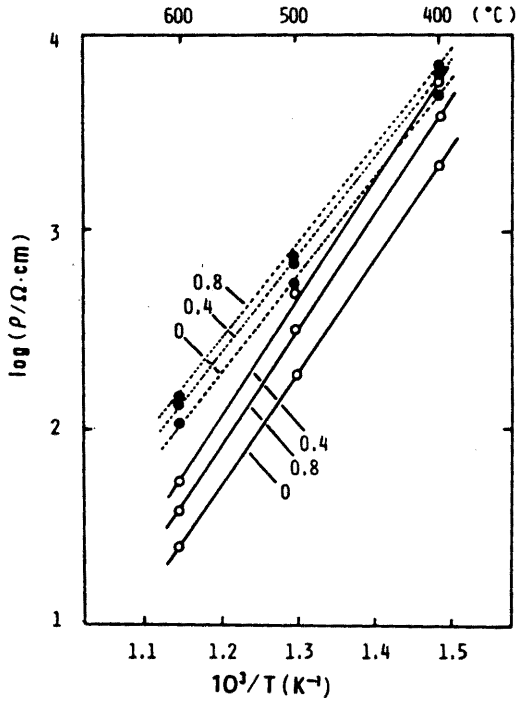

Fig. 2-4.

Temperature dependences of (●) grain and (o) grain-boundary resistivity of YSZ containing Al_2O_3 in concentrations (mol%) indicated by numbers in figure.

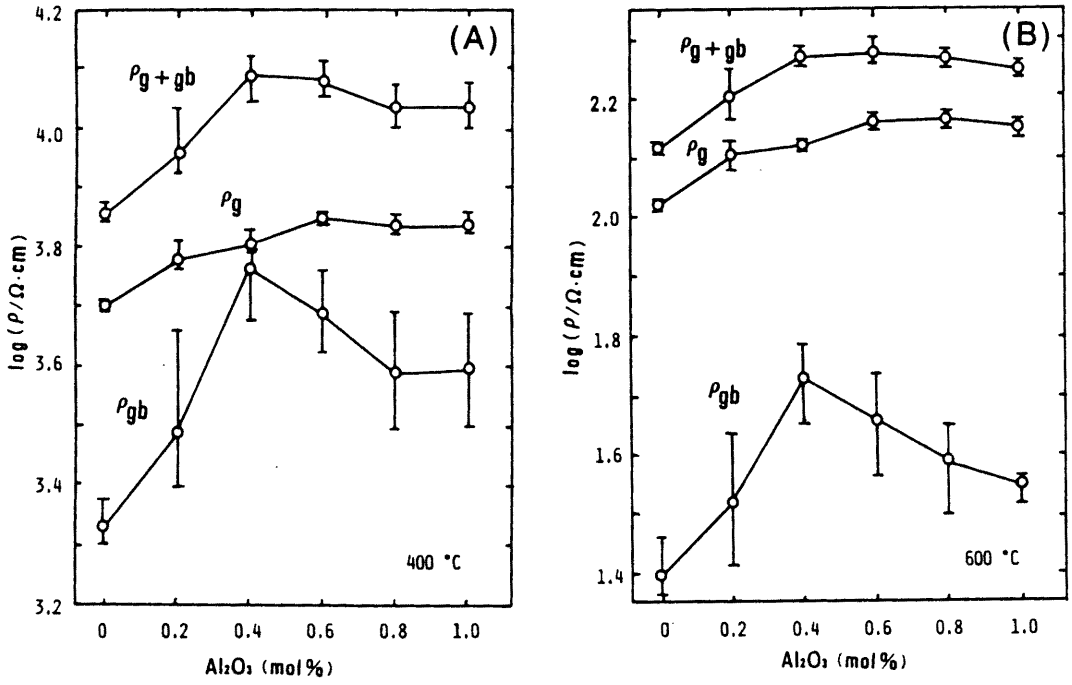

Fig. 2-5.

Al_2O_3 concentration dependence of grain (ρ_g), grain-boundary (ρ_{gb}), and total ($\rho_g + \rho_{gb}$) resistivities at (**A**) 400°C and (**B**) 600°C.

0.5 mol% Y_2O_3. This value is in agreement with the observed increase (2.5 kJ/mol) in E_g for the 0.6 mol% Al_2O_3 composition.

The increase in E_{gb} is a factor of two larger than that of E_g. Verkerk et al. reported and increase in E_{gb} from 107 to 125 kJ/mol for $(ZrO_2)_{0.82}(YO_{1.5})_{0.17}$ containing 0.78 mol% Al_2O_3, although they found no increase in E_g.[6] Increases of ρ_{gb} and E_{gb} in YSZ by the incorporation of impurities can be accounted for by impurity segregation, second pfase phase formation, and subsequent changes in space charge distribution at grain boundaries.[14] The large increase in E_{gb} cannot be explained by an interference of oxygen vacancy migration due to residual Al_2O_3 particles, if presented. Although Al_2O_3 of concentration up to 0.5 mol% appears to dissolve in YSZ, slight segregation of dissolved Al_2O_3 at grain boundaries may have occurred during slow cooling process, even in the low Al_2O_3 concentration range. In addition, if a small amount of other impurity insoluble in YSZ is present, a decrease in grain-boundary density for YSZ containing below 0.6 mol% Al_2O_3would lead to an enrichment of impurity per unit area of the grain-boundary surface. Assuming the segragation of Al and/or other impurities and subsequent changes in space charge distribution at grain boundaries, they may cause a trapping of oxygen vacancies due to associate formation or ordering, resulting in a decrease in mobility or concentration of oxygen vacancies. These phemonema can explain the large increases in E_{gb} and ρ_{gb} in the low Al_2O_3 concentration range. However, it cannot be concluded without precise surface analysis of the grain boundary.

Compared with those of ρ_g and E_g, the Al_2O_3 concentration dependence of ρ_{gb} is not in good agreement with that of E_{gb}. There is no marked maximum for E_{gb} in Fig.6 as shown for ρ_{gb} at 0.4 mol%Al_2O_3 inFig.5. In order to eliminate microstructural effects, the resistance per square centimeter of grain-boundary surface (R_{gbs}) was calculated from[15]

$$R_{gbs} = \rho_{gb}/D \qquad (4)$$

Figure 7 shows R_{gbs} as a function fo Al_2O_3 concntraion for

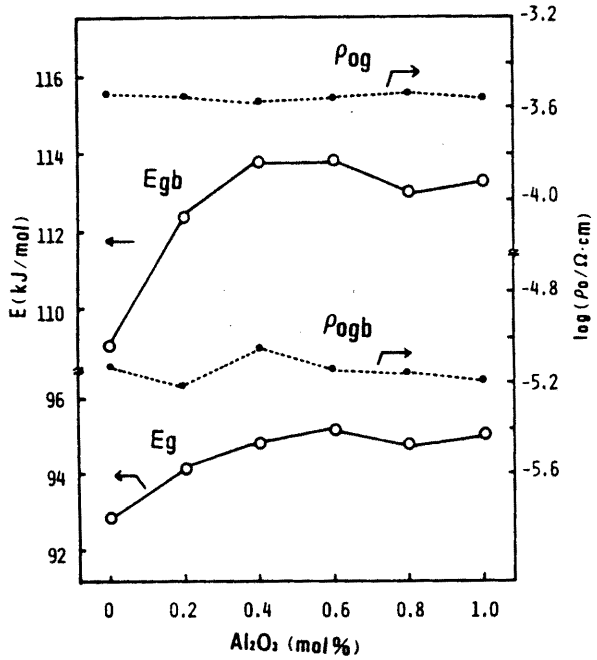

Fig. 2-6.
Al_2O_3 concentration dependence of activation energies (E_g, E_{gb}) and pre-exponential terms (ρ_{og}, ρ_{ogb}) for grain and grain-boundary resistivity.

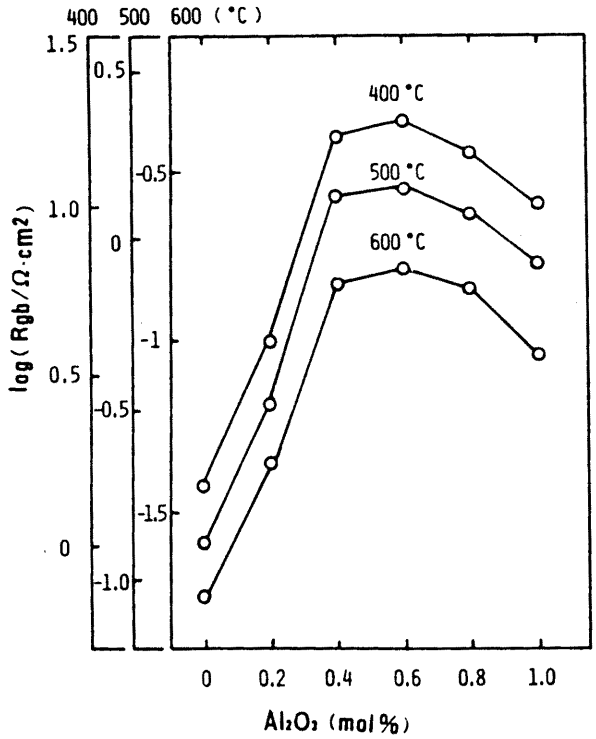

Fig. 2-7.
Al_2O_3 concentration dependence of resistance per cm^2 of grain-boundary surface at 400°, 500° and 600°C.

temperatures in the range 400 - 600°C. In each case, there is a sharp initial increase in R_{gbs} with increaseing Al_2O_3 concentration, to a maximum at 0.6 mol% Al_2O_3, followed by a decrease. The composition showing a maximum in R_{gbs} and E_{gb} agreed well.

The decrease in R_{gbs} in the composition containing more than 0.6 mol% Al_2O_3 appears to be larger than that expected from the decrease in E_{gb}. Butler and Drennan[12] found that Al_2O_3 particles, in Y_2O_3/Yb_2O_3stabilized zirconias with Al_2O_3 and SiO_2 present (see Table 1), contained Zr or Si and Zr rich inclusions. The Al_2O_3 particles were frequently associated with amorphous crusp areas rich in Si and Al. These results suggest that Al_2O_3 acts as a scavenger for SiO_2 which is present at grain boundaries as a second phase and interferes with ionic conduction. Although SiO_2 concentration have not been determined for the present system, a similar scavenging effect of Al_2O_3 could explain the decrese in R_{gbs} and ρ_{gb} in YSZ containing more than 0.6 mol% Al_2O_3.

CONCLUSION in **IV**-2

(1) Alumina of concentration up to 0.5 mol% dissolved in 8 mol%-YSZ, sintered at 1700°C and cooled at the rate of 220°C/h.

(2) Grain-boundary density decreased (grain size increased) with increasing Al_2O_3 concentration up to 0.6 mol% but increased at 1.0 mol% Al_2O_3.

(3) Grain resistivity and the resistance of the grain-bounary surface both increased with increasing Al_2O_3 concentration up to 0.6 mol%. The resistance of grain-boundary surface decreased when the Al_2O_3 concentration was > 0.6 mol%. It is suggested that soluble and insoluble Al_2O_3 have opposite effects on resistivity and grain gr owth in YSZ.

REFERENCES in **IV**-2

1. K.C. Radford and R.J. Bratton, J. Mater. Sci., 14, 59 (1979).
2. E. Schouler, Ph.D. Thesis, National Polytechnic Institute of Grenoble, France, 1979.
3. S.P.S. Badwal, J. Mater. Sci., 19, 1767 (1984).
4. K.C. Radford and R.J. Bratton, ibid., 14, 66 (1979).
5. R.V. Wilhelm and D.S. Howarth, J. Am. Ceram. Soc., 58, 228 (1979).
6. M.J. Verkerk, A.J.A. Winnubst and A.J. Burggraaf, J. Mater. Sci., 17, 3113 (1982).
7. K. Keizer, M.J. Verkerk and A.J. Burggraaf, Ceramurgia Int., 5, 143 (1979).
8. K. Keizer, A.J. Burggraaf and G. De With, J. Mater. Sci., 17, 1095 (1982).
9. N.M. Beekmans and L. Heyne, Electrochim. Acta, 21, 303(1976).
10. H. Bernard, Rep. CEA-R-5090, Commissariat a l'Energie Atomique, CEN-Saclay, France, 1981; pp.117.
11. M.V. Inozemtsev and M.V. Perfil'ev, Sov. Electrochem., 11, 951 (1975).
12. E.P. Butler and J. Drennan, J. Am. Cearm. Soc.,65, 474(1982).
13. A.I.Ioffe, et al., Phys. Status Solidi A, 30, 87 (1975).
14. M.J. Verkerk, B.J. Middelhuis and A.J. Burggraaf, Solid State Ionics, 6, 159 (1982).
15. C.S. Smith and L. Guttman, J. Met., 5, 81 (1953).
16. M.I. Mendelsson, J. Am. Ceram. Soc., 52, 443 (1969).
17. R.D. Shannon and C.T. Prewitt, Acta Cryst., B25, 925 (1969).
18. J.E. Bauerle, J. Phys. Chem. Solids, 30, 2657 (1969).
19. E.C. Subbarao, Science and Technology of Zirconia ; Advances in Ceramics, Vol.3. pp.1-24, The American Ceramic Society, Inc., Columbus, OH, 1981.
20. R.E.W. Casselton, Phys. Status Solidi A, 2, 571 (1970).

IV - 3. Conclusion in Chapter IV

The grain-boundary resistivity in stabilized ZrO_2 ceramics becomes comparable to the grain-interior resistivity at low temperatures, and it depends on microstructure(grain size et.al), composition and impurity concentration. In Chapter **IV**, it was tried to make clear those influences on the grain-boundary resistivity. Obtained results are summarized as ;

(1) There were two types of dependence of (total) grain-boundary resistivity on grain-boundary density D. The grain-boundary resistivity increased with D in the high-D region ($\simeq 2\times10^3 cm^{-1}$) but was independent of D in the low-D region. Estimated resistance per cm^2 of grain-boundary surface was constant in the high-D region but decreased with increasing D in the low-D region.

(2) Two factors are assumed as origins for resistance of grain-boundary surface ; an intrinsic factor such as lattice irregularity or segregation of princepal components, and an extrinsic factor such as impurity segregation or second phase forming. The intrinsic factor (independenct of D) and the extrinsic factor (dependent of D) are assumed to be predominant for the high-D and low-D region, respectively.

(3) Alumina of concentration up to 0.5 mol% can dissolve in Y_2O_3-stabilized ZrO_2 at 1700 C.

(4) It was suggested that Al_2O_3 additions have a dual role according to their concentration level. Below the solubility limit, grain-boundary resistivity is increased and grain growth is promoted. The reverse applied when the Al_2O_3 concentration is above the solubility limit.

It was found that the grain-boundary resistivity is affected by the impurity concentration and the fabrication process (microstructure) with their mutural interactions. In order to analyze the grain-boundary resistivity, those two factors have to be evaluated separately. The determination of the resistance of grain-boundary surface would be a useful aid to the analysis of conduction behavior at grain boundaries.

Chapter V

Electrical Conduction in Some Oxides Used as Dopants

V - 1. P-type electronic conduction in Sb_2O_4

INTRODUCTION

A series of antimony oxide compounds was applied as an additive to semiconducting materials. When antinomy sesquioxide (Sb_2O_3) is doped to tin oxide, trivalent antimony ions are known to be partially oxidized to pentavelent ions and to work as electron doners.[1,2] The network structure of the orthorhomic α-Sb_2O_4 was shown to contain equal amounts of Sb^{3+} and Sb^{5+} by X-ray and neutron diffraction [3,4] and Mossbauer analysis.[5]

However, the electrical properties of antimony oxide compounds are still not clear because of the polymorphic transitions[6] and vaporization at relatively low temperatures.[7]

In the present study electrical conductivity and thermoelectric power were measured on α-Sb_2O_4 to clarify the electrical conduction mechanism.

EXPERIMENTAL

Alpha Sb_2O_4 powder was prepared by heating Sb_2O_3 (99.99%) at 650°C for 2 h in air. X-ray diffraction patterns showed a

complete oxidation to α-Sb_2O_4. The cold-pressed bodies were covered with Al_2O_3 powder and hot-pressed at 900°C for 5 h under a pressure of 49 MPa in air. Surfaces of the spacimen were polished with emery paper after hot-pressed. Above 900°C in air, wight loss by vaporization was found in TG-DTA. The apparent densities of sintered specimems were 66 to 68% of theoretical.

The concentrations of Sb^{3+} and Sb^{5+} were determined by titrimetric analysis with potassium permanganate for Sb^{3+} and potassium iodide and sodium thiosulfate for Sb^{5+}. The concentration ratio Sb^{3+}/Sb^{5+} was 1.02 and 1.04 in the specimens after annealing at 700°C for 8 h under an oxygen partial preesure (PO_2) of $10^{4.31}$ (air) and 10^1 Pa, respectively.

Electrical condudtivity was measured at 250°C to 780°C by a two-probe ac method at a frequency of 10 kHz with sputtered Au electrodes and by a four-probe dc method with baked Pt paste electrodes. Ohmic contacts within 1 V were confirmed by measuring V-I plots. The dependence of electrical conductivity on oxygen partial pressure was measured by using Ar-O_2 mixed gas as a carrier gas and a stabilized zirconia cell for monitoring the PO_2. Thermoelectric power measurements were conducted in the same manner described in II-3.

RESULTS AND DISCUSSION

Figure 1 shows the temperature dependence of the electrical conductivity. Three regions with different activation energies appeared. The activation energies were 122 above 700°C, 96 between 450°C and 700°C, and 37 kJ/mol below 450°C. In the low-temperature region, deviations in conductivity among several spacimens were rather large, which may be due to differences in impurity concentration or microstruture of the specimens.

Figure 2 shows the PO_2 dependences of the conductivity at several temperature above 600°C. The conductivities were propor-

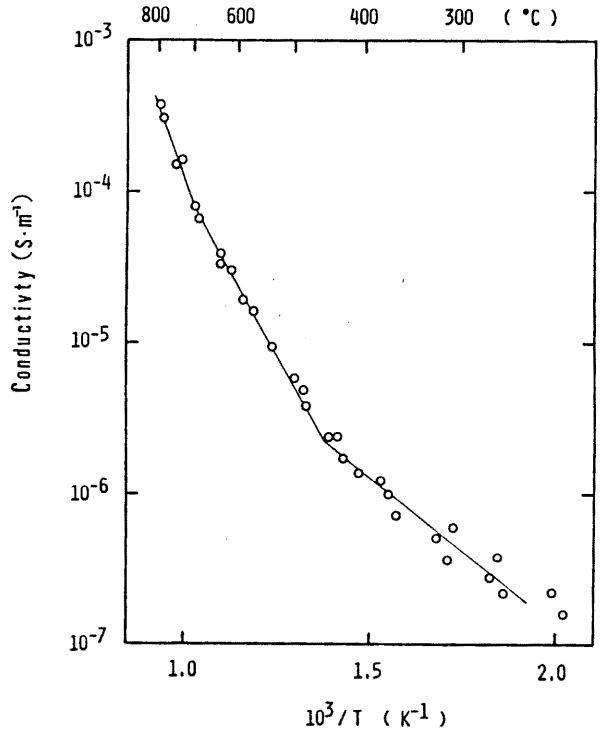

Fig. 1-1.

Temperature dependence of electrical conductivity of α-Sb_2O_4 in air.

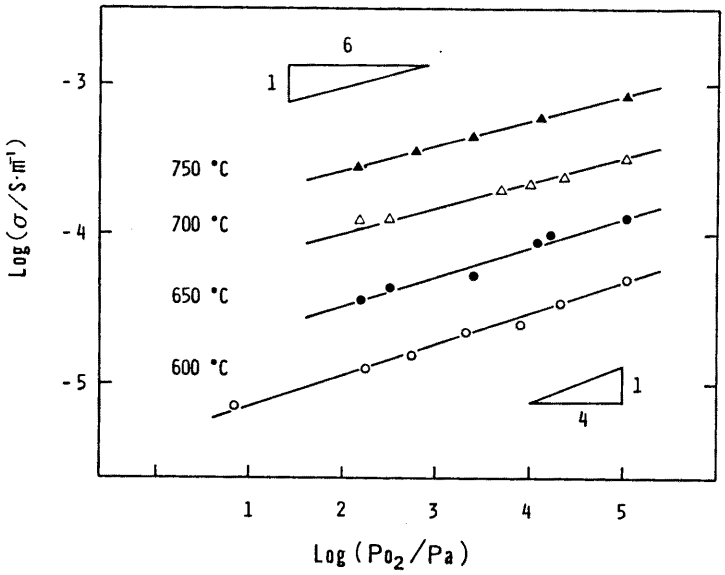

Fig. 1-2.

Oxygen partial pressure dependence of electrical conductivity of α-Sb_2O_4.

tional to $PO_2^{1/n}$ between 10^5 and 10^2 Pa, where 1/n was always positive and 1/4.8 to 1/5.1 below 700°C and 1/5.99 above 700°C. The sign of the observed Seebeck coefficient measured in air was also always positive. These results indicate that α-Sb_2O_4 is a p-type semicondudtor. The changes in activation energy and PO_2 dependence of the condudtivity above and below 700°C suggest a slightly different mechanism in the formation of electronic carriers. Below 10^1Pa, the conductivity became independent of PO_2 down to 10^{-9} Pa. The sample weight was constant through annealing at 700°C under 10^1Pa, whereas a weight loss of 2 wt% was observed for the specimen annealed under 10^{-9} Pa. These results suggest the vapolization of α-Sb_2O_4 and a subsequent change of the conduction mechanims below a PO_2 of 10^1Pa.

When positive holes are the only charge carrier for a nondegenerate semiconductor where Boltzmann statistics can be applied, the Seebeck coefficient Q can be written as;

$$Q = (k/e)[\ln(P_o/p) + A] \qquad (1)$$

where k is the Bolzmann constant, e the electronic charge, P_o the effective density of states, p the hole concentration, and A an energy-transport term.[8] The electrical condudtivity σ is written as;

$$\sigma = ep\mu \qquad (2)$$

where μ is the mobility of the charge carrier. Therefore, combining Eqs. (1) and (2) gives

$$\frac{d\log\sigma}{d(kT)^{-1}} + \frac{e}{2.303k}\frac{dQ}{d(kT)^{-1}} = \frac{d}{d(kT)^{-1}}\left[\log\mu + \log P_o + \frac{A}{2.303}\right] \qquad (3)$$

Since $dA/d(kT)^{-1}$ is negligibly small, the right side in Eq.(3) could be approximated to zero for a broad-band conduction.

Figure 3 shows log σ and eQ/2.303k vs 1/T for α-Sb_2O_4 measured in air in the mid-temperature range. The apparent activation energies were 96 kJ/mol for log σ and 83 kJ/mol for eQ/2.303k. This difference in activation energy suggests the thermally activated process in the movement of electron holes. If all the trivalent antimony ions are equivalently available for

the transport sites of electron holes and A = O, as in the case of a narrow polaron band, the concentration and mobility of electron holes could be calculated using Eqs.(1) and (2) and the reported lattice canstant[3] as

$$p = 7.65\times10^{24} \exp[-83(kJ/mol)/RT] \quad (cm^{-3}) \quad (4)$$

$$\mu = 1.71\times10^{-4}T^{-1} \exp[-18(kJ/mol)/RT] \quad (cm^2/V\cdot s) \quad (5)$$

The mobility of electron holes in the temperature range 450 to 700°C was 1.4 to $2.3\times10^{-8}(cm^2/V.s)$.

The results that the hole mobility has a very small value and an activation energy indicate that hopping conduction is dominant in the mid-temperature region in α-Sb_2O_4. However, Abnormally low hole mobility in the present study may be due to the low density of spacimen or to a reduced density of states (P_o) for polarons shared by cation pairs or clusters.[9]

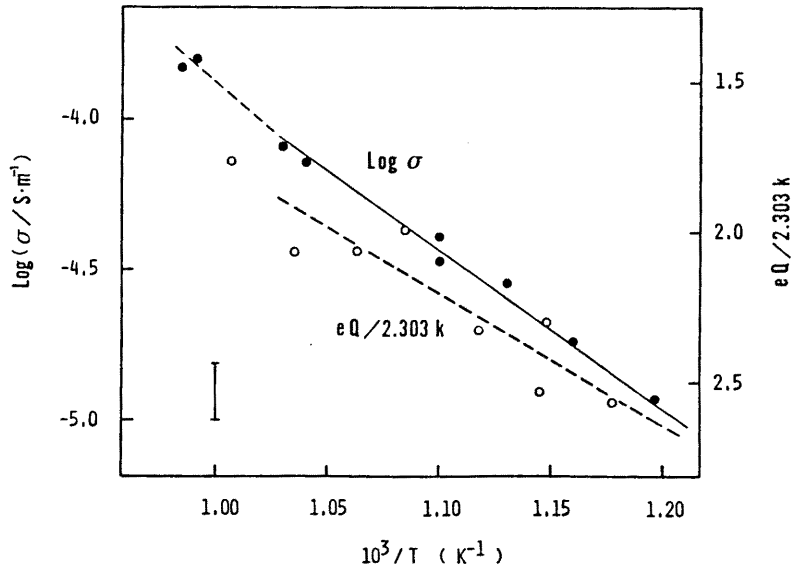

Fig. 1-3.

(●) Electrical conductivity and (o) eQ/2.303k vs. 1/T for α-Sb_2O_4 in air. Bar : experimental error in eQ/2.303k.

CONCLUSION in **V**-1

(1) Oxygen partial pressure (PO_2) dependence of conductivity and the sign of the Seebeck coefficient showed α-Sb_2O_4 to be a p-type semiconductor above 600°C in the PO_2 range of 10^5 to 10^2 Pa.

(2) A hopping conduction was proposed from very small hole mobility with an activation energy of 18 kJ/mol.

REFERENCES in **V**-1

1. L.D. Loch, J. Electrochem. Soc., 110, 1081 (1963).
2. T. Matushitaand I. Yamai, Yogyo Kyaki Shi, 80, 305 (1972).
3. P.S. Gopalakrishman, and H. Monohar, Cryst. Struct. Comm., 4, 203 (1975).
4. G. Thornton, Acta Crystallogr., Sect.B, 33, 1271 (1977).
5. G.G. Long, L.G. Stevens, and L.H. Bowen, Inorg. Nucl. Chem. Lett., 5, 799 (1969).
6. C.A. Cody, L. Dicarlo, and R.K. Darlington, Inorg. Chem., 18, 1572 (1979).
7. R.G. Behrens, and G.M. Rosenblatt, J. Chem. Thermodyn., 5, 173 (1973).
8. J.M. Wimmer, and I. Bransky; pp.269-311 in Electrical Conductivity in Ceramics and Glass, Part A. Edited by Norman M. Tallan. Marcel Dekker, New York, 1974
9. J.B. Goodenough, Mater. Res. Bull., 5, 621 (1970).

V - 2. Ionic conduction in pure- and ZrO_2-doped Y_2O_3

INTRODUCTION

Yttrium oxide (Y_2O_3) has the C-type cubic rare-earth-oxide crystal structure. This structure is described as a modified fluorite-type structure with one fourth of the anion sites vacant and regularly arranged. Instead of such a high concentration of oxygen vacancy, it is reported that the electrical conduction of Y_2O_3 in air is predominantly p-type and the contribution of ionic conduction is negligibly small.[1,2]

According to the phase diagram of Y_2O_3-ZrO_2 system[3], Y_2O_3 solid solutions exist up to 18 mol% at 1375°C and to 23 mol% ZrO_2 at 2000°C. Bratton suggested on the bases of density measurements that interstitial oxygen ions are generated in Y_2O_3 by doping of ZrO_2.[4] Ando et.al also reported that self-diffusion coefficients of the oxygen ion increase with an increase of ZrO_2 content.[5,6] To understand the conduction mechanism in the fluorite-related structure with a high concentration of oxygen vacancy, it is desirable to clarify the conduction behavior in the Y_2O_3-ZrO_2 system. For this purpose, electrical conductivity was measured as a function of temperature, PO_2 and ZrO_2 concentration.

EXPERIMENTAL

Powders of $Y(NO_3)_3.6H_2O$ and $ZrOCl_2.8H_2O$ in a desirable ratio were dissolved into water. Aquaous solution (28 %) of NH_3 was dropped slowly into the Y-Zr solution under stirring until the PH of the solution reachs about 9. Precipitated compound was filtered, washed by water and dried at 80°C for 10 h. Aggregates obtained were heated at 600°C, ground finely, pressed into bars, sintered at 1800°C for 20 min in N_2 and finally annealed at 1200 °C for 10 h in air. Lattice constants were calculated by the least-square method using Si as aninternal standard.

The conductivity was measured at 900-1200°C under PO_2 of 10^5 to 10^{-4} Pa by the complex impedance method. The PO_2 was controled by using $Ar-O_2$ or $CO-CO_2$ mixed gases and checked by a zirconia concentration cell. Platinum paste was baked as electrodes.

RESULTS AND DISCUSSION

X-ray diffraction showed that pure and ZrO_2-doped Y_2O_3 specimens were in single phases. The lattice constant decreased with increasing ZrO_2 content up to 16 mol%, as shown in Fig.1. However, the slope in Fig.1 seems to be different for below and above 4 mol% ZrO_2.

Figure 2 shows the temperature dependence of the conductivity of Y_2O_3 doped with 0 to 16 mol% ZrO_2 measured in air. The conductivity of ZrO_2-doped Y_2O_3 increased with an increase of ZrO_2 content. Activation energy was 110 kJ/mol for pure Y_2O_3 and 170 ± 5 kJ/mol for doped specimens.

Figure 3 shows the PO_2 dependence of conductivity for pure and 16 mol%-doped Y_2O_3 at 1000°C. The doped Y_2O_3 showed a constant conductivity, suggesting oxygen ionic conduction. In contrast, for pure Y_2O_3, conductivity increased in proportion to $PO_2^{1/6}$. From the difference in activation energy and PO_2

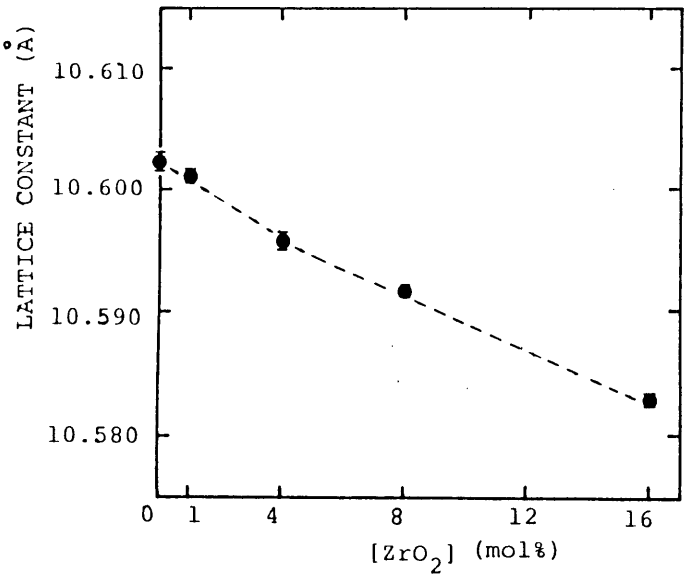

Fig. 2-1.

Lattice constant of Y_2O_3 doped with ZrO_2.

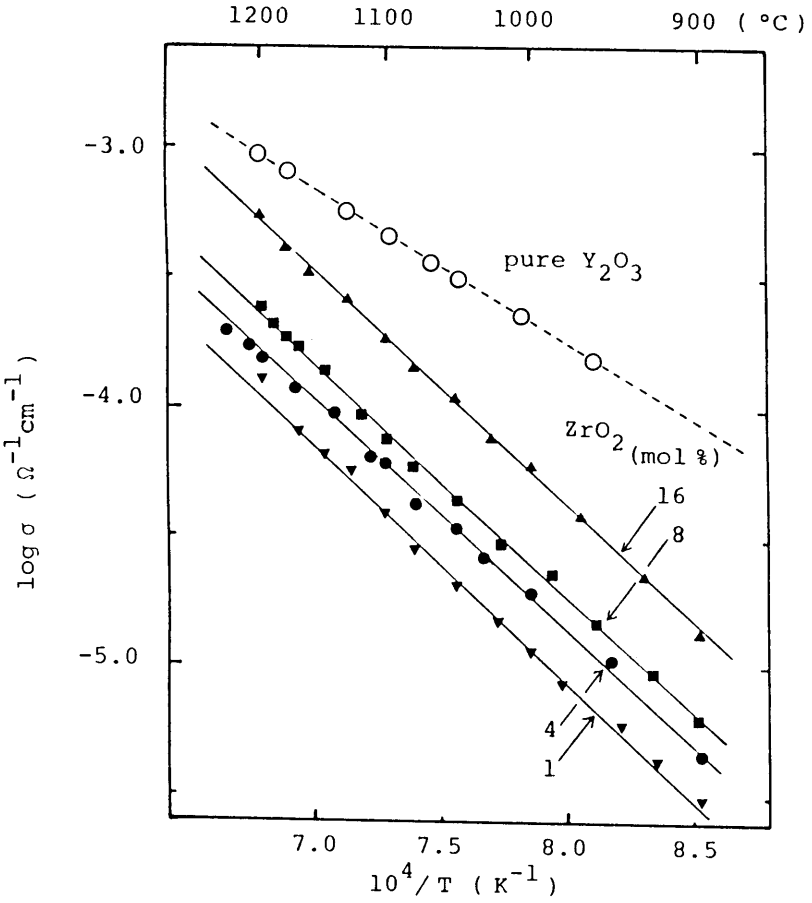

Fig. 2-2.

Electrical conductivity of pure and ZrO_2-doped Y_2O_3 in air. Numbers indicate ZrO_2 concentration in mol%.

dependence of conductivity, oxygen ionic conductivity is assumed to be prediminant in the ZrO_2-doped Y_2O_3 specimens.

On the bases of density change reported by Bratton[4], the dissolution of ZrO_2 into Y_2O_3 can be expressed as,

$$2\ ZrO_2 \xrightarrow{Y_2O_3} 2Zr_Y^{\cdot} + 3O_O^{*} + O_i'' \qquad (1).$$

Accordingly, it can be concluded that the oxygen ionic conduction is due to the interstitial oxygen ions introduced by dissolution of ZrO_2. The composition dependence of ionic conductivity ($\log\sigma$ vs. logx in $(Y_2O_3)_{1-x}(ZrO_2)_x$) is shown in Fig.4. When all interstitial oxygen ions contribute to ionic conduction, the slope ($\log\sigma/\log x$) in Fig.4 must be 1. However, the observed slope was rather smaller than 1 in low ZrO_2 region (especially below 4 mol%) although the slope was 1 in high ZrO_2 region. this suggests that all interstitial oxygen do not necessarily work as ionic carriers.

The composition dependence of lattice constant seems a little steeper below 4 mol% ZrO_2 than that above 4 mol%. In the crystal structure of pure Y_2O_3, two interstitial oxygen sites can be possible ; the vacant oxygen sites (48(e) in Ia3 space group) and the center position in a fluorite unit cell. It is also reported that the positions of Y^{3+} and O^{2-} ions deviate from their ideal positions in the pure Y_2O_3. Probably, introduced oxygen ions would occupy the vacant oxygen sites when the content of doped ZrO_2 is small(below 4 mol%). The mobility of these oxygen ions are expected to be small as for the oxygen ions present originally in the lattice. As the amount of introduced oxygen ions further increases, slight positional deviations of oxygen ions would be diminished or some oxygen ions would occupy the center of fluorite unit cell. These phenomena can be expressed as an increase in disorder in the oxygen sublattice. In this state, all introduced oxygen ions contribute to the ionic conduction and the conductivity increse in proportion to the concentration of introduced oxygen ions.

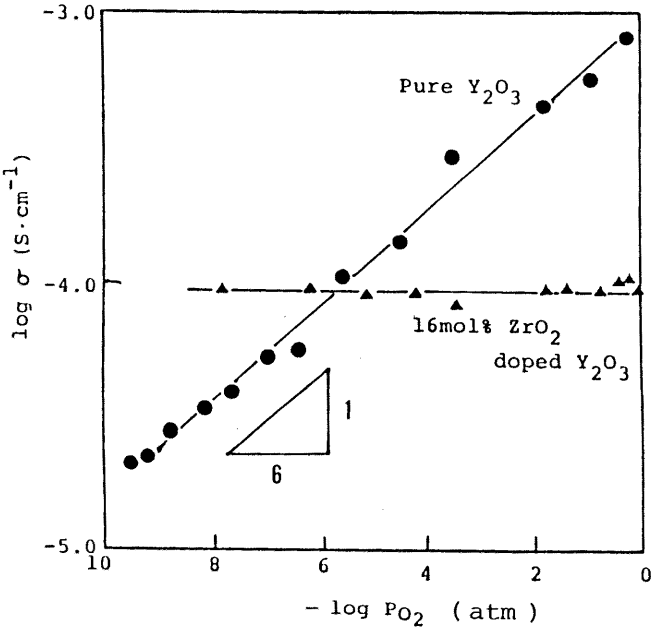

Fig. 2-3.

PO_2 dependence of conductivity for pure and ZrO_2-doped Y_2O_3 at 1000°C.

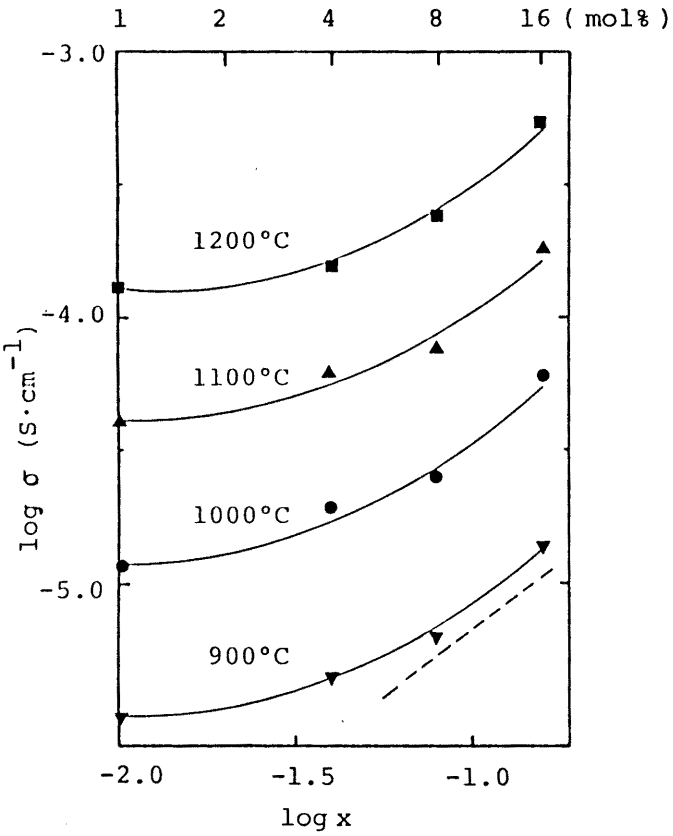

Fig. 2-4.
Composition dependence of oxygen-ion conductivity σ.
[log σ vs. log x in $(Y_2O_3)_{1-x}(ZrO_2)_x$]

CONCLUSION in V-2

(1) The vacant oxygen sites, which are regularly arranged in the C-type structure of pure Y_2O_3, was found not to contribute effectively to ionic conduction.

(2) The oxygen ion conductivity increased with increasing ZrO_2 content.

(3) Interstitial oxygen ion, introduced by doping of ZrO_2, seems to work as an effective ionic carrier when its concentration is above some value (about 4 mol% ZrO_2).

REFERENCES in V-2

1. N.M. Tallan and R.W.Vest, J. Am. Ceram. Soc., 49, 401 (1966).
2. J. Schieltz, J.W. Patterson and D.R. Wilder, J. Electrochem. Soc., 118, 1140 (1971).
3. V.S. Stubican, R.C. Hink and S.P. Ray, J. Am. Ceram. Soc., 61, 17 (1978).
4. R.J. Bratton, J. Am. Ceram. Soc., 52, 213 (1969).
5. K. Ando, Y. Oishi and H. Hase, J. Am. Ceram. Soc., 66, c-222 (1983).
6. K. Ando, K. Sogabe, Y. Oishi and K. Kitazawa, Proceedings of the annual meeting of Yogyo Kyokai, A-31, 145 (1984).
7. F. Hanic et al. Acta Cryst. B40, 76 (1984).

Acknowledgment

The author is deeply indebted to Professor Dr. Hiroaki Yanagida for providing him with the opportunity and the philosophical foundation for the present thesis. Professor Yanagida's continuing interest and encouragement are also greatly appreciated.

Associate professor Dr. Masasuke Takata of The Technological University of NAGAOKA is sincerely acknowledged for encouragement and suggestions in both academic and private aspects.

Associate professor Dr. Kunihito Koumoto is greatfully acknowledged for many valuable discussions.

Mr. Shunji Takeda is acknowledged for his help in many kinds of measurements.

Drs. Kimihiro Yamashita, Shunichi Hishida and Mr. Satoru Fujitsu are greatly acknowledged for many helpful discussions and comments.

The author wish to thank Hiroya Terada, Shinichi Katsuta, Yoshihiro Suenaga, Yukihiko Shimizu, Tetsuya Nishi, Munenori Iwabuchi, Toshihiko Hanada of Chiba Institute of Technology, and Kanji Takashima, Akira Tanigawa of The Science University of Tokyo for undertaking the research together.

In the end, the author is grateful to many people who encouraged him to accomplish his research, and especially to his parents and his wife Saeko.

LIST OF PUBLICATION

1. "Polymorphic Transformation and Electrical Resistivity of Bismuth Oxide", M. Miyayama, M. Takata and H. Yanagida, Yogyo-Kyokai-Shi, 87(10), 536-40 (1979) (in Japanese).

2. "Stabilization of β-Bi_2O_3 by Sb_2O_3 Doping", M.Miyayama, H. Terada and H.Yanagida, J. Am. Ceram. Soc.,64(1), c-19 (1981).

3. "Electric Conduction of Metastable Pure β-Bi_2O_3", M. Miyayama, S. Katsuta and H. Yanagida, Nippon-Kagakukai-Shi, 1981(10), 1583-88 (in Japanese).

4. "Electrical Conduction in Sintered α-Sb_2O_4", M. Miyayama, S. Ogi and H. Yanagida, J. Am. Ceram. Soc., 66(5), 351-52 (1983).

5. "Electrical Conduction in β-Bi_2O_3 Doped with Sb_2O_3", M. Miyayama, S. Katsuta, Y. Suenaga and H. Yanagida, J. Am. Ceram. Soc., 66(8), 585-88 (1983).

6. "Grain Boundary Resistivity of Stabilized Zirconia Films", M. Miyayama, H. Inoue and H. Yanagida, J. Am. Ceram. Soc., 66(9), c-164-7 (1983).

7. "Mixed Electrical Conduction in Sintered bcc $6Bi_2O_3.SiO_2$", M. Miyayama, Y. Suenaga and H. Yanagida, J. Mater. Sci., 18(10), 3023-30 (1983).

8. "Dependence of Grain-Boundary Resistivity on Grain-Boundary Density in Yttria-Stabilized Zirconia", M. Miyayama and H. Yanagida, J. Am. Ceram. Soc., 67(10), c-194-95 (1984).

9. "Oxygen Ion Conduction in γ-Bi_2O_3 Doped with Sb_2O_3", M. Miyayama and H. Yanagida, J. Mater. Sci., 21(4), 1233-36 (1986).

10. "Effects of Al_2O_3 Additions on Resistivity and Microstructure of Yttria-stabilized Zirconia", M. Miyayama, H. Yanagida and A. Asada, J. Am. Ceram. Soc., 65(4), 660-64 (1986).

11. "Oxygen Ion Conduction in fcc Bi_2O_3 Doped with ZrO_2 and Y_2O_3", M. Miyayama and H. Yanagida, Mat. Res. Bull.,in press.

12. "Oxygen Ionic Conduction in Composites Consisting of Bi_2O_3 and ZrO_2 Both Stabilized with Y_2O_3", M. Miyayama, T. Nishi and H. Yanagida, J. Mater. Sci., accepted.

13. "Electrical Conduction in Sintered Y_2O_3 Doped with ZrO_2 and CaO", M. Miyayama, T. Nonaka and H. Yanagida, in preparation.